Application of Different Model Concepts for Simulation of Two-Phase Flow Processes in Porous Media with Fault Zones

vorgelegt von
Master of Science

SONG PHAM VAN

aus Thaibinh, Vietnam

von der Fakultät VI Planen Bauen Umwelt
der Technischen Universität Berlin
zur Erlangung des akademischen Grades
Doktor der Ingenieurwissenschaften
Dr.-Ing.

genehmigte Dissertation

Promotionsausschuss:

Vorsitzender:	Prof. Dr. Gerd Wessolek
Gutachter:	Prof. Dr.-Ing. Reinhard Hinkelmann
Gutachter:	Prof. Dr.-Ing. Erwin Zehe (TU München)

Tag der wissenschaftlichen Aussprache: 09.02.2009

Berlin 2009

D83

Acknowledgement

This dissertation was written during my employment time as a research associate at the Chair of Water Resources Management and Modeling of Hydrosystems (WAHYD), Institute of Civil Engineering, Technische Universität Berlin in Germany.
A significant part of the work presented here was supported by a scholarship program NaFöG initiated by the Land Berlin which is gratefully acknowledged and I feel very honored for the support. The presented work was partially conducted within the framework of the project "Coupling of Flow and Deformation Processes for Modeling the Movement of Natural Slopes", financed by the German Research Foundation (DFG).

First of all, I would like to express my deep gratitude to my supervisor, Prof. Reinhard Hinkelmann, Head of the Chair of Water Resources Management and Modeling of Hydrosystems, Institute of Civil Engineering, Technische Universität Berlin for his long time proper guidances and valuable suggestions which make this thesis successful.
Next, I would like to express my sincere thanks to Prof. Erwin Zehe, Institute of Water and Environment, Technische Universität München for his useful suggestions and for his support as the second supervisor.

Gratitude goes to my colleagues from WAHYD for making my time at the institute not only pleasant but also a learning experience. A very special thanks to Leopold Stadler and Mirko Schanka, who have spent the time for the useful suggestions and correction of my thesis. Thanks to Tobias Busse, my office room-mate, who always make the warm and frendly atmosphere in the office. Thanks goes of course to Ms. Mata Krishna for her helping and advices during my work, Ms. Christl Mohamed for correcting me German languge through her pronunciation. Thanks to Ralf Duda - Computer's Doctor who has always been ready when my computers have troubles.

I also would like to thank to my friends in our badminton club (SV Berliner Brauereien e.V.) who help me to reduced stress through very interesting matches and training camps: Thanh Trung, Le Hung and my trainer Lutz Friedrich.

Many from my family have encouraged me all the way long. I want to express my special gratitude to my parents, my aunts, my sisters, my girlfriend and my big family in Vietnam for all their love, constant support and encouragement during the long time I have been away.

Berlin, November 2008

Pham Van Song

Abstract

This dissertation focuses on the modeling of two-phase flow processes including the water and gas phase in porous media with fault zones which consist of fractures or macropores. The aim of the thesis is to make applications and comparisons of different model concepts in order to improve the process understanding and to reveal possibilities and limitations of the different approaches as well as to provide knowledge related to the potential for investigations of two-phase flow modeling in porous media with fault zones. Here, three different model concepts were investigated: *2D fracture model concept*, *1D fracture model concept* and *fracture with pipe model concept*.

Generally, the choice of model concept is strongly depending on the characteristics of the problems being considered, for example, the scales of the problem. The modeling of two-phase flow processes in porous media with fault zones has been applied to domains with different scales (small scale (< 1m), laboratory scale (1-10m) and small field scale (10-100m)).

The first application is carried out in a small scale domain. Water infiltration processes in a single vertical fracture are analyzed. The numerical simulation results show an overall very good agreement between two model concepts: 2D fracture model concept and 1D fracture model concept. The pipe model concept is not suitable in this case.

The second application is carried in a laboratory scale domain. Seepage processes through a dike are investigated for systems with one horizontal fault zone on different locations ont the land or sea side. To check the model concepts, experiments from the laboratory were compared to the numerical simulations. The 2D fracture model concept and 1D fracture model concept are suitable for numerical model in this case, as a good agreement between the experimental and numerical results was obtained. However, the results show an over-estimation of the seepage processes for the pipe model concept. Therefore, this model concept is not further recommended.

The last application is carried out in a small field scale domain. A slope which is idealized from a natural hillslope in Vorarlberg Alps is chosen as a case study for the simulation. The results show considerable influences of the preferential flow in macropores on the water infiltration processes in the slope. Due to the property of macropores, the infil-

tration is strongly speeded up. However, the maximum water pressure in the system is somewhat smaller due to the macropores. The fast pressure increase in lower parts of a layered hillslope is one main factor influencing the slope stability. The numerical results are in principal agreement with observations in the field. For investigation the influences of small-scale heterogeneities, geostatistical methods are used to generate permeability fields. Comparative studies have been carried out and analyzed for cases with different parameters like correlation lengths, variances, and anisotropies. The simulation results illustrate a more or less strong influence of small-scale heterogeneities on the saturation and pressure fields of the slope.

Kurzfassung

Diese Arbeit konzentriert sich auf die Modellierung von Zweiphasenströmungen der Phasen Wasser und Gas in porösen Medien mit Störungszonen, wobei Klüfte und Makroporen berücksichtigt werden. Die Zielstellung der Arbeit besteht aus der Anwendung und dem Vergleich unterschiedlicher Modellkonzepte, um auf der einen Seite das Prozessverständnis zu verbessern und um auf der anderen Seite die Möglichkeiten und Grenzen der verwendeten Modellkonzepte sowie das Potential von Zweiphasenströmungssimulationen in porösen Medien mit Störungszonen aufzuzeigen. Es werden hier drei unterschiedliche Modellkonzepte untersucht: *2D-Kluft-Modellkonzept*, *1D-Kluft-Modellkonzept* und *Kluft mit Rohrströmungsmodellkonzept*.
Im Allgemeinen hängt die Wahl des Modellkonzepts stark von den Eigenschaften des Systems und der Problemstellung ab, beispielsweise von den zu berücksichtigenden Skalenbandbreiten. Daher wurden Untersuchungen auf unterschiedlichen Skalen (kleine Skala ($<$ 1m), Laborskala (1-10m) und kleine Feldskala (10-100m)) durchgeführt.
Im ersten Anwendungsbeispiel werden Wasserinfiltrationsprozesse in einer vertikalen Kluft auf einer kleinen Skala analysiert. Die numerischen Simulationen zeigen eine sehr gute übereinstimmung zwischen dem 2D- und dem 1D-Kluft-Modellkonzept. Das Rohrströmungsmodellkonzept ist in diesem Fall nicht geeignet.
Das zweite Anwendungsbeispiel befasst sich mit der Durchsickerung von Deichen auf der Laborskala, wobei eine horizontale Störungszone jeweils an verschiedenen Stellen land- und seeseits angeordnet wurde. Die numerischen Untersuchungen wurden mit Laborexperimenten verglichen. In diesen Untersuchungen konnten gute übereinstimmungen zwischen den numerischen Berechnungen mit dem 2D- und 1DKluft- Modellkonzept sowie mit den Experimenten erzielt werden. Das Rohrströmungsmodellkonzept führt zu einer überschätzung der Durchsickerung, so dass dieses Modellkonzept nicht weiter empfohlen wird.
Im letzten Anwendungsbeispiel wird ein idealisierter Ausschnitt eines natürlichen Hanges aus den Vorarlberger Alpen auf der kleinen Feldskala betrachtet. Die Ergebnisse belegen den großen Einfluss der preferentiellen Strömungen in Makroporen auf die Wasserinfiltration am Hang. Aufgrund der Makroporen wird die Infiltration stark beschleunigt, je-

doch ist der maximale Wasserdruck im System etwas kleiner. Der schnelle Anstieg des Wasserdrucks in den unteren Bereichen geschichteter Hänge hat einen maßgeblichen Einfluss auf die Stabilität solcher Hänge. Die numerischen Ergebnisse sind in prinzipieller übereinstimmung mit Beobachtungen aus dem Feld. Auswirkungen von kleinskaligen Heterogenitäten auf die Simulationsergebnisse werden mit geostatistisch generierten Permeabilitätsfeldern abgeschätzt. Vergleichende Studien zu unterschiedlichen Korrelationen, Varianzen und Anisotropien zeigen teilweise große und teilweise kaum Einflüsse der kleinskaligen Heterogenitäten auf die Sättigungs- und Druckverteilungen im Hang auf.

Contents

List of Figures

List of Tables

Nomenclature

terms with Latin letters

symbol	dimension	definition
a		range
an		anisotropic ratio
b	$[m]$	constant aperture
cl	$[m]$	correlation length
g	$[m/s^2]$	gravity
$\underline{g}$	$[m/s^2]$	gravity vector $(0, 0, -g)^T$
g		gas phase
h	$[m]$	piezometric head
h	$[m]$	water level
h		variance
n, m	$[-]$	*Van Genuchten* (VG) parameter
m		population mean
ne		nugget effect
p	$[Pa]$	pressure
p_c	$[Pa]$	capillary pressure
p_d	$[Pa]$	*Brooks-Corey* (BC) parameter, entry pressure
p_d^f	$[Pa]$	BC parameter, entry pressure in the fault zone
p_d^m	$[Pa]$	BC parameter, entry pressure in the matrix
p_g	$[Pa]$	pressure of gas phase
p_g^w	$[Pa]$	partial pressure of water vapor in the gas phase
q_c	$[kg/(m^3 s)]$	sink or source of concentration
q_w	$[kg/(m^3 s)]$	sink or source of water
q_n	$[kg/(m^3 s)]$	flux of non-wetting phase
q_w	$[kg/(m^3 s)]$	flux of wetting phase
t	$[s]$	time

v	$[m/s]$	flow velocity
$\underline{v}_f$	$[m/s]$	filter or *Darcy* velocity
z	$[m]$	vertical space coordinate
B_i	$[m^3]$	control volume
C		Sill
C		variance
$Cov(h)$		Covariance function
E		expected value
$\underline{\underline{K}}$	$[m^2]$	permeability tensor
$\underline{\underline{K}}_\alpha$	$[m^2]$	effective permeability tensor
$N(h)$		number of pairs of the locations separated by h
K_f	$[m/s]$	hydraulic conductivity
K_m	$[m^2]$	arithmetric average permeability
K^f	$[m^2]$	permeability of the fault zone
K^m	$[m^2]$	permeability of the matrix
P		probability of occurrence
Re	$[-]$	*Reynolds* number
R_g	$[J/(mol\,K)]$	universal gas constant, $(R = 8.31451)$
S	$[-]$	saturation
S_α	$[-]$	saturation of phase α
S_e	$[-]$	effective saturation
S_n	$[-]$	non-wetting phase saturation
S_{gr}	$[-]$	residual gas saturation
S_w	$[-]$	wetting phase saturation
S_{wr}	$[-]$	residual water saturation
T	$[\,^\circ C, K]$	temperature
Z	$[Nm/(kg\ K)]$	real gas coefficient
Z		random variable
W	$[-]$	weighting function

terms with Greek letters

symbol	**dimension**	**definition**
α		phase
α	$[-]$	upwind parameter

α	$[1/Pa]$	*Van Genuchten* (VG) parameter
λ	$[-]$	*Brooks-Corey* (BC) parameter
λ^f	$[-]$	*Brooks-Corey* (BC) parameter of the fault zone
λ^m	$[-]$	*Brooks-Corey* (BC) parameter of the matrix
λ	$[-]$	mobility
λ_α	$[-]$	mobility of phase α
μ	$[kg/(ms)]$	dynamic viscosity
ν	$[m^2/s]$	kinematic viscosity, $\nu = \mu/\varrho$
ρ	$[kg/m^3]$	density
ρ_a	$[kg/m^3]$	density of air
ρ_w	$[kg/m^3]$	density of water
ϕ	$[-]$	porosity
ϕ^f	$[-]$	porosity of the fault zone
σ	$[N/m]$	surface tension
θ	$[^\circ]$	contact angle
Θ	$[m^3.m^{-3}]$	volumetric soil water content
Γ		boundary of domain Ω
$\gamma(h)$		variogram function
Δt	$[s]$	time step
$\Delta x, \Delta y$	$[m]$	element length
Ω		solution domain

abbreviations

symbol	**definition**
1D	one-dimensional
2D	two-dimensional
3D	three-dimensional
ART	Almost Regular Triangulation
BC	*Brooks-Corey*
bc	boundary condition
FE	Finite Element
FR	Fractured Rock
FPR	Fractured Porous Medium
BiCGSTAB	Biconjugate Gradient Stabilized

MIMD	Multiple Instruction Multiple Data
NAPL	Non-Aqueous Phase Liquid
PPM	Portable Pixmap
REV	representative elementary volume
UG	Unstructured Grid
VG	*Van Genuchten*
VTK	Visualization ToolKit

Chapter 1

Introduction

1.1 Motivation

Multiphase models for the simulation of processes in the subsurface are widely used in different fields of technical applications. Characteristic for such models is that they consider flow of more than one fluid phase (e.g. water, gas, oil, alcohol). One major difficulty in numerical simulation of multiphase flow in subsurface arises from the strongly heterogeneous and anisotropic nature of soils. The typical heterogeneous porous media are often porous media with fault zones including fractured porous media and macroporous media. The description of multiphase flow in porous media with fault zones becomes a challenging problem, because of the multiple scales involved and because of the non-linearity of the governing equations.
Multiphase flows in heterogeneous porous media or porous media with fault zones are described by the generalized Darcy law for the multi-fluid, coupled by a global continuity equation, and supplemented with constitutive equations for the relative permeabilities and capillary pressures being function of the saturations. The system of equations is generally non-linear. With the presence of heterogeneties (e.g fault zones (fractures or macropores)), the difficulty of the simulation stems from this non-linearity, from the sharp contrast of the matrix and fault zone properties and from the random character of the medium geometry (HELMIG (1993 [38]), BOGDANOV et al. (2003 [14]), EWING (2003 [32])).
Figure 1.1 shows a schematic cut-out of the hydrosystem subsurface where the flow and transport processes are actived. The upper part of this subsurface system corresponds to the unsaturated zone, where air and water fill the void space between the soil particles. This area is mainly considered in this study.

Popular multiphase problems occurring in nature are two-phase flows such as water-gas flow that can be activated in fractured porous media like in coal mines, CO_2 storage

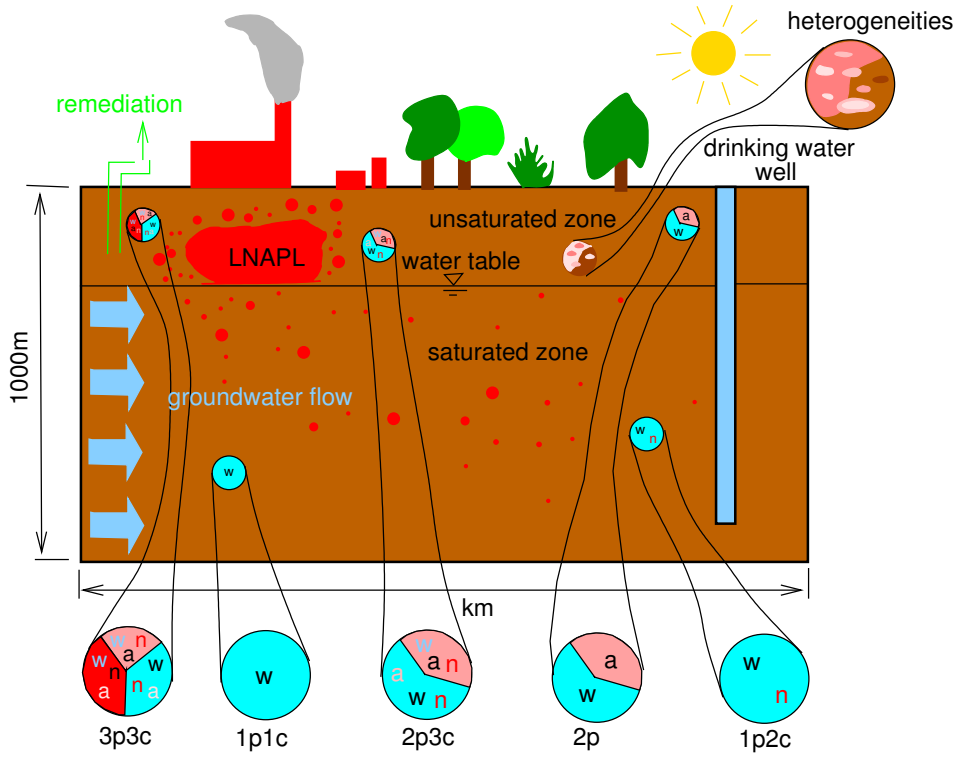

Figure 1.1: Processes in the hydrosystem subsurface (NIESSNER and HELMIG (2006 [61]))

in the subsurface and seepage processes through dikes or water infiltration processes in hillslopes.

- In coal mining areas, methane is degasing out of coal and migrating through the saturated and the unsaturated zone of the subsurface to the surface of the earth. At several locations, the methane fluxes are so high that they cause danger for human life as well as restrictions for the use of buildings. A two-phase (water, methane) flow model has to be chosen for simulating these problems (BREITING et al. (2000 [19]), HINKELMANN et al. (2002 [44])).

- In coastal areas, most of the dikes which serve as flood defense structures are made of layered material, especially soils. As a consequence of increasing height and frequency of storm surge levels, the probability of overtopping dikes increases, too. Overtopping evokes complex gas-water flow processes inside the flood defense structure, enhances the stress, and thus has a significant influence on the stability of such systems. The existing fault zones in dikes such as macropores, void spaces or inhomogeneities caused by animals, roots of dead plants or construction measures

can increase the failure mechanisms of the dikes. The water infiltration processes in the dikes can be investigated by numerical simulation. The two-phase (water and gas) flow model concept for fractured porous media has been applied for such problems (PAUL et al. (1999 [66]), HINKELMANN (2005 [42]), PHAM VAN et al. (2008 [75])).

- Landslides are one of the most dangerous natural hazards in mountainous regions that have a severe impact on the welfare of societies. A landslide is the sliding movement of masses of loosened rock and soil down a hillside or slope. In some moutain areas, the hillslopes consist of a large number of macropores. Then, the soil is a kind of fractured porous media. Due to the extreme rainfall situations, e.g. heavy rainfall or long periods of rainfall, the water is transported very fast via runoff and macropores into the subsurface. Many researches show that infiltration and the preferential flow through the macropores in unsaturated zone are the major factors influencing stability in shallow slopes (e.g. BOOGARD (2001 [13]), RAHARDJO et al. (2005 [81]), LINDENMAIER et al. (2005 [55])). The two-phase flow model including gas and water phases is being suitable for numerical simulation of the occurring processes (HINKELMANN and ZEHE (2007 [45]), STADLER et al. (2008 [93])).

- Carbon dioxide (CO_2) is a greenhouse gas, whose release into the atmosphere from combustion of fossil fuels contributes to global warming. During the past few years, focus has been made on new solutions that could prevent this by reducing the world wide CO_2 emissions. One of the good solutions is capturing and storing CO_2 from stationary point sources and pipe it into a geological formation where it is accumulated for long-term safe-keeping. These processes are called CO_2 sequestration. To simulate these processes, the two-phase model including water and CO_2 can be applied for the heterogeneous system.

In a number of cases, the dissolution of components in the phases as well as mass transfer processes must be considered. For such problems multiphase multicomponent model concepts are required (see HINKELMANN (2005 [42]), EBIGBO et al. (2006 [31]), BIELINSKI (2007 [11]), CLASS et al. (2007 [23])).
These examples represent only small part of wide field of multiphase flow processes. In this research, the progress in two relatively new application fields of flow in porous media with fault zones is chosen for simulation: seepage processes through dikes with fault zones and water infiltration in natural slopes with macropores. These two application fields are presented in detail in chapter 5 and chapter 6.

1.2 State of the Art

Flow in Unsaturated Zone without and with Fault Zones: Many models of varying degree of complexity and dimensionality have been developed during the past several decades to quantify the basic physical and chemical processes affecting water flow and pollutant transport in the subsurface. From that, several models can be distinguished. The physically-based hydrological model (e.g CATFLOW, SWAT) is based on the understanding of the physics of the hydrological processes which control catchment response and mainly use conceptual model to describe these processes. In this model, the domain is divided into spatially fixed subdomains: surface, unsaturated zone and groundwater where the boundaries, for example between the unsaturated zone and groundwater cannot move. The groundwater flow equation is applied to model the flow process in fully saturated subsurface in some models (e.g FEFLOW, MODFLOW). In the problems (e.g coastal zones), the groundwater table fluctuations are important. The moving boundary for variable groundwater table is applied in the models and an iterative approach is needed for the determination of the free groundwater surface. Often, the model concepts for flow in the unsaturated zone - also called vadose zone - are based on the Richards equation (RICHARDS (1931 [85])) and it is the standard method in soil science:

$$\frac{\partial \Theta(h)}{\partial t} - \nabla \cdot (K_f(h) \nabla (h + z)) = Q_0 \tag{1.1}$$

where h is the unknown pressure head, Θ is the volumetric soil water content, K_f is the soil hydraulic conductivity, z is the vertical space coordinate, t is the time and Q_0 is the source/sink term.
Combined with some parameterizations for the material properties, specifically for the soil water characteristic and for the hydraulic conductivity (e.g. BROOKS-COREY (1964 [21]), VAN GENUCHTEN (1980 [35]), BURDINE (1953 [24]), MUALEM (1976 [60]) it is possible to solve the system of equations numerically. This approach makes the assumption that the air phase essentially remains at a constant pressure, equal to atmospheric; the system is then reduced to the consideration of the water phase only. The approach has been shown to be a good approximation for most applications in soil sciences, however, problems occured in some situations where air phase can significantly retard the movement of the water phase.

In the following part, several numerical codes for modeling of flow in vadose zone and multiphase/multicomponent flow in subsurface systems which are widely used in the 'water world' are introduced.

The physically-based hydrological model CATFLOW was developed and expanded in the hydrology section at the Universität Karlsruhe (TH) (MAURER (1997 [57]), ZEHE (1999 [109]) and ZEHE et al. (2001 [110]))). The model permits the consideration of the interaction between all relevant hydrological processes based on field observations. These are: evapotranspiration, interception, inltration in micro- and macropores and two-dimensional soil water movement (saturated/unsaturated) as well as surface runoff and channel flow (including runoff from sealed surfaces). In the unsaturated zone, the water and soil dynamics in the soil matrix are modeled my means of 2-D Richards equation. By using a simplified approach, the flow in macropores is taken into account in CATFLOW model.

FEFLOW (Finite Element subsurface FLOW system) is is one of the most sophisticated software packages available for the modeling of flow and transport processes in porous media under saturated and unsaturated conditions in both 2D and 3D. The software is is developed by DHI-WASY GmbH, the German branch of the DHI group. Dealing with problems in unsaturated zone, the program uses a finite element analysis to solve the Richards equation. Different parameter models (e.g., Van Genuchten, Brooks-Corey) can be invoked for unsaturated flow and transport problems. Primary variable switching is used for an efficient simulation of unsaturated flows. Dealing with fractures, discrete-fracture modeling approach is can be used in FEFLOW. The software incorporate fractures as discrete feature elements (lower dimensional elements) (see FEFLOW by DHI-WASY ([33])).

HYDRUS models and various modifications and extensions (e.g. SWMS-2D, HYDRUS-1D, HYDRUS-2D, HYDRUS (2D/3D)) were developed jointly by the U.S. Salinity Laboratory (USSL) and the University of California, Riverside (UCR) (SIMUNEK et al. (2008 [89])). These tools include numerical models for one- or multidimensional variably saturated flow and transport (e.g. HYDRUS-1D, HYDRUS-2D, and HYDRUS (2D/3D)), analytical models for solute transport in soils and groundwater (e.g., CXTFIT and STANMOD), and tools or databases for analyzing or predicting the unsaturated soil hydraulic properties (e.g., RETC, Rosetta, and UNSODA). These modeling tools cover a large number of processes, from relatively simple one-dimensional solute transport problems to multidimensional flow and transport applications to relatively complex problems involving a range of biogeochemical reactions. The HYDRUS2 model is a finite element model simulating water flow in two-dimensional variably saturated domains as described with the Richards equation. The fracture-matrix interactions are handled using a dual-continua approach, such as the double- or multiple-porosity, or dual-permeability.

Multiphase Flow Models for Porous Media without and with Fault Zones: When we consider more than one fluid, the multiphase flow models are applied. Here, if two or more fluids fill a volume (e.g. the pore volume) and are immiscible and separated by a sharp interface, each fluid is called a phase of the multiphase system. The first numerical simulators for the computation of multiphase flow in porous media were developed in the petroleum industry in the 1960s (BARENBLATT et al. (1960 [20]), WARREN and ROOT (1963 [101])). Since the 1980s numerical multiphase models are also applied to environmental problems, e.g. the simulation of groundwater remediation technologies in the saturated as well as unsaturated zone.
BEAR et al. (1993 [10]) has extensively reviewed the research on fracture flow phenomena. DIDATO (1994 [30]) has reviewed many software packages, claimed to solve problem of the fluid flow in fractured porous media. In this part, some well-known numerical codes for multiphase flow in subsurface systems are introduced.

TOUGH2, the successor of TOUGH, is one of the best-known codes for the modeling of multiphase/ multicomponent systems (PRUESS (1991 [76]). It was developed at Lawrence Berkeley National Laboratory of the U.S. Department of Energy (DOE). TOUGH2 is a numerical simulator for non-isothermal flows of multicomponent, multiphase fluids in one, two, and three-dimensional porous and fractured porous media. The chief applications for which TOUGH2 is designed are in geothermal reservoir engineering, nuclear waste disposal, environmental assessment and remediation, and unsaturated and saturated zone hydrology. The numerical solution of multiphase flows in TOUGH2 employs space discretization by means of Integral Finite Difference Method (IFDM). The package TOUGH2 does not incorporate fractures as discrete elements. The fracture-matrix interactions are handled using a dual-continua approach, such as the double- or multiple-porosity, or dual-permeability (see section 2.4).

The computer model Subsurface Transport Over Multiple Phases (STOMP) was designed by Mark White of Pacific Northwest Laboratory in order to simulate the flow and transport of fluids in variably saturated soil (WHITE and OOSTROM (1996 [103])). The STOMP simulator has been designed to solve a wide variety of non-linear multiphase, flow and transport problems for variably saturated geologic media. The STOMP simulator solves the partial differential equations that describe the conservation of mass or enegry quantities by employing an integral finite difference method for the spatial discretization and a backward Euler scheme for the temporal discretization. The solver for the resulting non-linear coupled algebraic equations is based on Newton-Raphson

method. The simulator has been written with a variable source code that allows the user to choose the solved governing equations (e.g., water mass, air mass, dissolved-oil mass, oil mass, salt mass, thermal energy). Depending on the chosen operational mode, the governing transport equations will be written over one to four phases (e.g., aqueous phase, gas phase, (non-aqueous phase liquid) NAPL phase, ice phase, solid phase).

Finite Element Heat and Mass Transfer Code (FEHM) was developed by Hydrology, Geochemistry and Geology Group, Los Alamos National Laboratory, USA (ZYVOLOSKI et al. (1999 [112])). FEHM is a numerical simulation code for subsurface transport processes. It simulate 2D, 2D radial, or 3D geometries, time-dependent, multiphase, multicomponent, non-isothermal, reactive flow through porous media and fractured porous media. FEHM has been used for simulation of hydrothermal oil, and natural-gas reservoirs, nuclear-waste isolation, and groundwater modeling. The equations of heat and mass transfer for multiphase flow in porous media are solved using the finite element method. To solve the non-linear coupled algebraic equations, the Newton-Raphson iterative procedure is used. Using either double-porosity/double-permeability or dual-porosity models, FEHM can simulate flow that is dominated in many areas by fracture and fault flow. Both TOUGH and FEHM are used for simulation of flow and transport in variably saturated fractured systems at Yucca Mountain, Nevada, the proposed high-level radioactive waste disposal site.

The software package ROCKFLOW (KOLDITZ et al. 1998 ([50])) was developed by the Institute of Fluid Mechanics and Computer Applications in Civil Engineering, University of Hannover, Gemany. ROCKFLOW can be used for numerical simulation of fractures, porous media, and fractured porous media. The program is based on the finite element method in a approach which can combine elements of different dimensions. As such, it is possible to simulate, for example, discrete fracture networks with 2D elements with arbitrary orientation in space embedded in a matrix of 3D elements. Recently, a Lagrangian scheme for transport in fracture networks was added. The simulator uses a dynamic hierarchical grid adaptation strategy (BARLAG (1997 [4])), which adapts the grid during runtime on the basis of multiple indicators. The simulator consists of multiple kernels for fully or partially saturated single-phase flow, multiphase flow and transport of one or more components.

The numerical simulator MUFTE-UG is developed at the Institute of Hydraulic Engineering, University of Stuttgart in cooperation with the Chair of Water Resources Management and Modeling of Hydrosystems, Technische Universität Berlin (part MUFTE

(Multi-Phase Flow, Transport and Energy Model)) and the Technical Simulation Group of the Interdisciplinary Center for Scientific Computing, University of Heidelberg (part UG (Unstructured Grids)) (HELMIG et al. (1998 [40]), BREITING et al. (2002 [18]) and HINKELMANN (2005 [42])).
The simulator provides several modules for the numerical simulation of isothermal and non-isothermal multiphase / multicomponent flow and transport processes in porous and fractured porous media. MUFTE-UG incorporates several different types of spatial discretization methods (e.g. BOX, CVFE method) and the non-linearities are handled with the Newton-Raphson Method, and the linearized equations are solved with the BiCGSTAB Method using Multigrid preconditioning. MUFTE-UG currently supports the following schemes: single-phase stationary, solute transport (implicit/explicit/characteristics), non-linear transport-reaction systems (implicit), two-phase (implicit, sequential and IMPES), two-phase in fractured porous media (implicit), two-phase/ three-component non-isothermal (implicit), three-phase/ three-component nonisothermal (implicit).
MUFTE-UG simulation is based on the discrete model concept for fractured porous media. From 2008 the double continuum model concept was developed for numerical simulation in the framework of project "Großshang" (HINKELMANN and ZEHE (2007 [45]), STADLER et al. (2008 [92]), MAYER (2008 [58])). The development processes are still underway.
As I introduced in above part, there are several numerical codes for modeling of flow in unsaturated zone. However, several deficits of the numerical simultion should be mentioned. Modeling of flow and transport in porous media with fault zones including fractured porous media and macroporous media, numerical problems can occur because of strong heterogeneities. With macroporous media which consist of many macropores inside, there is 'no' physically proven concept for simulating two-phase flow processes.

1.3 Goal and Structure

This thesis focusses on the modeling of two-phase (gas and water) flow in porous media. The porous media that we consider here are the porous media with fault zones including fractured porous media and macroporous media. Resulting from the motivation, the goals of the thesis can be summarised as following:

Normally, the choice of model concepts for description of flow processes in porous media with fault zones is strongly depending on the characteristics of problems being considered, for example, the scale of the problem. Before applying the numerical simulation in the

field scale, the model concepts should be investigated in different scales from small scale to large scale. Here, three scales are used for simulation: *small scale, laboratory scale and medium/small field scale.*
The overall objective of this work is to make an application and comparison of different model concepts for the simulation of two-phase flow processes in porous media with fault zones. The numerical simulation considers different applications from small scales to large scales. Comparative studies using the results from different model concepts for accounting for the fault zones are carried out in order to reveal possibilities and limitations of the different approaches and provide knowledge related to the potential for investigation of two-phase flow in heterogeneous structures. In oder to check the numerical model, laboratory experiments have been used for comparisons. Through all these comparisons, the process understanding is improved.
Modeling of flow and transport in porous media is always associated with uncertainties coming from small-scale heterogeneities. The distribution of small-scale heterogeneities can have a high impact on all flow and transport processes. In the thesis the influences of small-scale heterogeneities are investigated by using geostatistical methods.

This dissertation is organized in seven chapters. It is structured as follows:

- Chapter 1 gives the introduction and the state of the art of flow models in the unsaturated zone. Chapter 2 describes model concepts for flow in fault zones. Before presenting different model concepts for flow in fractured porous media and macroporous media, the flow process in a single fracture based on two parallel plates model is explained in this chapter.

- In chapter 3, firstly, the physical fundamentals used for the model are introduced. Then, the mathematical model of two-phase flow in porous media including governing equations, constitutive relationships, and several formulations is explained. Different model concepts for modeling fault zones (fractures, macropores) are introduced. Based on the governing equations, the numerical model concept is given. For the numerical model, an overview of the different numerical methods is presented and discretization techniques both in space and time are explained in detail, followed by the introduction of the modeling system MUFTE-UG. Additionally, the introduction to geostatistical methods with some theoretical variogram models is presented in this chapter and it can be applied for analysing the influences of the small-scale heterogeneities in subsurface.

- Depending on the mathematical and numerical model which are presented in chapter 3, different model concepts are applied for numerical simulation. Chapter 4, 5 and

6 strongly focus on comparisons of model concepts for two-phase flow in fractured porous media. Different model concepts are applied for numerical simulation of two-phase flow processes in different scale domains (*small/academic scale)*, *laboratory scale* and *medium/small field scale*). Based on these investigations, the suitable model concept can be chosen for the large field scale.

In chapter 4, a *small scale (academic scale)* system with a single fracture is applied for the simulation.

- Chapter 5 focuses on *laboratory scale* problems. A dike with fault zones is introduced for investigation. The seepage through the dike is investigated in detail by both the numerical and experimental simulations.

- In chapter 6, the numerical simulation of two-phase flow processes is applied in a *medium scale (small field scale)* domain. A slope (Heumoes slope) which is idealised from a natural hillslope in the Vorarlberg Alps area is chosen as a case study domain for the simulation. The landslide problems which can occur in mountain areas are briefly introduced and discussed in this chapter. The influences of small-scale heterogeneities on the water infiltration processes in a slope are also investigated using a geostatistical method.

- Chapter 7 concludes with a summary of this work and suggestions for future research.

Chapter 2

Model Concepts for Porous Media with Fault Zones

2.1 Basic Definitions

The understanding and prediction of fluid flow in porous media and fractured porous media are of great importance in various areas of research and industry. Table 2.1 lists the areas where flow in porous media plays an important role. Petroleum engineers and hydrogeologists need to model mulphiphase flow for production of hydrocabons from petroleum reservoirs. Hydrologists and soil scientists are concerned with underground water flow in connection with applications to civil, environmental and argiculture engineering. In other disciplines, for example, fuel cells or solar cells are investigated.
In hydrogeology the term "fracture" is defined as planar stress features, which can be found in stiff soil, e.g. clay deposits, and in most near surface rock units. It has a special configuration: one of its dimensions - the aperture - is much smaller than the other two ones. The term fractured rock (FR) is used when the blocks of rock surrounded by fractures contain no void space. We shall employ the term fractured porous medium (FPR), or fractured porous rock, when the blocks are porous. Thus, in a FPR, the void space is composed of two parts: a network of fractures and blocks of porous media. Fractures are described by a variety of properties (e.g. fracture width, length, aperture and roughness). Figure 2.1 shows some parameters of the fractures which can be used in this thesis.

In soil science, the "fracture" term can be called by the name that related to the soil structure: "macropore". The term macropore simply refers to a large soil pore. Macropores are defined either by their size, their forming process (soil fauna, decay of plant roots, wetting and drying processes, freeze-thaw cycle, the erosive action of

Hydrology	Groundwater flow, flow in unsaturated soil, salt water intrusion into coastal aquifers, soil remediation
Geology	Petroleum reservoir engineering, geo-thermal energy, CO_2 sequestration
Agriculture	Irrigation, drainage, contaminant movement in soils, soilless cultures
Chemical engineering	Packed bed rectors, filtration, fuel cells, drying of granular materials
Mechanical engineering	Solar cell design, wicked heat pipes, heat exchangers, porous gas burners
Industrial materials	Rubber foam, glass fiber mats, concrete, brick manufacturing

Table 2.1: Areas where flow in porous media plays an important role (HOFFMANN (2003 [47]))

subsurface flow) or the dominant type of flow (laminar and turbulent) in macropores. They are found in many types of soils and are typically of organic origin, including worm holes, animal burrows, and root channels (see Figure 2.2).

The flow in fractures and macropores is commonly denoted preferential flow in natural porous media. It occurs predominantly in fine-textured soils or media with pronounced structure. In order to unify the names, the term “fault zone” in this study is understood a synonym for the terms “fracture” or “macropore”.

In summary, the porous media with fault zones including fractured porous media and soils with macropores represent a system that principally consists of properties:

- The fault zone system has a high permeability, a high porosity, a low total volume, and low storage capacity.
- The matrix (or soil matrix) has a low permeability, a low porosity, a high total volume, and a high storage capacity.

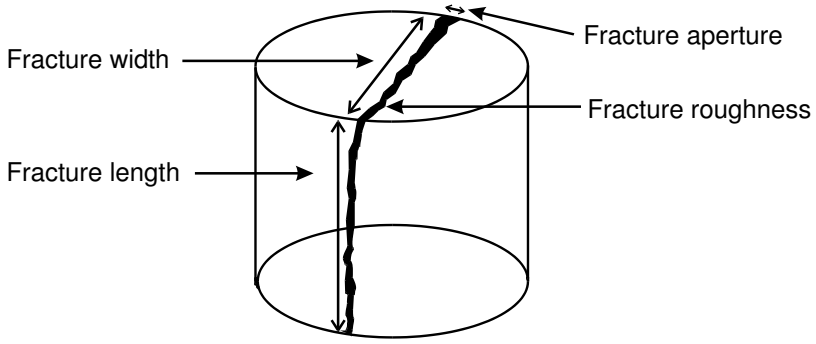

Figure 2.1: Definition of some fracture parameters (DIETRICH et al. (2005 [28]))

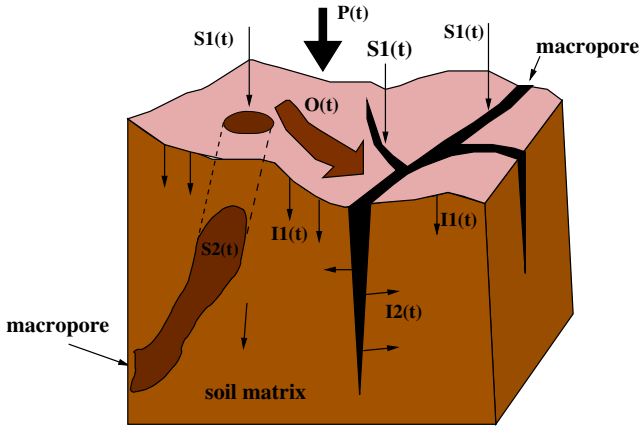

Figure 2.2: Definition diagram for water flows in a block of soil with macropores: P(t): Overall input (precipitation, irrigation); I1(t): Infiltration into the matrix from the surface; I2(t): Infiltration into the matrix from the walls of the macropores; S1(t): Seepage into macropores at the soil surface; S2(t): Flow within the macropores; O(t): Overland flow (BEVEN and GERMANN (1982 [12])

2.2 Fractures Determination

Naturally, a domain can have a large number of the fractures inside. Characterization of fractured systems is probably one of the most challenging problems that petroleum geologists as well as hydrogeologists have to face. In the continuum approach, fractures are considered to be sufficiently ubiquitous and distributed in such a manner that they can be meaningfully described statistically (BEAR (1993 [10])).
DIETRICH et al. (2005 [28]) have developed an anquifer-analogue approach in a research project to investigate the complex structure of natural fractured systems as well as

flow and transport processes inside (Figure 2.3). The approach is based on the so-called outcrop-analogue method, in which well defined samples from sandstone outcrops (quarries) are used as a realistic representation of those sections of the (aquifer) system where access is limited to (a few) boreholes.
In the above mentioned research, the complexity of natural fracture geometries is described using statistical distribution functions and/or geostatistical parameters. From the observations (borehole samplings, measurements on exposed rock surfaces), geometries of fractured aquifer systems have been characterised and transfered mostly from a smaller scale to the entire fractured aquifer. Hence, the assumption has been made that the statistical patterns analyzed from observations can, to some extent, represent the fracture geometries of the complete system. The geometries of fractures (e.g. orientation, aperture, size, density) are generally described with log-normal or the exponential distributions. Based on both the spatial characteristics of a fracture network and the statistical distribution of fracture geometries, the representative fracture network is created by a geostatistical fracture generator (see SILBERHORN-HEMINGGER (2002 [88])).

2.3 Flow in a Fault Zone

The flow in a single fault zone (i.e. single fracture or single macropore) is well introduced in many text books and article (e.g. HELMIG (1997 [39]), SPILLER (2004 [90]), BRUSH and THOMSON (2003 [16])). Most of the approaches depend on the geometry of the fault zone. An overview of the most important approaches is given in Figure 2.4. Fundamentally, single phase flow in single fracture is governed by Navier-Strokes equations which express momentum and mass conservation over the fracture void space. Generally, laminar flow of a Newtonian fluid with constant density and viscosity through a fracture is assumed. The idealized parallel plate model is a model which consists of two plane parallel plates, representing the fracture walls. The length scale l of the plates is much larger than the distance between them b ($l >> b$). Figure 2.5 visualises this concept and Figure 2.6 shows the two parallel plates and the parabola shaped velocity profile indicating laminar flow.
The Navier-Strokes equations may be written in vector form as:

$$\rho(\underline{u}\cdot\nabla)\underline{u} = \mu\nabla^2\underline{u} - \nabla p \tag{2.1}$$

$$\nabla\cdot\underline{u} = 0 \tag{2.2}$$

where ρ is the fluid density, μ is the fluid viscosity, $\underline{u} = (u_x, u_y, u_z)$ is the velocity vector, and $p(x, y, z)$ is the hydrodynamic pressure. In equation 2.1 $\rho(\underline{u}\cdot\nabla)\underline{u}$ denotes the inertial forces, $-\nabla p$ stands for the pressure forces, and $\mu\nabla^2\underline{u}$ represents the viscous forces.

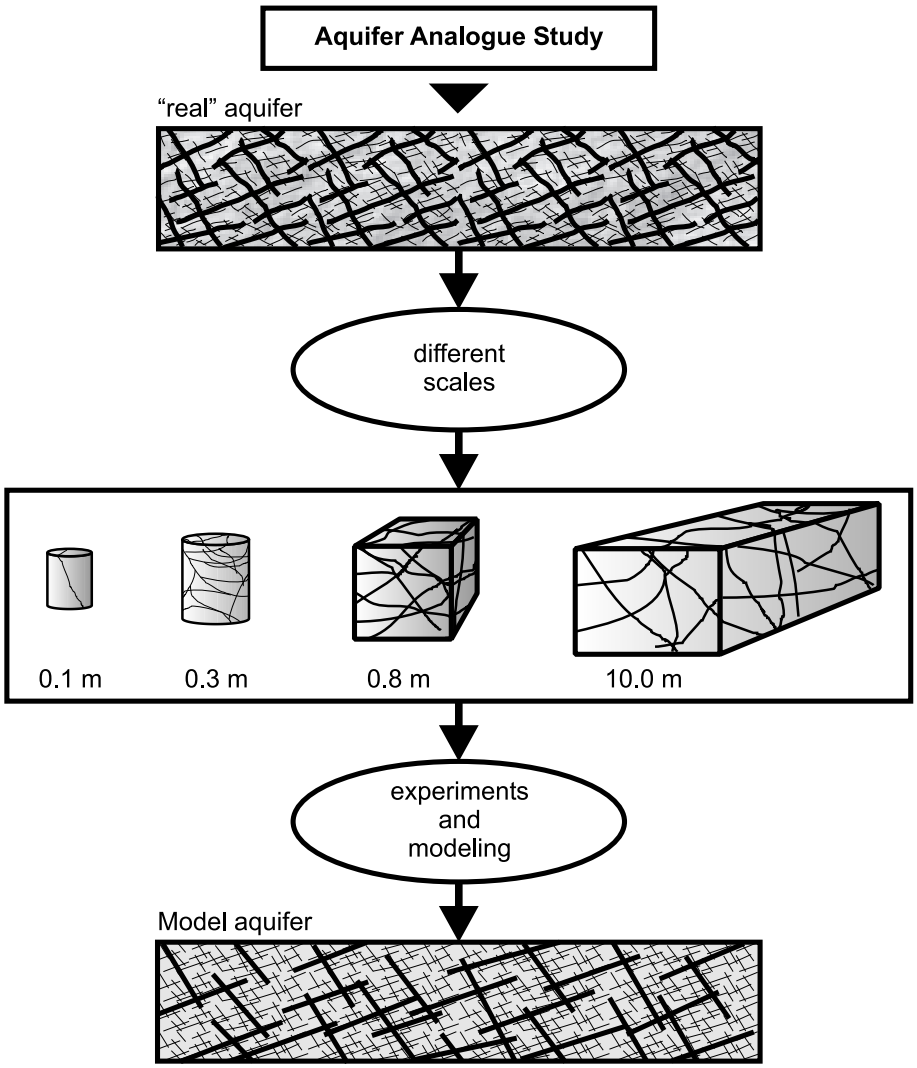

Figure 2.3: Aquifer-analogue approach (DIETRICH et al. (2005 [28]))

The Navier Stokes equations form a non-linear system of partial differential equations which are difficult to solve in irregular geometries and even in domains with simple geometry, such as a set of parallel plates and there are different methods for simplifications of the Navier Stokes equations presented by BRUSH and THOMPSON (2003 [16]).
The first level of simplification is to assume that the inertial forces in the flow field are negligible compared to the viscous and pressure forces. The Reynolds number is defined as:

$$Re = \frac{\text{inertial forces}}{\text{viscous forces}} = \frac{u_0 \cdot l_v}{\nu} \tag{2.3}$$

where ν denotes the kinematic viscosity, l_v is the characteristic length of the viscous forces and defined as mean fracture aperture, u_0 is the characteristic velocity for the inertial forces. The flow is in the validity of *Darcy's law* having the range of Reynolds

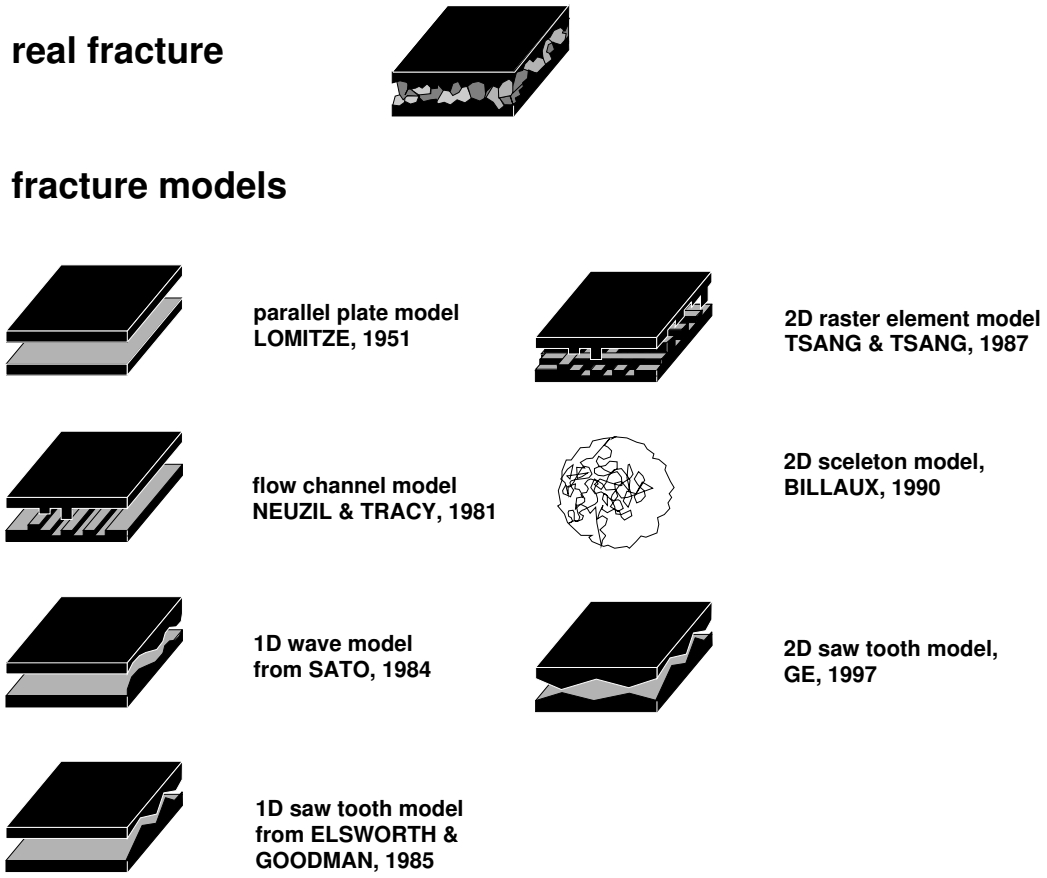

Figure 2.4: Overview on models for a single fracture (DIETRICH et al. (2005 [28]))

number is up to 1...10 (see Figure 2.7). For larger Reynolds numbers ($Re > 10$), the so-called *Forchheimer's law* with non-linear equation can be applied (FORCHHEIMER (1901 [36])).
In the case of small Reynolds numbers (Re = 1...10), equation 2.1 reduces to:

$$\mu \nabla^2 \underline{u} = \nabla p \tag{2.4}$$

Combining equation 2.4 with equation 2.2, we have a linear system of equations called

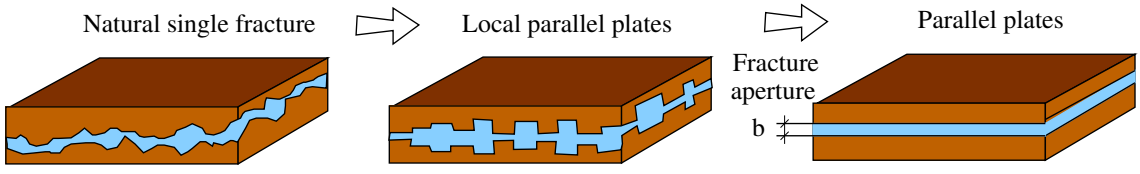

Figure 2.5: From the nature to the parallel plate concept (SILBERHORN-HEMINGGER (2002 [88]))

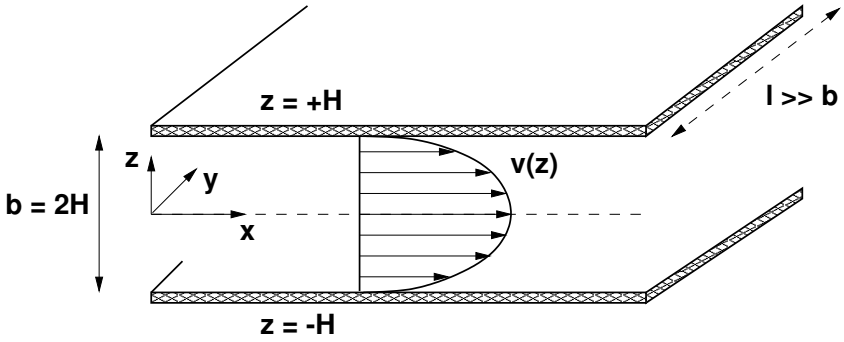

Figure 2.6: Laminar flow between two parallel plates: Parabola shaped velocity profile

the *Stokes* or *creeping flow equations.*
From a numerical point of view, the three-dimensional Stokes equations are also hard to solve. The *second simplification* is to approximate the three-dimensional flow field given by the Stokes equations with a two-dimensional description. Assuming that the variability in the fracture aperture is gradual. Then, the velocity normal to the fracture walls will be approximately zero ($u_n = 0$) and the viscous forces will be dominated by the shear forces acting normal to the fracture wall ($\nabla^2 \underline{u} = \partial^2 \underline{u}/\partial n^2$). Incorporating these velocity conditions into equation 2.3 and assuming that the fracture walls are approximately normal to the z-axis gives:

$$0 = \mu \frac{\partial^2 \underline{u}}{\partial z^2} - \nabla p \tag{2.5}$$

where $\underline{u} = (u_x,\ u_y,\ 0)$ is a two-dimensional velocity vector with a direction parallel to the x-y plane. Incorporating the no-slip condition ($u=0$) at the fracture walls, equations 2.5 and 2.4 may be integrated across the local aperture. With the help of the *Hagen-Poiseuille's law* of the flow in parallel plates, the average velocity in fault zone can be determined (SNOW (1969 [87]), TSANG and TSANG (1987 [94])):

$$\underline{u} = \frac{b^2}{12} \frac{\rho g}{\mu} \nabla h \tag{2.6}$$

$$\nabla \cdot (b \cdot \underline{u}) = 0 \tag{2.7}$$

where b is the fault zone aperture, ρ is the fluid density, g is the acceleration of gravity, μ is fluid viscosity, h is the average hydraulic head.
Inserting the equation 2.6 into 2.7 one obtains:

$$\nabla \left(\frac{b^3}{12} \frac{\rho g}{\mu} \nabla h \right) = 0 \tag{2.8}$$

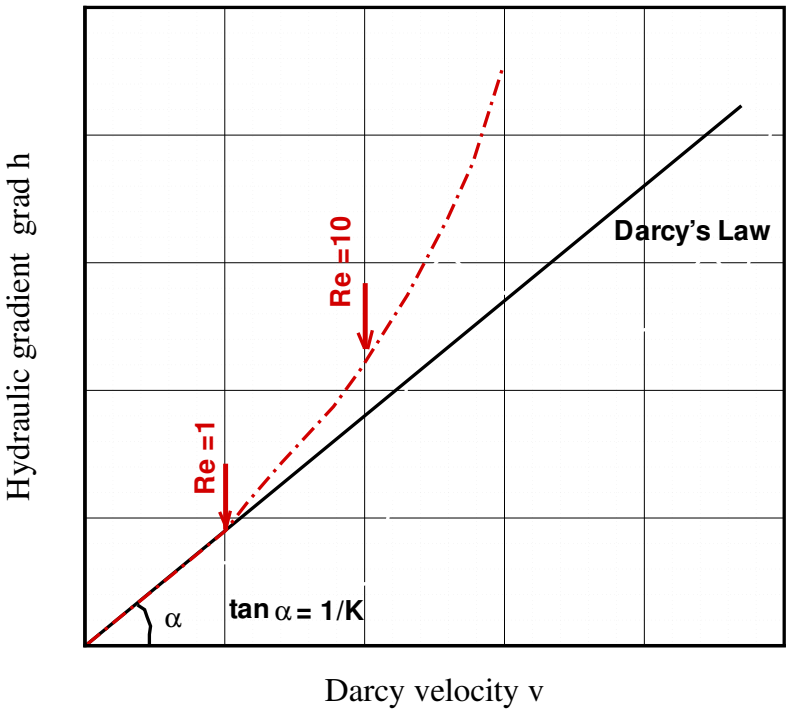

Figure 2.7: Deviation of Darcy's law (BEAR (1972 [9]))

This relation is commonly called *local cubic law* for fluid flow in a rough-walled fracture. With the validation of the Darcy law the permeability of the fault zone is chosen:

$$K = \frac{b^2}{12} \tag{2.9}$$

2.4 Model Concepts

Numerous researchers have developed model concepts describing fluid flow in porous media with fault zones, mainly for fractured porous media and a few for macropores porous media and several different model concepts have been proposed (e.g. HELMIG (1997 [39]), REICHENBEGRER (2004 [83]), HINKELMANN (2005 [42]), DIETRICH et al. (2005 [28])). Fundamentally, each method can be distinguished on the basis of the storage and flow capabilities of the porous medium and the fault zone. The storage characteristics are associated with porosity, and the flow characteristics are associated with permeability. The most common concepts which stem from the field of fractued porous media can generally be distinguished into the following categories: *discrete model concepts, equivalent model*

concepts and hybrid model concepts.
Discrete model concepts are subdivided into fracture-network approach and combined approach. For these model concepts, two different types of overlapping domains are introduced, the fracture network and the matrix.
In *fracture-network approach*, the matrix is assumed to be impermeable. The flow and transport processes are only activated in fracture network and the exchange of fluid and solutes between matrix and fracture network is neglected. However, some experimental and numreical investigations have shown that the matrix and fracture network interaction cannot be neglected for transport simulation (see KRÖHN (1991 [52]), HINKELMANN (2005 [42])).
When the *combined approach* is applied, the fracture network and the matrix are considered. The fractures are treated as a porous medium; generally with a much higher permeability and lower storage capacity compared to the matrix. They can be modeled as equidimensional elements, for example, two-dimensional fracture in a two-dimensional domain (which implies very high demands on net generation and the numerical tools for solving the resulting equation system). The fractures can also be discretized as elements of lower dimension (or mixed dimensional elements), for example, as one-dimensional fracture in two-dimensional domain or as one-dimensional fracture or two-dimensional fracture plain in a three-dimensional domain.
In *equivalent model concepts (or continuum model concepts)*, the domain is homogenized based on assumptions about the regularity of fractures. It is assumed that an REV cannot only be obtained for the porous medium but also for the fractured system. In these approaches, *single-continuum, double-continuum* and *multi-continua* approaches are distinguished (see Figure 2.11).
In the *single-continuum approach*, the whole fractured porous domain is represented as an equivalent porous medium. That means its properties are averaged and assumed to be constant over the REV.
In the *double-continuum models*, the fractured porous medium is represented as two distinct, overlapping and interacting continua, one consisting of the network of fractures and the other of the porous blocks. The interaction between both continua is formulated by an exchange function.
In some researches (e.g. PRUESS et al. (1985 [78]), ZIMMERMANN et al. (1999 [111]), MORTENSEN (2001 [1]), WU et al. (2004 [104])), the double-continuum models can be divided into the *double-porosity (or dual-porosity)* and *double-permeability* (or *dual-permeability*) models. If flow only occurs in the fractures, the model is known as double-porosity. Flow in the matrix is thus neglected and the matrix only contributes as an additional storage term. If flow occurs within the fracture and the matrix, the model is

known as a double-permeability model. Flow and transport are described using flow and transport equations for the separated domains of the fracture and the matrix, respectively. In a case where fractures of different scales are considered (e.g. small scale fissures and medium scale fractures), the double-continuum concept can be extended to include more than two continua; this is known as a *multi-continua model* (see Figure 2.8).

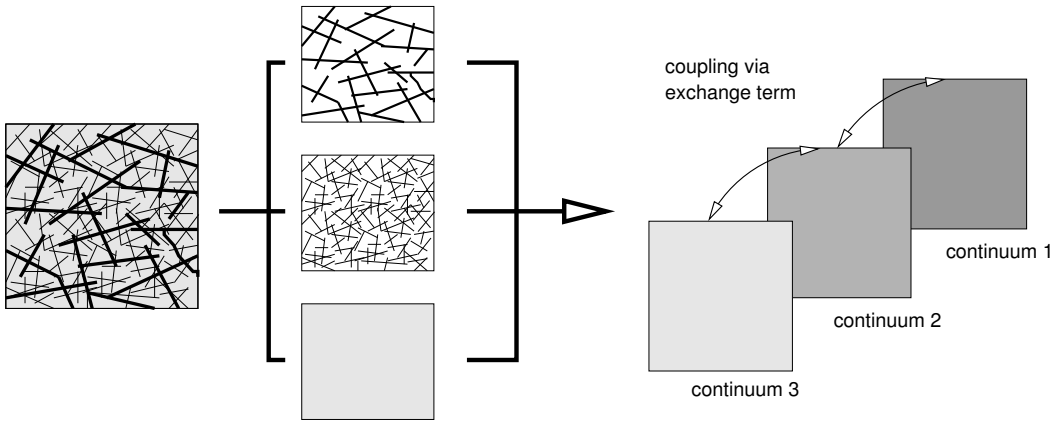

Figure 2.8: Proceduce for the multi-continua model (SILBERHORN-HEMINGGER (2002 [88]))

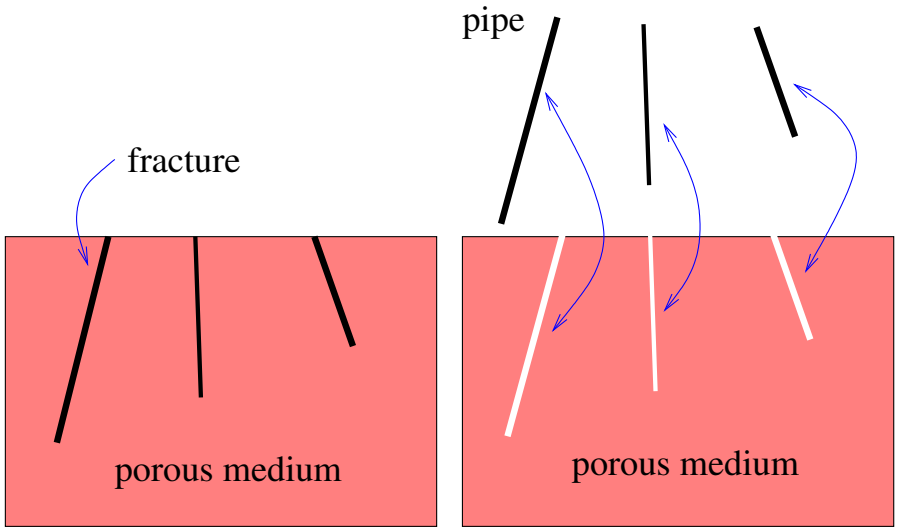

Figure 2.9: Combined model approach and coupling porous media with pipe flow

Additionally, the fractures can be excluded from the porous medium. The flow in the fractures can be modelled, for example, as pipe flow, which is coupled to the porous media flow along the common boundaries (see Figure 2.9). The exchange (leakage) parameters must be determined.

Hybrid model concepts (known as mixed discrete-continuum model concepts) have been proposed as a method that combines discrete model concepts with the continuum model concepts, for example, a discrete fracture-network approach is coupled with a single-continuum, double-continuum or multi-continua approach (see Figure 2.11). The equivalent continua are not located between the fractures but are coupled with the fracture network by sink and source terms.
In principle, most model concepts for single phase (water phase) flow in porous media are also applicable for two-phase flow in fractured media. However, due to very high pemeabilities in fractures and macropores, the physical process can hardly be described as posous medium flow and the numerical problems can occur in the simulation.

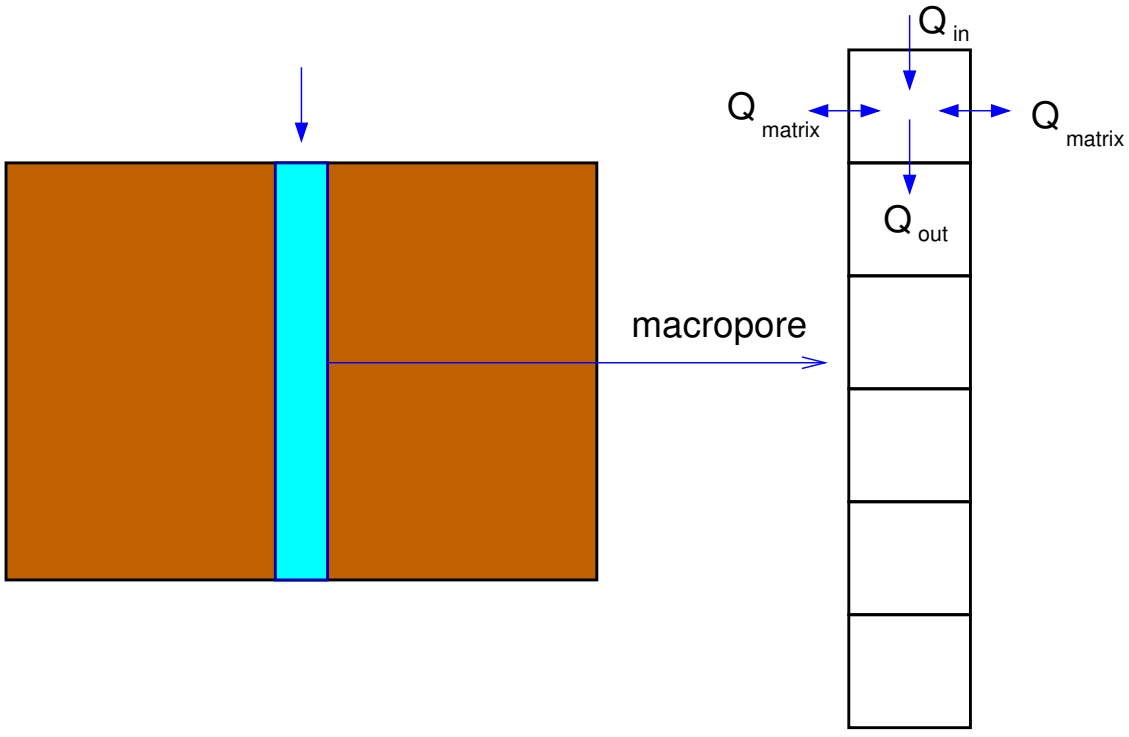

Figure 2.10: The idea of the CASCADE model concept (STADLER et al. (2008 [91]))

Dealing with macroporous soils, WEILER (2001 [102]) has developed a special model concept (*INfiltration-INitiation-INteraction Model* (IN^3M)) to model the infiltration into the soil with macropores. In this model, the macropore system is characterized by the macropore density and the average macropore radius. Only vertical flow is assumed in the macropores. The vertical infiltration in the soil matrix is calculated like the horizontal infiltration using the Green-Ampt approach.

In the framework of the reseach project "Großshang" (Natural Slopes), STADLER et al.

(2008 [91]) have developed a so-called *CASCADE model concept* and applied it for modeling the fluid flow in a single macropore and the exchange with the matrix. The numerical results have been compared to experimental results. Like for hydrological concepts, the idea of this model is to ensure the mass continuity in the macropore. The macropore is modelled as a cascade of volumes where water is shifted through and exchanged to the matrix driven by pressure gradients (see Figure 2.10).
The choice of model concepts for the description of flow processes in fractured media is strongly depending on the characteristics of problems being considered. Some factors that need to be taken into account include: the scale of the problem, the amount of data available, the fracture characteristics (e.g. connectivity, spacing, and aperture), the matrix characteristics (e.g. permeability and block size). In the researches of BEAR (1993 [10]), KRÖHN (1991 [52]) and DIETRICH et al. (2005 [28]), the choice of model concepts is denpending on the scale of the problem. For this point of view, the investitation domain can be classified into four different types:

- **The very near field:** Interest is focused on flow and transport processes within small-scale fractures and the pore space. Flow and transport processes are considered in a well-defined single fracture.

- **The near field:** The flow and transport processes are considered in a relatively small domain, which contains a small number of well-defined small and intermediate fractures. The geometries of the individual fractures are deterministically defined or they can be generated stochastically, based on statistical information from the real system.

- **The far field:** On this scale, the flow and transport processes are regarded as taking place, simultaneously, in at least two continua. One continuum is composed by the network of large scale fractures and the other one by the porous rock. Mass of the fluid phase and its components may be exchanged between the two continua.

- **The very far field:** The entire fractured medium is considered as one single continuum, possibly heterogeneous and anisotropic if geological layers and fault zones on a large scale are taken into account.

The choice of different model concepts which depends on the scale of the investigated problem is presented in Figure 2.12.

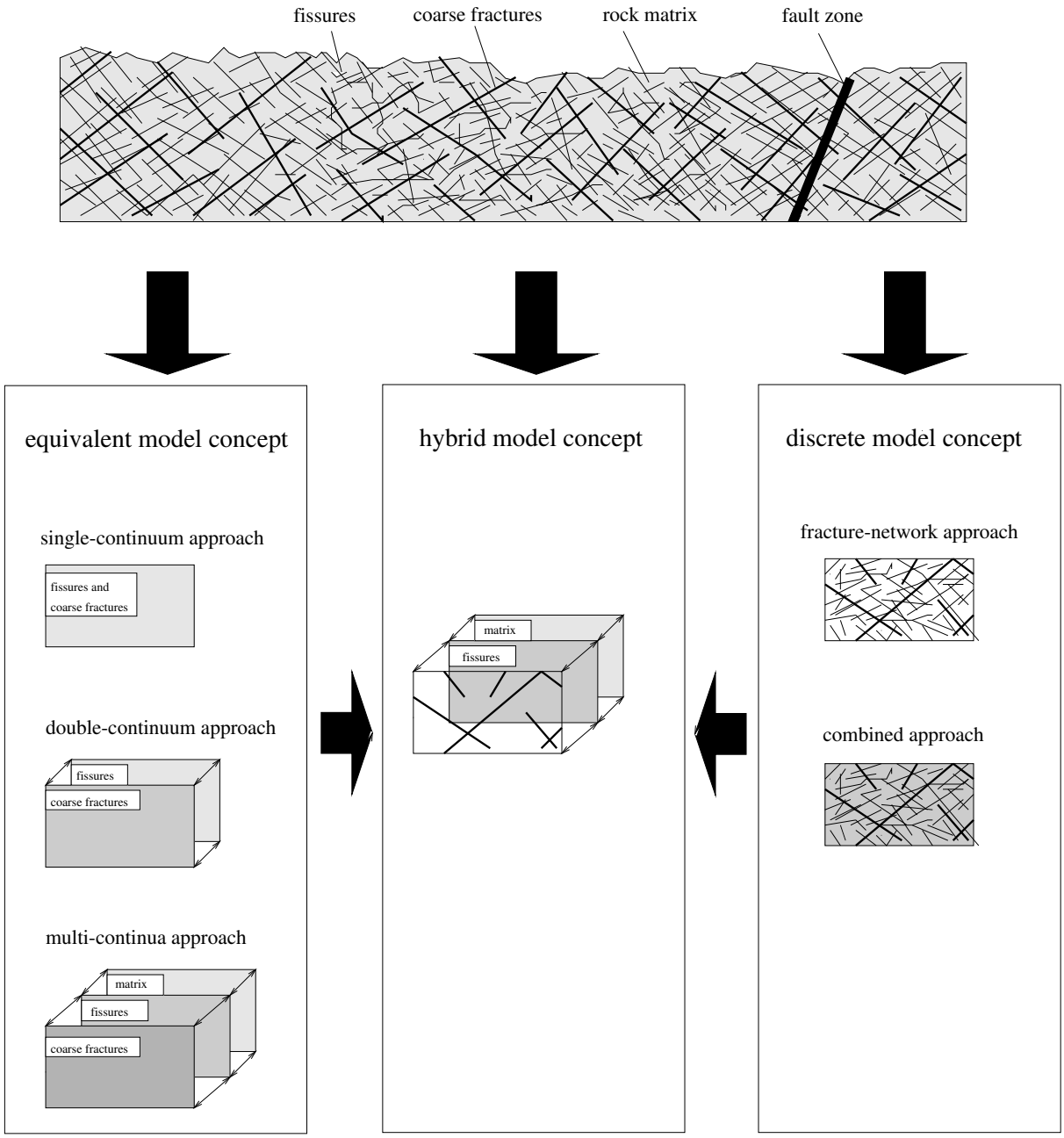

Figure 2.11: Model concepts for fractured-porous media (HINKELMANN (2005 [42])

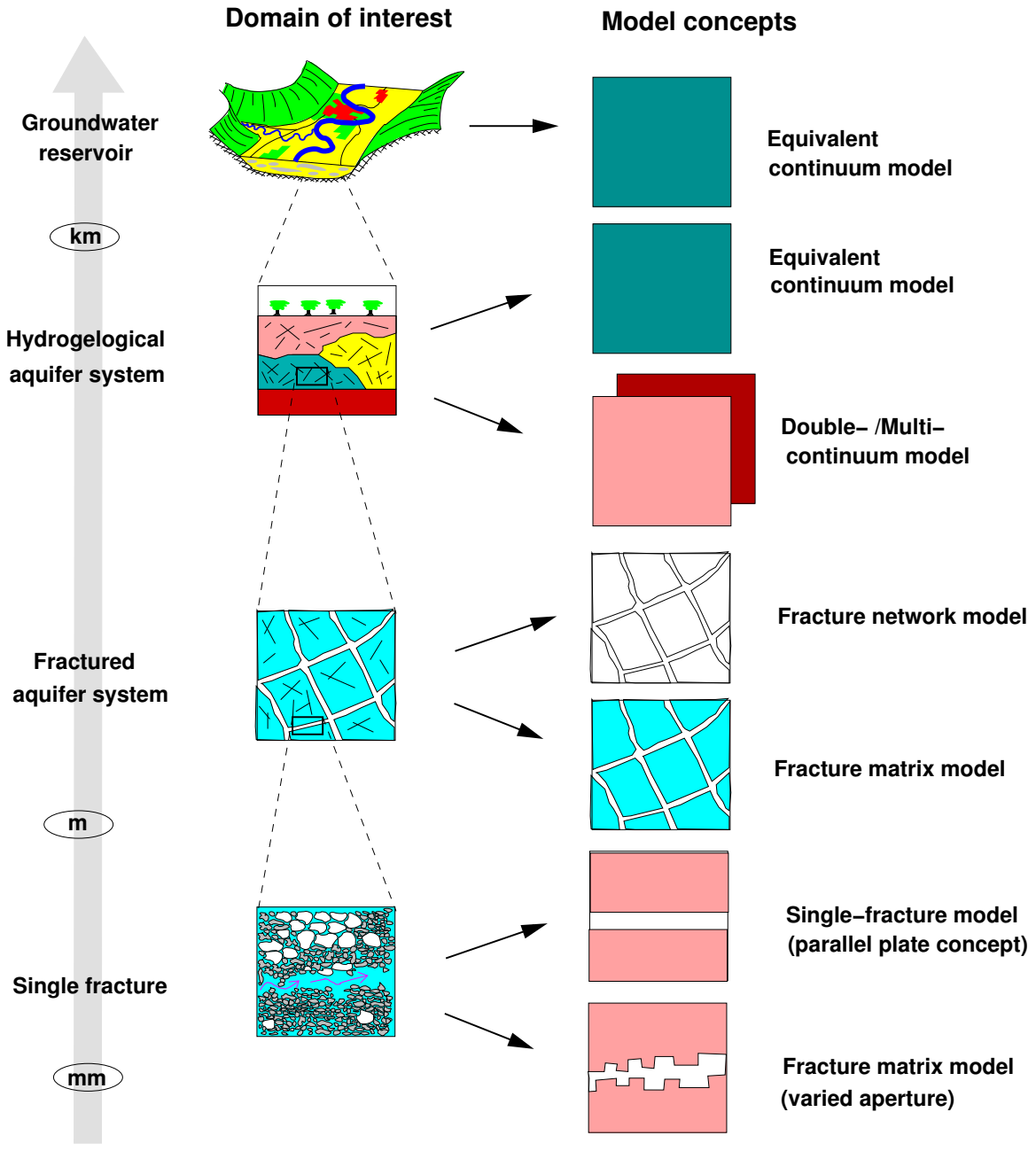

Figure 2.12: Relations between model concepts and scales of the investigated domain (KRÖHN (1991 [52]), DIETRICH et al. (2005 [28]))

Chapter 3

Two-Phase Flow Model

3.1 Fundamental Principles

3.1.1 Phase and Component

For the multiphase/multicomponent system, the terms "phase" and "component" are important terms. They are defined in many books and articles (e.g. HELMIG (1997 [39]), KOBAYASHI (2004 [48])).

- Phase
  An important point is that different types of phases are associated with different physical properties. A term phase is defined as a matter which has a homogeneous chemical composition and a physical state. Normally, three phases can be distinguished: a solid, a liquid, and a gas phase. However, speaking of phases in this work, it is only referred to fluid phases, i.e. a two-phase system represents a system with two fluids which are not soluble in one another and a solid matrix and the solid phase are not treated here.

  In the case of a *single-phase system*, the void space of the porous medium is filled by a single phase fluid (e.g. water) or by several fluids completely *miscible* with each other (e.g. fresh water and salt water). In a *multiphase system*, the void space is filled by two or more fluids which are *immiscible* with each other (e.g. water and gas, water and oil). In this thesis, a two-phase system represents a system with gas and water and a solid matrix.

- Component
  The term component stands for a constituent of a phase which can be associated with a unique chemical species. The number of the components in a system is the minimum number of independent chemical species necessary to define the compo-

sition of all the phases present in the system. A phase usually consists of several components considering the fact that in reality phases are never absolutely insoluble. A component can consist of a chemical element (e.g. hydrogen, nitrogen), as well as of a molecular substance (e.g. pure water, sodium chloride), or a mixture of different substances (e.g. alkalinity).

In this work, the two-phase flow including water and gas phase in soils is investigated and the components are not considered. Some simplifications are assumed as followings:

- In the two-phase system, the temperature change is negligible and thus iso-thermal conditions are assumed. The gas phase is considered to be compressible and the ideal gas law is assumed to be valid.
- Porous media are compressible. However, a pressure dependence of the porosity is supposed to be negligible, here.
- Effects of hysteresis are not considered, which means gravity is always in equilibrium with capillarity.

3.1.2 Issue of Scales

Two-phase flow in porous media involves several complex processes that are relevant to different spatial and temporal scales. A process that is dominant on one scale may become insignificant if the same system is considered on a different scale. Having a clear definition of scales and understanding their role is particularly crucial for the discussion of two-phase flow in porous media.
The length scale of interest in porous medium systems may vary from a molecular level on the order of 10^{-11} to $10^{-9}m$ to a mega level on the order of $10^{3}km$ (or even more) for some regional applications. Figure 3.3 graphically depicts the range of the spatial scales of concern in a typical porous media system. The following scales can be distinguished:

- molecular scale [$\sim pm$]
- continuum scale [$\sim\mu m$]
- micro-scale (pore scale) [$\sim mm$]
- local scale (REV scale) [$\sim m$]
- meso-scale [$\sim 10^{2}m$]
- field scale [$\sim km$]

On the *molecular scale*, single molecules are considered. These are decisive for fluid properties such as viscosity, density, and interfacial tensions. The Lattice-Boltzmann methods for small system can be applied. The numerical simulation of multiphase flow processes is not feasible on this scale.
By averaging over a large number of molecules, the *continuum scale* is reached (see Figure 3.1). The transition from the molecular to the continuum consideration also allows for the definition of continuum variables, such as pressure, temperature (see BEAR (1972 [9])). Based on this concept, pressure is an averaged effect that arises from forces exerted by a large number of molecules. Navier Stokes equations can be used for simulation of fluid flow on this scale.
The consideration of several pore spaces leads to the *micro-scale* or *pore scale*. On this scale, we consider a point within the considered phase or at the interface between phases. The microscopic consideration implies that discontinuities (i.e. micro-cracks), which are small compared to the pore or grain diameter or the fracture aperture, can still be clearly recognized.
When talking about the *local scale* or *REV scale* (range from cm to m), the micro-scale properties are averaged over a *representative elementary volume (REV)* that gives realistic information on the porous medium. On this scale, we describe the porous medium as a *continuous* medium (although the medium is discontinuous on smaller scales). This leads to new parameters like porosity or saturation with new equations. Figure 3.2 shows the search for a REV. As an example, a typical porous medium property is considered, the porosity. Porosity of a porous medium is defined as the ratio of the volume of the pores to the total volume of the considered medium. The pore geometry of a porous medium is not recognizable and therefore the description of flow can be realized only with averaged properties. If a very small averaging volume is chosen for the REV, the porosity fluctuates between zero and one depending on whether a pore or a grain is being considered. Enlarging this volume we will encounter oscillations starting from extreme values and stabilizing at a more or less constant value, until larger scale heterogeneities are included into the averaging volume. If the volume is increased to values that are too large, heterogeneities on the macroscale of the porous medium start to have an effect on the value of the averaged porosity.
On the *meso-scale* different macroscopic properties are assigned to sub-areas of the system. Macroscopic heterogeneities have to be considered on this scale. The porous media cannot be represented by a single REV as on the local scale. In Figure 3.2 this is represented by the fact that in volume L macroscopic heterogeneities result in a change in the porosity.
Field scale has a range from m to km. The structures of different geological periods are considered. These structures commonly involve several types of materials with different

properties. If one tries to characterize porous media for a volume at this scale ($[m]-[km]$), effective parameters may vary within it. In other words, the concept of the REV has also an upper boundary due to large-scale heterogeneities. The concept is however the same as the one used on the local scale: to build models on the field scale, a field scale domain is split into several smaller local-scale sub-domains according to the geology, and the same equations for flow as in the local scale are applied.

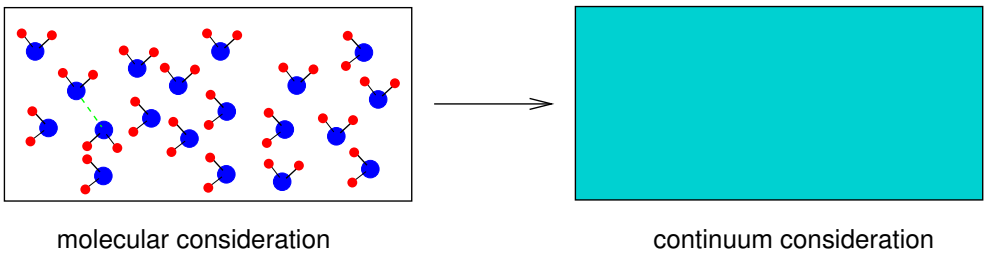

Figure 3.1: Consideration of water as a continuum

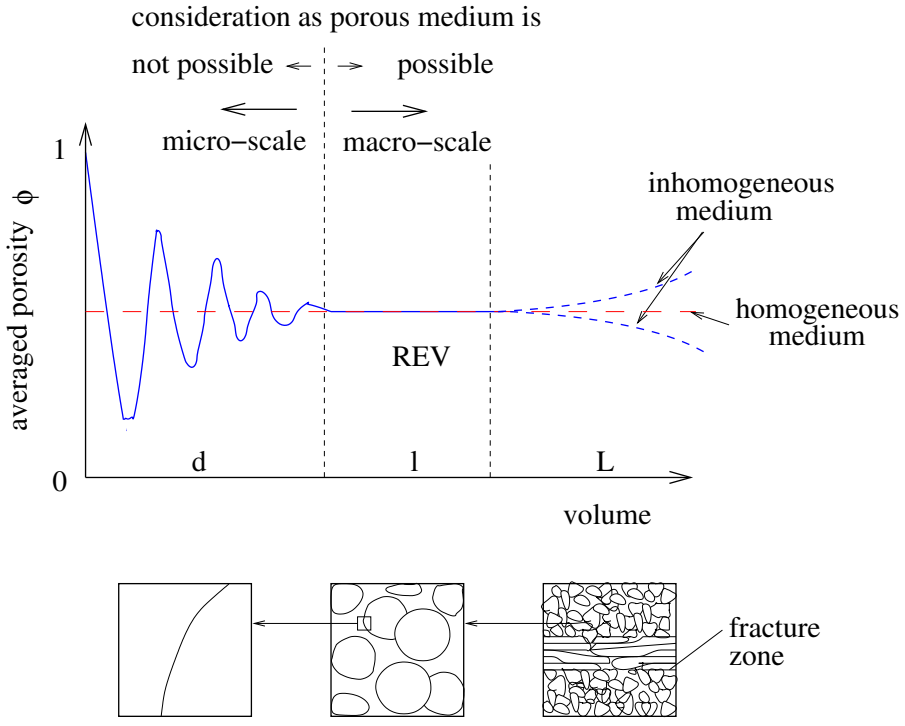

Figure 3.2: Definition of the REV (BEAR (1972 [9]), HELMIG (1997 [39]), HINKELMANN (2005 [42]))

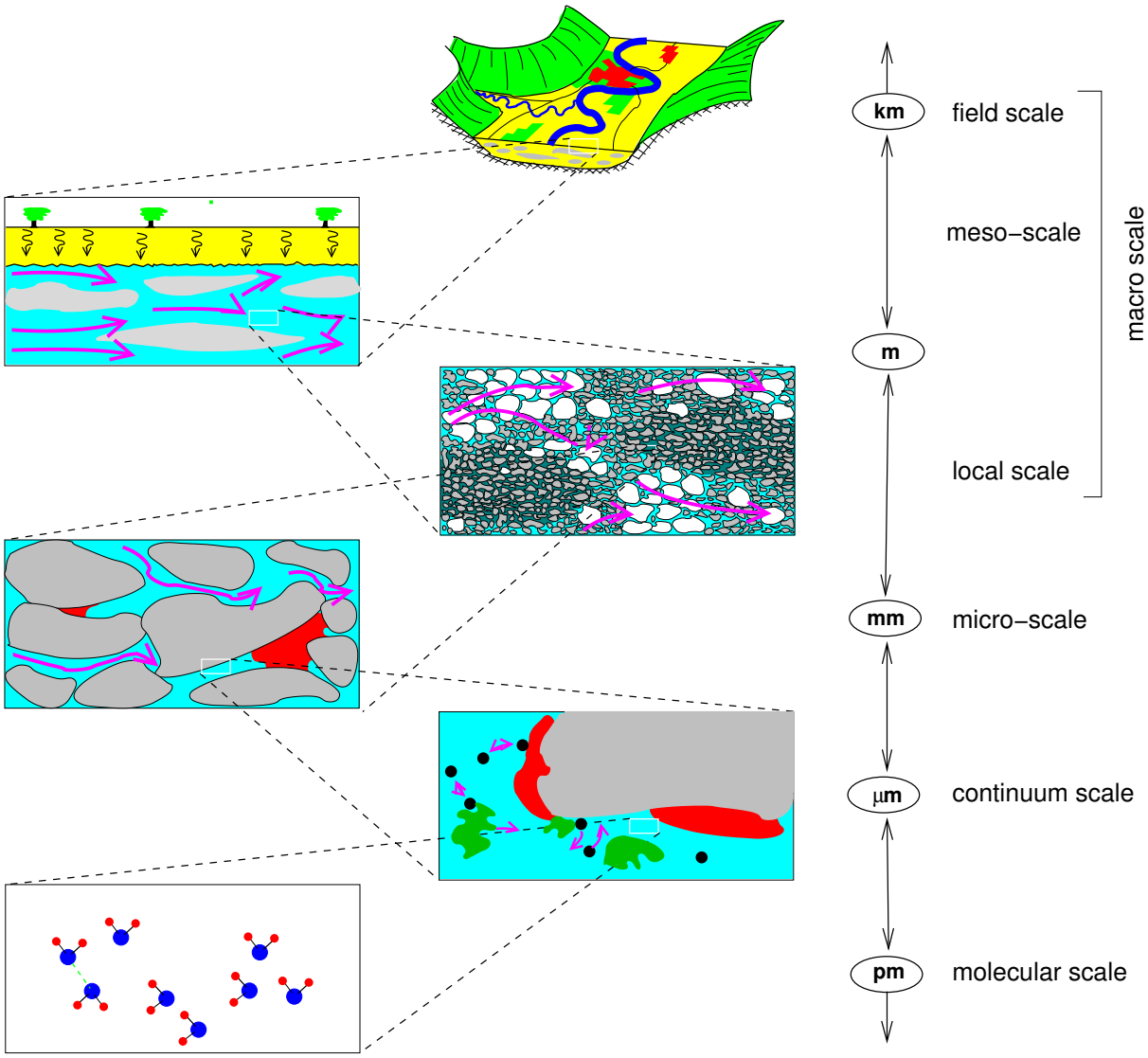

Figure 3.3: Spatial scale considerations in subsurface systems (KOBUS and DE HAAR (1995 [49]), OCHS (2007 [62]))

3.1.3 Porosity

A porous medium consists of a solid matrix and the pores. The porosity ϕ can be defined as the ratio of the pore space within the REV and the total volume of the REV:

$$\text{porosity} = \frac{\text{volume of the pore space within the REV}}{\text{volume of the REV}} \tag{3.1}$$

In reality, the fluids can only pass through when the pore spaces are connected, these are called flow paths. The pores in which flow cannot exist are often called dead-end pores. This characteristic leads to define the effective porosity:

$$\text{effective porosity} = \frac{\text{volume of flow paths}}{\text{volume of the REV}} \tag{3.2}$$

In this case, only the part of the pore volume is considered which is usable for the flow. Thus, the effective porosity is always equal to or smaller than the porosity defined in equation 3.1.

3.1.4 Saturation

The saturation of the phase α is defined to be the ratio of the volume of fluid α within the REV to the volume of the pore space within the REV:

$$S_\alpha(x,t) = \frac{\phi_\alpha(x,t)}{\phi} = \frac{\text{volume of fluid phase } \alpha \text{ within REV}}{\text{volume of pore space within REV}} \tag{3.3}$$

The following relationships are valid:

$$\sum_{\alpha=1}^{n_{phase}} \phi_\alpha = 1 \quad for \quad 0 \leq \phi_\alpha \leq 1 \tag{3.4}$$

$$\sum_{\alpha=1}^{n_{phase}} S_\alpha = 1 \quad for \quad 0 \leq S_\alpha \leq 1 \tag{3.5}$$

where n_{phase} is the number of phases in the model. In a two-phase system (gas-water phase), like porosity, the concept of so-called effective water saturation S_e is defined:

$$S_e = \frac{S_w - S_{wr}}{1 - S_{wr}} \tag{3.6}$$

where S_{wr} is the residual saturation of the water. This concept tries to account for the mobile portion of the water only in the pore space; thus the residual saturation is subtracted from the saturation.

3.1.5 Capillary Pressure

When a fluid is in contact with another immiscible fluid or solid, there is free energy present at the interface, causing the surface to contract. The force present at the interface between two fluids is called *interfacial tension* σ. The pressure discontinuities occur across the fluid-fluid interfaces due to the interfacial tension. The difference between the pressures of the non-wetting fluid and the wetting fluid is known as the capillary pressure p_c , which is a basic parameter in the study of the behavior of multiphase flow in porous media:

$$p_c = p_n - p_w \tag{3.7}$$

where p_n is the pressure of the non-wetting phase and p_w the pressure of the wetting phase. The fluid with a boundary angle $\theta < 90^0$ is referred to as the wetting fluid with respect to the solid phase, the fluid with an obtuse boundary angle $1 - \theta > 90^0$ is the non-wetting fluid. In Figure 3.4, the contact angle for the water is smaller than 90, thus water is notated as the wetting phase (w) and gas is the non-wetting phase (n), θ denotes the contact angle. Equilibrium requires that:

$$\sigma_{wn} cos(\theta) = \sigma_{sn} - \sigma_{sw} \tag{3.8}$$

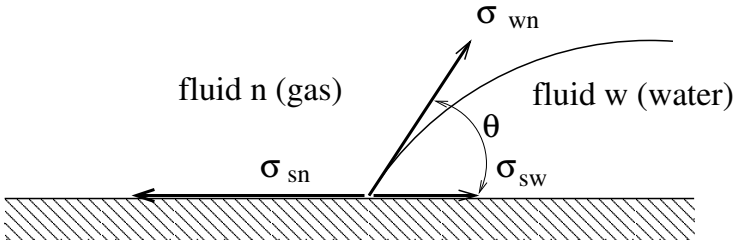

Figure 3.4: Contact angle between a fluid-fluid interface (BEAR (1972 [9])), σ_{wn} represents the interfacial tension between fluid phases, and θ denotes the contact angle

The capillary pressure can be defined quantitatively by considering a fluid-fluid interface within a pore, as shown in Figure 3.5, where the wetting/non-wetting interface has two principle radii of curvature, r_1 and r_2. The pressure difference across the interface can be defined according to a balance of forces acting on the opposite side:

$$p_c = p_n - p_w = \sigma_{wn} \left(\frac{1}{r_1} + \frac{1}{r_2} \right) = \frac{2\sigma_{wn}}{r^*} \tag{3.9}$$

Equation 3.9 is known as Laplace's law for capillary pressure, where r^* is the mean radius of curvature.

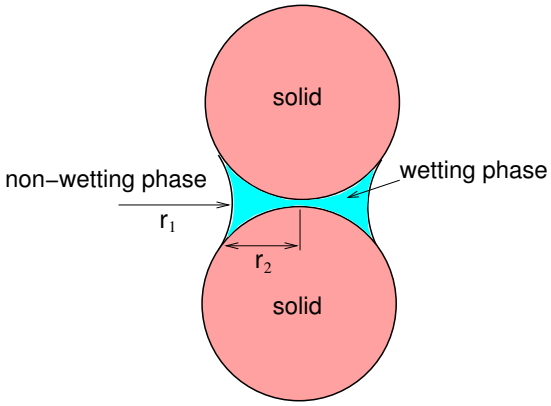

Figure 3.5: Equilibrium at a wetting/non-wetting fluid interface within pores (BEAR (1972 [9]))

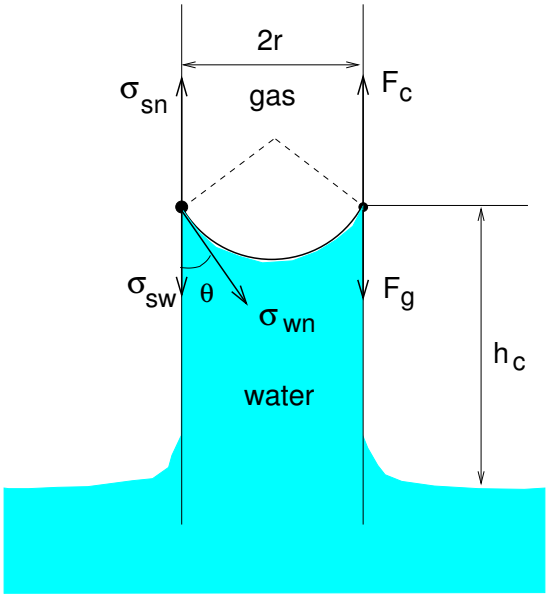

Figure 3.6: Capillary pressure in a cylindrical capillary tube with radius r

In the case of a cylindrical capillary tube with radius r, the water level in the capillary tube is elevated up to a height h_c at which the capillary forces (F_c) equal to gravity forces (F_g) (see Figure 3.6), the capillary pressure is written as following:

$$A \cdot \frac{2\sigma_{wn} cos\theta}{r} = \rho_w A h_c g \tag{3.10}$$

$$p_c = \rho_w g h_c = \frac{2\sigma_{wn}}{r} cos\theta \tag{3.11}$$

The above equation is called Young-Laplace's equation, in which θ is the contact angle between the fluid interface and the capillary wall.
On the macro-scale (local scale), the capillary pressure is dependent on the saturation. If the saturation ratio of the wetting fluid decreases it retreats to smaller and smaller pores which leads to an increase in capillary pressure. Thus, a macroscopic consideration of capillary leads to a relationship of the form:

$$p_c = p_c\left(S_w\right) \tag{3.12}$$

3.1.6 Permeability

The *absolute (intrinsic or saturated) permeability* K is a measure of the resistance of a particular porous medium towards flow of a fluid in its pores. It is a material property of the porous medium and assumed to be independent of the fluid. The absolute permeability is linked to the hydraulic conductivity K_f by taking into account the viscosity μ and density ρ of the fluid:

$$K_f = K\frac{\rho g}{\mu} \tag{3.13}$$

On the micro-scale, saturated permeability K is uniquely determined by the pore structure. It is the key parameter describing the mobility of a viscous fluid in a porous medium. For multiphase flow, when considering the flow of one fluid phase, the permeability of the medium appears to be reduced with respect to the fluid considered since part of the pore space is occupied by another fluid phase. The concept of the *effective permeability* K_α is then adopted, defined as the permeability of the medium to the flow of a specific phase α:

$$K_\alpha = K k_{r\alpha} \tag{3.14}$$

where $k_{r\alpha}$ is the *relative permeability* and K is the absolute (intrinsic or saturated) permeability described above. Like for capillary pressure, the relative permeability for a REV is a function of the saturation:

$$k_{r\alpha} = k_{r\alpha}\left(S_w\right) \tag{3.15}$$

The relations given in 3.14 and 3.15 depend on the material and two-phase systems as well. They should determined by fitting the parameters of analytical functions to measured data (see subsection 3.2.4).

3.1.7 Fluid Parameters

In this study, the model consists of two-phase flow which implies the two fluid flows: water and gas. Due to the big difference of the two fluid properties, some parameters like density, viscosity should be explained.
The density ρ of a fluid is the ratio of the mass m of that fluid in a certain volume V over that volume:

$$\rho = \frac{m}{V} \tag{3.16}$$

Generally, the density of fluid phase α depends on the pressure p_α, temperature T as well as on the composition x_α^k of the phase. Here, two phases are considered and components are not included. For the water phase, the pressure dependence is neglected, the water is assumed to be an incompressible fluid. For gas phase, the gas density is determined by the *real gas law*:

$$\rho_g = \frac{p_g}{Z R_g T} \tag{3.17}$$

In this equation Z stands for the real gas factor. For a simple case, Z is chosen to be 1 which implies the ideal gas law. R_g stands for the universal gas constant and T for the temperature.
Viscosity can be understood as the internal resistance of a fluid to flow. The dynamic viscosity of water and gas is primarily determined by the temperature. With increasing temperature, the viscosity of water decreases. Contrarily, the gas viscosity increases with increasing temperature. The viscosity of the gas phase is about two order of magnitude lower than that of water phase.
The relations for density and viscosity as a function of temperature for water and gas are shown in HELMIG (1997 [39]).

3.2 Two-Phase Flow Equations

Usually, the model concepts for the subsurface and surface-water hydrosystems are based on continuum-mechanical considerations. Therefore, the processes occurring on the micro-scale must be averaged in space and/or time in order to serve as physical quantities, i.e. effective parameters and processes, on meso-scale. The model concept of two-phase flow in porous media assumes that the two fluids, here water (w) and gas (g), are not miscible in each other and that mass transfer processes, for example evaporation or condensation, are negligible. The processes on the micro-scale are averaged to the REV scale (see Figure 3.7).

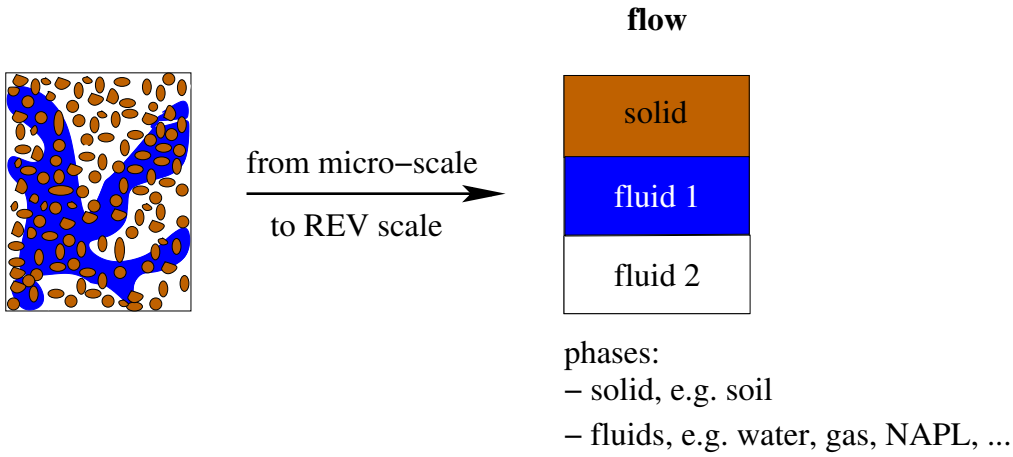

Figure 3.7: Phases in REV concept (HINKELMANN (2005 [42]))

3.2.1 Mass Balance Equation

The flow of two immiscible fluid phases in porous media can be described by the balance equations for mass and for momentum (the generalized Darcy Law).
To formulate a model for two-phase flow in porous media, mass balance equations are accounted for the individual phases in a control volume B. Based on an Eulerian approach, a mass balance can be formulated for each phase α in a non-deforming control volume with the *Reynold's transport theorem*. The storage and sources/sinks terms are described with volume integrals over B, while the flux term is described with an area integral of fluxes over the boundaries Γ of the control volume:

$$\frac{\partial}{\partial t}\int\limits_{B}\phi S_\alpha \rho_\alpha dB + \int\limits_{\Gamma}\phi\rho_\alpha \underline{u}_\alpha d\Gamma - \int\limits_{B}\rho_\alpha q_\alpha dB = 0 \tag{3.18}$$

Applying the Gaussian integral theorem, the equations are reformulated in the form:

$$\frac{\partial}{\partial t}\int\limits_{B}\phi S_\alpha \rho_\alpha dB + \int\limits_{B}\nabla(\phi\rho_\alpha \underline{u}_\alpha) dB - \int\limits_{B}\rho_\alpha q_\alpha dB = 0 \tag{3.19}$$

The Darcy velocity $\underline{v}$ is defined as:

$$\underline{v}_\alpha = \phi \underline{u}_\alpha \tag{3.20}$$

Inserting the Equation 3.20 into Equation 3.19 and choosing an infinitesimally small control volume is equivalent to the consideration at a point for which is now formulated the balance equation in its differential form (this equation is also known as continuity equation):

$$\frac{\partial(S_\alpha \phi \rho_\alpha)}{\partial t} + \nabla \cdot (\rho_\alpha \underline{v}_\alpha) - \rho_\alpha q_\alpha = 0 \tag{3.21}$$

Here, α is a subscript for the phases, the wetting phase w (e.g. water) and the non-wetting phase n (e.g. NAPL, gas), respectively.

3.2.2 Momentum Equation

Darcy's law can be extended to multiphase flows and it is then called generalised Darcy's law. Thus, it represents the momentum equation:

$$\underline{v}_\alpha = -\frac{1}{\mu_\alpha}\underline{\underline{K}}_\alpha(\nabla p_\alpha - \rho_\alpha \underline{g}) \tag{3.22}$$

$$\underline{v}_\alpha = -\frac{k_{r\alpha}}{\mu_\alpha}\underline{\underline{K}}(\nabla p_\alpha - \rho_\alpha \underline{g}) \tag{3.23}$$

In these equations, K_α is the effective permeability for phase α, ϕ stands for the porosity, S for the saturation, ρ for the density, t for the time, q for a sink / source term, $\underline{v}$ for the Darcy-velocity vector, k_r for the relative permeability, μ for the dynamic viscosity, $\underline{\underline{K}}$ for the intrinsic permeability tensor, p for the pressure and $\underline{g}$ for the gravity vector.

3.2.3 System of Two-Phase Flow Differential Equations

If the momentum equation 3.23 is inserted into the continuity equation 3.21, the following system of two-phase differential equations is obtained:

$$\frac{\partial(S_\alpha \phi \rho_\alpha)}{\partial t} - \nabla \cdot \left[\rho_\alpha \frac{k_{r\alpha}}{\mu_\alpha}\underline{\underline{K}}(\nabla p_\alpha - \rho_\alpha \underline{g})\right] = q_\alpha \rho_\alpha,\ \alpha \in (w,n) \tag{3.24}$$

or written in another way:

$$\frac{\partial(S_\alpha \phi \rho_\alpha)}{\partial t} - div\ \left[\rho_\alpha \lambda_\alpha \underline{\underline{K}}(grad\, p_\alpha - \rho_\alpha \underline{g})\right] - q_\alpha \rho_\alpha = 0,\ \alpha \in (w,n) \tag{3.25}$$

In the last equation, $\lambda_\alpha = k_{r\alpha}/\mu_\alpha$ denotes the mobility of phase α.
The system is completed by two further algebraic conditions. The void space in the porous medium is completely filled by the different fluid phases (wetting and non-wetting phase):

$$S_w + S_n = 1 \tag{3.26}$$

At the interface between two phases, the difference of the pressure at every point is a function of the capillary pressure p_c :

$$p_c = p_n - p_w \tag{3.27}$$

with the definition of the capillary pressure given above, p_c and $k_{r\alpha}$ still depend on the saturations of phases and the following relationships are needed (see subsection 3.2.4):

$$p_c = p_c\,(S_\alpha) \tag{3.28}$$

$$k_{r\alpha} = k_{r\alpha}\left(S_\alpha\right) \tag{3.29}$$

3.2.4 Constitutive Relationships

3.2.4.1 Capillary Pressure - Saturation Relationships

On the macro-scale both capillary pressure and relative permeability depend on the saturation. If the water saturation decreases, the wetting phase retreats into smaller and smaller pores and thus the capillary pressure increases. The macroscopic consideration of the capillarity results in a relationship given in Equation 3.12.
In general, there are two possibilities how to obtain capillary - saturation relationships. The first method is direct measurement. The second method is to derive the functional relationship between capillary pressure and saturation from theoretical considerations. Usually, these models contain several parameters which are fitted to experimental data. Several empirical models for the parameterization of a general capillary pressure - saturation functional relationship have been proposed (i.e. BROOKS AND COREY (1964 [21]), VAN GENUCHTEN (1980 [35]), CAMPBELL (1974 [22]), BRUTSAERT (1967 [17]); for an overview see SHETA (1999 [86])). Among the most common ones are the relationships of BROOKS-COREY (BC) and VAN GENUCHTEN (VG).
The capillary pressure - saturation relationship according to Brooks-Corey is defined with the help of the *effective saturation* S_e:

$$S_e\left(p_c\right) = \frac{S_w - S_{wr}}{1 - S_{wr}} = \left(\frac{p_d}{p_c}\right)^\lambda \quad for \quad p_c \geq p_d \tag{3.30}$$

or

$$p_c = p_d S_e^{-\frac{1}{\lambda}} \tag{3.31}$$

In these equations, p_c denotes the capillary pressure, p_d the entry pressure, S_e the effective water saturation, and λ is the form parameter. The λ-parameter usually lies between 0.2 and 3. A very small λ-parameter describes a single-grain size material, while a very large λ-parameter indicates a highly non-uniform material. The entry pressure p_d is considered as the capillary pressure required to displace the wetting phase from the largest occurring pores.
In the model of Van Genuchten, the following capillary pressure - saturation relationship is introduced:

$$p_c(S_w) = \frac{1}{\alpha}(S_e^{-\frac{1}{m}} - 1)^{\frac{1}{n}} \qquad \text{for} \quad p_c > 0 \tag{3.32}$$

Here, the parameter m in the VG function is usually chosen as $m = 1-1/n$, and therefore, only two free parameters n and α remain to be fitted. Typical values for n range from 2 to 5, α is a form parameter characterizing the pore-space geometry.
A correspondence between the Brooks and Corey and the van Genuchten models was deduced by LENHARD et al. (1989 [54]). The parameters n and α in VG model can be computed from the parameters P_d, λ in the BC model by following functions:

$$m = 1 - \frac{1}{n} \tag{3.33}$$

$$\lambda = \frac{m}{1-m}\left(1 - 0.5^{\frac{1}{m}}\right) \tag{3.34}$$

$$S_{ex} = 0.72 - 0.35e^{-n^4} \tag{3.35}$$

$$\alpha = \frac{S_{ex}^{\frac{1}{\lambda}}}{p_d}(S_{ex}^{-\frac{1}{m}} - 1)^{1-m} \tag{3.36}$$

with S_{ex} is the a special effective saturation (see SHETA (1999 [86])).
In Figure 3.8, the capillary pressure - saturation relationship is shown for the BC and VG models on equal physical conditions ($p_d = 700[Pa]$, $\lambda = 2.3$ in BC model and $n = 5$ and $\alpha = 0.0011$ in VG model).
The principle difference between the two types of relationships is the behavior of the function at $S_w = 1$. Whereas for Van Genuchten, the capillary pressure is equal to zero for a fully water saturated soil, the Brooks-Corey relation involves a displacement pressure (the pressure needed to displace the wetting phase from the largest pore, p_d).
The BC parameters (p_d, λ) or the VG parameters (n, α) should be determined from controlled experiments or they should be estimated from soil properties or taken from the literature.
In cases of lacking of experimental data, LEVERETT (1941 [53]) introduces a function to transfer known parameters, for example, to another medium with a different permeability or porosity or another two-phase system (from water-gas to water-NAPL) with different capillary pressure. The assumption is that the scaling factor $\frac{p_c}{\sqrt{k\theta}}$ equals the one in the other porous medium or another two-phase system. This function is so-called Leverett function (further information in LEVERETT (1941 [53]), SHETA (1999 [86])).
For fractured porous media, fractures are discretely taken into account. Two different possibilities of capillarity can be determined. The fracture can be treated as a porous medium as already described. The capillarity can also be formulated as a function of the fracture-aperture distribution by a geostatistical model (see PRUESS and TSANG (1990 [77]), SILBERHORN-HEMMINGER (2002 [88])).
For the problems with small-scale heterogeneities, the geostatistical methods are applied to generate the permeability field. The parameter p_d can be determined according to the Leveret function (see section 6.4).

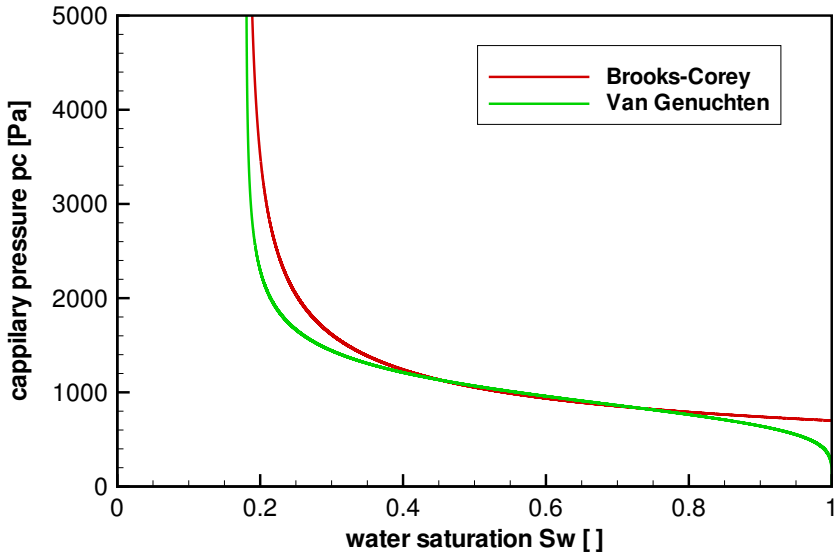

Figure 3.8: p_c - S_w relationship after BC and VG, on equal physical conditions, ($p_d = 700[Pa]$, $\lambda = 2.3$ in BC model and $n = 5$ and $\alpha = 0.0011[1/Pa]$ in VG model)

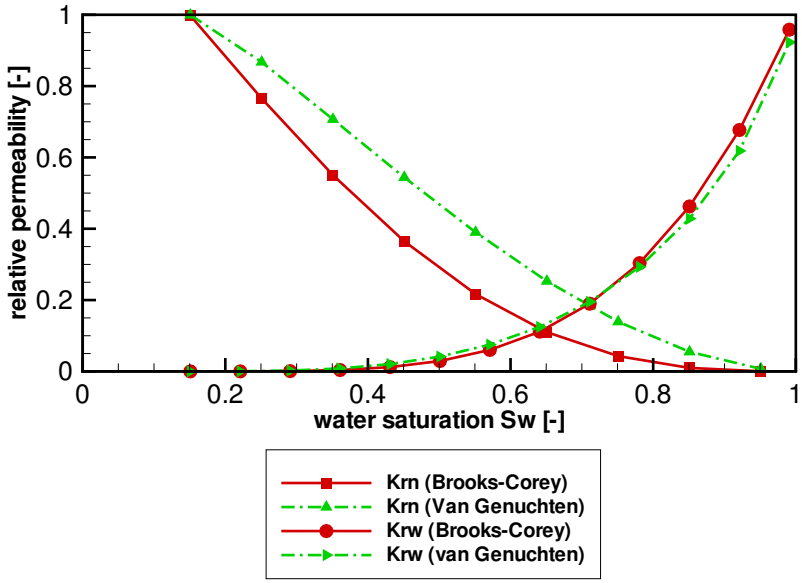

Figure 3.9: Relative permeability - saturation relationship after BC and VG, on equal physical conditions, ($\lambda = 2.3$, $n = 5$, $\alpha = 0.0011[1/Pa]$, $S_{wr} = 0.18$)

3.2.4.2 Relative Permeability - Saturation Relationships

Based on pore-network models, relative permeability - saturation relationships are determined by integrating over the capillary pressure - saturation relationship. The BROOKS-COREY (1964 [21]) model stems from the pore-network model of BURDINE (1953 [24]):

$$k_{rw} = S_e^{\frac{2+3\lambda}{\lambda}} \tag{3.37}$$

$$k_{rn} = (1 - S_e)^2 \left(1 - S_e^{\frac{2+\lambda}{\lambda}}\right) \tag{3.38}$$

The VAN GENUCHTEN model (1980 [35]) is determined by the pore-network model of MUALEM (1976 [60]) and has the form:

$$k_{rn} = (1 - S_e)^{1/3} \left[1 - S_e^{\frac{1}{m}}\right]^{2m} \tag{3.39}$$

The parameters are the same as in the context of the capillary pressure - saturation relationship. Figure 3.9 shows these relative permeability-saturation relationships.
In discrete fractured systems, linear relative permeability-saturation relationships can be used or other relations taking into account the fracture roughness, fracture aperture and the fracture contact area. For further reading, see HELMIG (1997 [39]), BREITING et al. (2002 [18]), HELMIG and CUNNINGHAM (2003 [41]) and HINKELMANN (2003 [42]).

3.2.5 Different Formulations

In Equation 3.25, the number of unknowns in the system is four (i.e. p_w, p_g, S_w, S_g), and there are two mass conservation equations and two constraints. Thus, the system is closed and it can be solved. Normally, in order to solve the equations, we first eliminate two unknowns using the constraints and then formulate the two mass conservation equations with the remaining two unknowns. Several possible formulations according to the choice of the primary variables for the unknowns exist: the pressure formulation, the pressure-saturation formulation and the saturation formulation. In the following steps, the three formulations are briefly introduced.

3.2.5.1 Pressure Formulation

The pressure formulation uses the wetting and non-wetting phase pressure (p_w and p_n) as the primary variables. Saturations are transformed to pressures by inverting the capillary pressure - saturation relationship (see subsection 3.2.4.1). The constraint for using this

formulation is, that the p_c - S_w function has to be strictly monotonic in order to be inversed:

$$S_\alpha = f_\alpha^{-1}(p_c) = f_\alpha^{-1}(p_n - p_w) \tag{3.40}$$

The p_w - p_n formulation reads as follows:

wetting phase:

$$-\frac{\partial(\phi\rho_w f_w^{-1}(p_c))}{\partial t} - div\left[\rho_w \frac{k_{rw}}{\mu_w}\underline{\underline{K}}(grad\, p_w - \rho_w \underline{g})\right] - \rho_w q_w = 0 \tag{3.41}$$

non-wetting phase:

$$\frac{\partial(\phi\rho_n f_n^{-1}(p_c))}{\partial t} - div\left[\rho_n \frac{k_{rn}}{\mu_n}\underline{\underline{K}}(grad\, p_c + grad\, p_w - \rho_n \underline{g})\right] - \rho_n q_n = 0 \tag{3.42}$$

These two equations are strongly coupled and a non-linear parabolic system. However, in many practical examples, for example, in case of discrete fractures or transitions between heterogeneities, the capillary pressure gradient ($\frac{\partial p_c}{\partial S_\alpha}$) is zero or close to zero, so that this formulation cannot be chosen. One major problem results of the effect that the total velocity must be known in advance and another of the hyperbolic character for small capillary pressure gradients.

3.2.5.2 Saturation Formulation

This formulation is only applicable to incompressible fluids. The saturation formulation ($S_w - S_n$) is determined after calculating the total velocity $v_t = v_w + v_n$ and several transformations. The system is reduced to one equation with only one primary variable S_w or S_n.

3.2.5.3 Pressure - Saturation Formulation

For many cases, the pressure - saturation formulation is most suitable. This formulation uses the pressure of one phase and the saturation of the other phase (p_w, S_n or p_n, S_w or p_w, S_w or p_n, S_n) as primary variables. The following relations are obtained:

$$\nabla\, p_n = \nabla\,(p_c + p_w) \tag{3.43}$$

$$\frac{\partial S_w}{\partial t} = \frac{\partial(1 - S_n)}{\partial t} = -\frac{\partial S_n}{\partial t} \tag{3.44}$$

Inserting Equation 3.43 and Equation 3.44 into the two-phase flow equation 3.25 leads to the p_w - S_n formulation (p_n - S_w, p_w - S_w, p_n - S_n accordingly):

wetting phase:

$$-\frac{\partial(S_n \phi \rho_w)}{\partial t} - div\ \left[\rho_w \frac{k_{rw}}{\mu_w} \underline{\underline{K}} (grad\, p_w - \rho_w \underline{g})\right] - \rho_w q_w = 0 \tag{3.45}$$

non-wetting phase:

$$\frac{\partial(S_n \phi \rho_n)}{\partial t} - div\ \left[\rho_n \frac{k_{rn}}{\mu_n} \underline{\underline{K}} (grad\, p_c + grad\, p_w - \rho_n \underline{g})\right] - \rho_n q_n = 0 \tag{3.46}$$

These two equations are strongly coupled, highly non-linear and mixed parabolic/hyperbolic type. The major advantage is that they are not limited to small capillary-pressure gradients, i.e. the pressure-saturation formulation can be applied to discrete fractured systems and heterogeneous media. Therefore, this formulation is chosen for the work here. For further reading, see PRUESS (1991 [76]), HELMIG (1997 [39]), PAUL (2003 [65]), HINKELMANN (2005 [42]).

3.3 Numerical Modeling of Two-Phase Flow in Porous Media

3.3.1 Introduction

In most cases, the systems of multiphase flow equations (Equation 3.25) lead to a system of non-linear coupled differential equations, apart from some exceptions. Generally, it cannot be solved analytically. Therefore, numerical methods, i.e. here discretization techniques are usually necessary.

The first numerical simulator for incompressible two-phase flow in porous media has been developed about 40 years ago. Since then, many different methods have been devised. In the incompressible case, the pressure equation is elliptic and a fully explicit treatment is not possible. Therefore, any numerical method for the multiphase flow problem has to solve systems of algebraic equations, various degrees of implicitness and coupling are possible (see BASTIAN (1999 [7])).

The development process of a numerical method is shown in Figure 3.10 starting with the selection of the mathematical model, followed by the space discretization, i.e. grid generation, on the one hand, and the discretization of the differential equation on the other hand.

For the discretization, the Fully Upwind Box Method is applied in space and the fully implicit Euler Method in time. The non-linearities are handled with the Newton-Raphson Method, and the linearized equations are solved with the BiCGSTAB Method using Multigrid preconditioning. A time-step adaptation depending on the number of non-linear iterations is carried out. For further reading see more in HELMIG (1997 [39]), BASTIAN (1999 [7]), BASTIAN et al. (2000 [8]) and HINKELMANN (2005 [42]).

3.3.2 Temporal Discretization

Discretization methods are used in order to replace the differential terms in the two-phase flow equations by algebraic terms. These methods approximate the solution function at discrete points or nodes. The requirements for convergence of discretization methods are, that they must be consistent and stable. Moreover, it is desirable to have a monotonic solution behavior (which means in our case a non-oscillating solution) in order to avoid over- or undershooting. To prevent the appearance of non-physical sinks and sources, a conservative discretization is to be used. In order to combine the advantages of the (cell-centered) finite volume (FV) discretization and the finite element (FE) discretization, the BOX scheme was developed. This discretization technique is not only locally conservative (like the FV method) but can also be applied to unstructured grids easily (like the FE method). An overview of different discretization schemes and their properties can be found, for example in HELMIG (1997 [39]), PAUL (2003, [65]) and HINKELMANN (2005 [42]).
For the temporal discretization in this work, the implicit Euler scheme (finite difference method of first order), a one-step scheme, is applied. Here, the time-dependent partial derivative of an unknown u is approximated by:

$$\frac{\partial u}{\partial t} = \frac{u^{n+1} - u^n}{\Delta t} = f\left(u^{n+1}\right) \quad with \quad \Delta t = t^{n+1} - t^n \tag{3.47}$$

The indices $n+1$ and n denote the point in time at which u is evaluated. The unknowns on the new time level n+1 depend on each other and a system of equations with all degrees of freedom has to be solved for each time step. So, the discretization with the implicit Euler scheme for the time dependent terms in Equation 3.45 and 3.46 will be:

wetting phase:

$$-\left([S_n\rho_w]_j^{n+1} - [S_n\rho_w]_j^n\right)\frac{\phi}{\Delta t} \tag{3.48}$$

non-wetting phase:

$$\left([S_n\rho_n]_j^{n+1} - [S_n\rho_n]_j^n\right)\frac{\phi}{\Delta t} \tag{3.49}$$

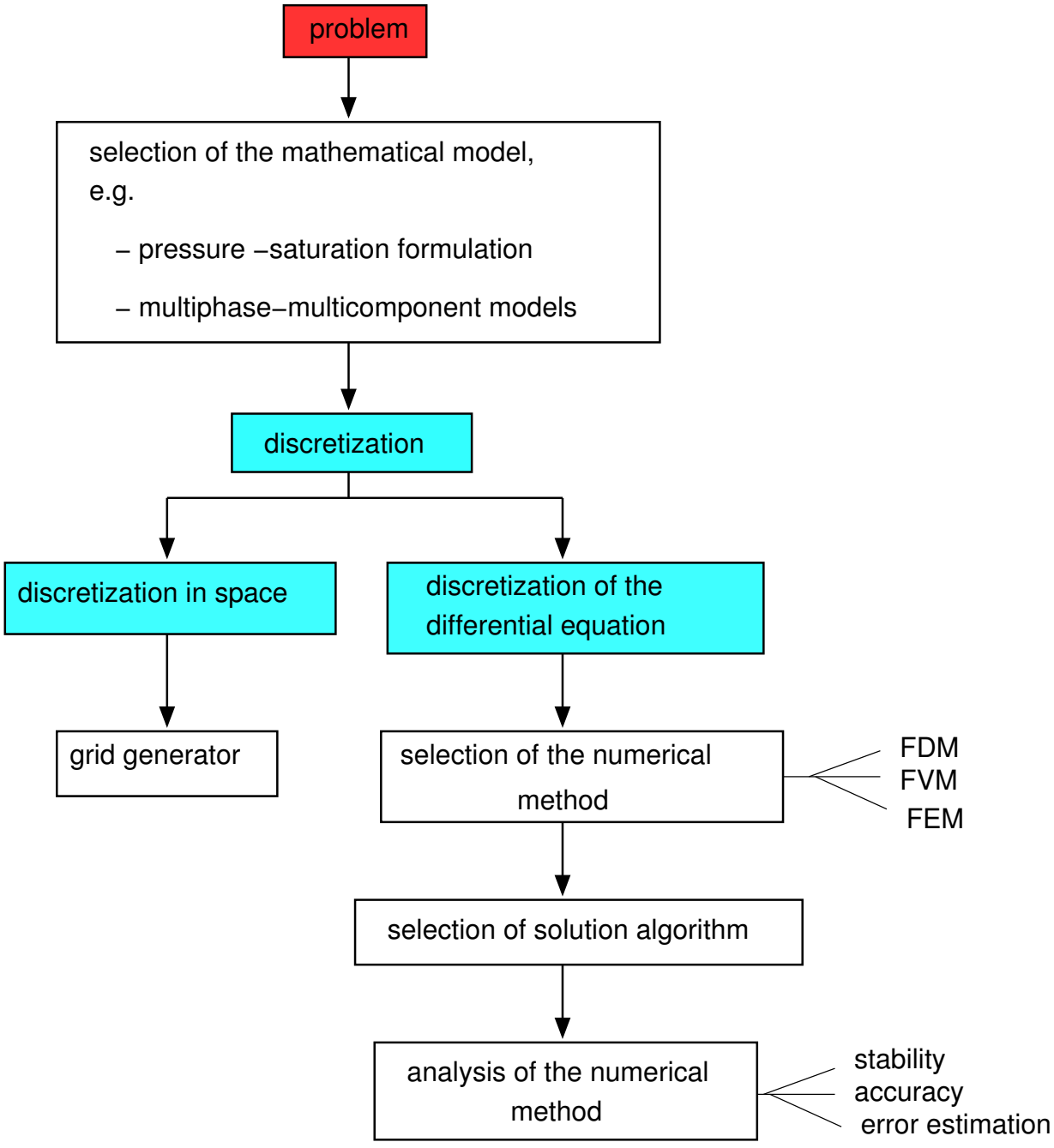

Figure 3.10: Development of a numerical solution method (HELMIG (1997 [39]))

3.3.3 Spatial Discretization

For the discretization in space, the BOX Method (subdomain collocation finite volume method) is used in the frame of this work. In this technique, two different meshes are needed. First, the model domain Ω is discretized with a finite element (FE) mesh that consists of n nodes $V = v_1, ..., v_n$ and m elements $E = e_1, ..., e_m$. Dirichlet and Neuman boundary conditions must be assigned along the boundaries of the domain. Then, a secondary control volume mesh is constructed in the following way: for each node v_i, a control volume or box B_i is constructed by connecting the mid points of the adjoining element sides and the barycenters of the neighboring elements. Each control volume B_i consists of l subcontrol volumes, which describe the intersection of elements connected to the node k_i (see Figure 3.11):

$$B_i = \sum_{i=1}^{l} b_i^l \tag{3.50}$$

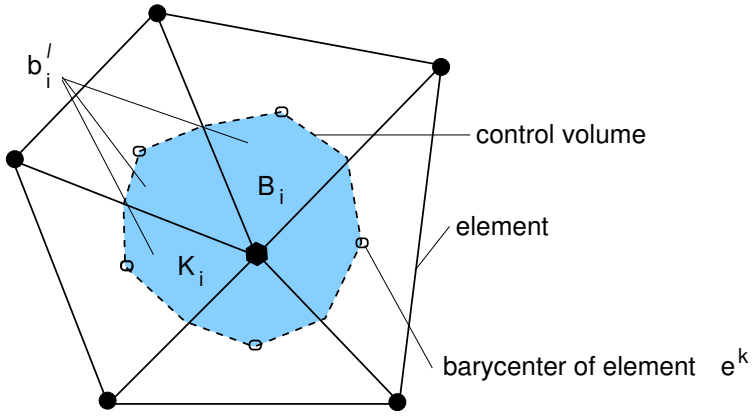

Figure 3.11: Construction of control volume

The spatial distribution of an unknown u in the model domain Ω is required for the solution of the equation system. To get this, discrete values of the unknown $\hat{u}$ are assigned to the nodes of the finite element mesh. In between the nodes, a basis function N_j is used for every node j to interpolate. (This function is also known as *ansatz function, interpolation function, or shape function*). The approximated values of the unknown $\tilde{u}$ are defined:

$$\tilde{u} = \sum_{j=1}^{n} \hat{u}_j \cdot N_j \tag{3.51}$$

where n is the number of nodes of in model domain. The value of N_j is always equal to 1 at nodes j and 0 at all other nodes. The function N_j can be described in Figure 3.12

for the one-dimensional case. Applying this approximation procedure to the unknowns of equations, some unknowns are given:

$$\tilde{p_w} = \sum_{j=1}^{n} \hat{p_{wj}} \cdot N_j, \qquad \tilde{S_w} = \sum_{j=1}^{n} \hat{S_{wj}} \cdot N_j \tag{3.52}$$

If the approximated unknown values are inserted into the weak formulation of balance equations (which is obtained intergration over a control volume G), the differential equations are not sastisfied exactly and an error, the so-called residual ε is produced. With a function W_i, ε can be weighted and intergrated over the whole domain G so that the average residual becomes zero.

$$\int_G W_i \cdot \varepsilon dG = 0, \qquad i = 1, 2, \ldots, n \tag{3.53}$$

For BOX method, a weighting function W_i is defined equal to 1 inside the control volume and 0 outside the control volume:

$$W_i(x) = \begin{cases} 1 & \text{if} \quad x \in B^i \\ 0 & \text{if} \quad x \notin B^i \end{cases} \tag{3.54}$$

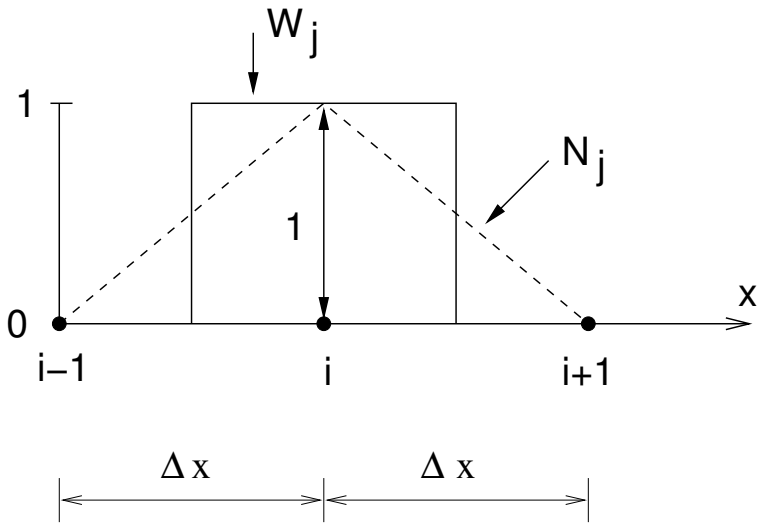

Figure 3.12: Shape and weighting function (HELMIG (1997 [39]))

The boundary and the volume integrals are solved for each control volume. The space terms in equation 3.45 and 3.46 are:

wetting phase:

$$-\rho_{w,ij}^{n+1}\lambda_{w,ij}^{n+1}\int_{\Gamma_i}\underline{\underline{K}}gradN_j\underline{n}dO\ \underbrace{(p_{w,j}^{n+1}-\rho_{w,j}^{n+1}g-p_{w,i}^{n+1}+\rho_{w,i}^{n+1}g)}_{discrete\ flow\ \ df_w}-q_{w,i}^{n+1}B_i=0 \tag{3.55}$$

non-wetting phase:

$$-\rho_{n,ij}^{n+1}\lambda_{n,ij}^{n+1}\int_{\Gamma_i}\underline{\underline{K}}gradN_j\underline{n}dO\ \underbrace{(p_{w,j}^{n+1}+p_{c,j}^{n+1}-\rho_{n,j}^{n+1}g-p_{w,i}^{n+1}-p_{c,i}^{n+1}+\rho_{n,i}^{n+1}g)}_{discrete\ flow\ \ df_n}$$
$$-q_{n,i}^{n+1}B_i=0 \tag{3.56}$$

In these equations, the densities can be defined by averaging along the edges:

$$\rho_{\alpha,ij}^{n+1}=0.5(\rho_{w,i}^{n+1}+\rho_{w,j}^{n+1}),\qquad \alpha=w,n \tag{3.57}$$

There are several ways to choose the mobility term λ. Here, the mobility term can be determined with fully upwinding. This method is called *Fully Upwind Box Method* and it is applied in this work. When the mobility λ is considered constant in an element, it gets the value of the mobility at the upstream node of the discrete flow direction:

$$\lambda_{\alpha,ij}^{n+1}=\begin{cases}\lambda_{\alpha,i}^{n+1} & if\quad df_\alpha\geq 0\\ \lambda_{\alpha,j}^{n+1} & if\quad df_\alpha<0\end{cases},\qquad \alpha=w,n \tag{3.58}$$

Several comparative studies of different discretization methods regarding monotocity, mesh geometry, convection/ diffusion and heterogeities have been carried out. The studies demonstrate that the Fully Upwind Box Method is monotonous, locally mass-conservative, applicable for unstructured grids and it represents the correct physical behavior. A certain numerical diffusion can occur (see HELMIG (1997 [39]), PAUL (2003 [65]), HINKELMANN (2005 [42])).

3.3.4 The Influence of Heterogeneties

With discontinuous porous media, such as fractured domains, we need a special treatment for the discretization (see HELMIG (1997 [39]), REICHENBERGER et al. (2004 [83]), REICHENBERGER et al. (2006 [84])). The whole domain Ω consists of different subdomains, e.g. the matrix Ω^m and the fracture Ω^f, with different absolute permeabilities. The flux of phases and the capillary pressure across the interface have to be continuous. We assume a mobile wetting phase in both matrix and fracture, hence we require that p_w

is continuous across the fracture-matrix interphase. The absolute permeabilities in their respective domains are:

$$K(x) = \begin{cases} K^f(x) & \text{if} \quad x \in \Omega^f \\ K^m(x) & \text{if} \quad x \in \Omega^m \end{cases} \tag{3.59}$$

Accordingly, the porosity ϕ depends on the domain as well as the capillary pressure function $p_c(S_w)$ and the relative permeability functions $k_{r\alpha}(S_w)$. The capillary pressure functions $p_c(S_w)$ are shaped like in Figure 3.13.
Two assumptions are essential without taking into consideration the blocking fractures (e.g. fractures filled with clay):

- The absolute permeability in the matrix is smaller than the absolute permeability in the fractures, $K_m(x) < K_f(y)$ for all $x, y \in \Omega$.
- The values of the capillary pressure function in the matrix are larger than these in the fractures for the same saturation (the entry pressure of the rock is larger than the one of the fractures).

For the Brooks-Corey capillary pressure relation, the entry pressure is positive, and there is a saturation S_w^* such that the continuity of the capillary pressure can only be achieved if $S_w < S_w^*$. S_w^* is called *threshold saturation*.
In VAN DUIJIN et al. (1995 [99]) it is shown for a one-dimensional problem that for $S_w > S_w^*$ the capillary pressure is discontinuous and that S_w is 1 in the matrix Ω^m. Physically, if the non-wetting phase is not present (i. e. $S_w = 1$ and $S_n = 0$), then p_n is undefined and p_c (which is defined as p_n - p_w) is also undefined. The proposed interface condition is called extended capillary pressure condition and is shown in Figure 3.13. We have:

$$S_w^m = \begin{cases} 0 & \text{if} \quad S_w^f > S_w^* \\ (p_c^m)^{-1}\left(p_c^f\left(S_w^f\right)\right) & \text{else} \end{cases} \tag{3.60}$$

In the discretization of two-phase flow in fractured media, we employ two fundamental properties of fractures being overlapping domains.
In the lower-dimensional fractures, the volumetric elements are complemented with lower dimensional elements, e.g. 1D line elements in 2D domain; 1D line elements and (or) 2D triangles/quadrilaterals in 3D domain (see Figure 3.15 (left)). The fractures appear as inner boundaries to the domain where material properties change.
In equi-dimensional fractures, both fracture and matrix elements have the same dimensionality (see Figure 3.15 (right)). A fracture can be a porous medium with a higher permeability. It can also be a void space with a small aperture b, then $K = b^2/12$.

Like the case of interface conditions, we assume that the interface between two domains are resolved by the grid and also that fractures are resolved by the grid. This situation is depicted in Figure 3.14, where a part of a fracture and the surrounding grid is shown. The vertex K_i in this figure is part of sub-domains: two matrix domains Ω^m and the fracture domain Ω^f.

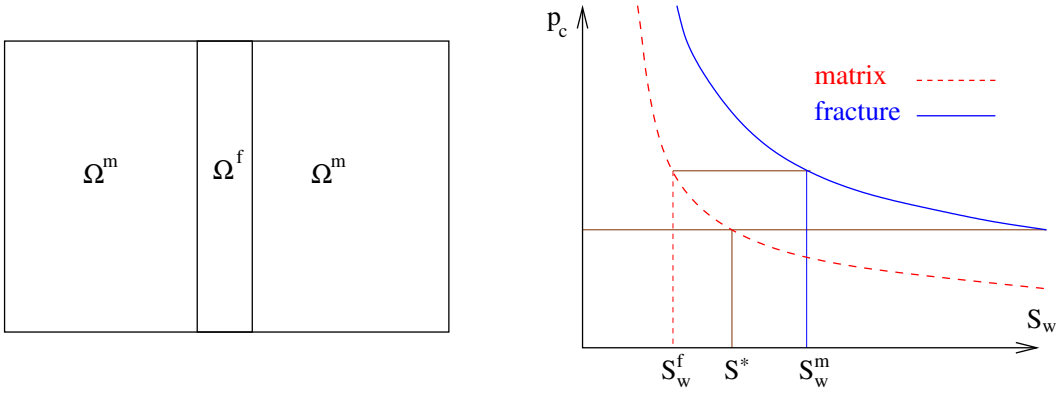

Figure 3.13: Brooks-Corey capillary pressure curve for discontinuous media

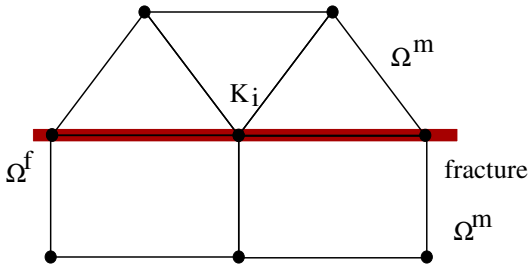

Figure 3.14: Example of a fracture in a grid

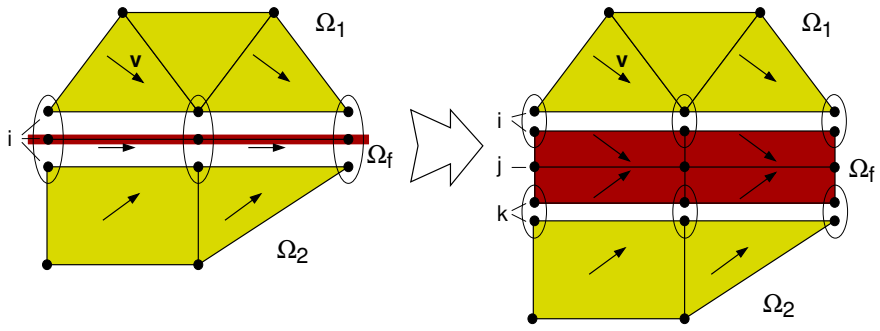

Figure 3.15: Spatial discretization of lower- and equi- /dimensional fracture approach

3.3.5 Numerical Simulator MUFTE-UG

Two-phase flow model concepts are implemented in the modeling system MUFTE-UG that is a combination of MUFTE and UG (see Figure 3.16). MUFTE stands for **MU**ltiphase **F**low, **T**ransport and **E**nergy model. UG is the abbreviation for **U**nstructured **G**rids. The numerical simulator is developed at the Institute of Hydraulic Engineering, University of Stuttgart in cooperation with the Chair of Water Resources Management and Modeling of Hydrosystems, Technische Universität Berlin (part MUFTE) and the Technical Simulation Group of the Interdisciplinary Center for Scientific Computing, University of Heidelberg (part UG).
The MUFTE software toolbox mainly contains the physical model concepts and discretization methods for isothermal and non-isothermal multiphase / multicomponent flow and transport process in porous and fractured porous media. In this toolbox, several modules for the numerical simulation of isothermal and non-isothermal multiphase / multicomponent flow and transport processes in porous and fractured-porous media have been provided including the system with single-phase, two-phase and three-phase problems. These problems can be illustrated in detail as following:

- single-phase systems
  - single-phase flow: liquids, e.g. water, NAPLs, ...; gases , e.g. air, methane,...; incompressible, compressible
  - single- and multicomponent transport: e.g. contaminants, dissolved gases, ...
  - fractures
  - 2D, 3D
- two-phase systems
  - two-phase flow: liquid / liquid, e.g. water / NAPL, water / oil, ...; liquid / gas, e.g. water / air, water / methane, ...; incompressible, compressible
  - two- and multicomponent transport: e.g. salt, dissolved gases, contaminants, ...
  - isothermal and non-isothermal (including phase transitions)
  - fractures
  - 2D, 3D
- three-phase systems
  - three-phase flow: liquid / liquid / gas, e.g. water / NAPL / air, ...; incompressible, compressible

– three- and multicomponent transport: e.g. contaminants, wator vapor, dissolved gases, ...

– isothermal and non-isothermal (including phase transitions)

– 2D

Several model concepts for fractured porous media including the discrete model concept (e.g. combined approach) and equivalent model concept (e.g. double-continuum approach) can be used in the MUFTE toolbox. Different flow laws and modeling techniques are available for the flow through fault zones and fractures. MUFTE provides a large set of constitutive relationships for the relative permeability and the capillary pressure as well as state equations for some parameters (e.g. densities, viscosities). The MUFTE toolbox includes also several different types of spatial discretization methods (e.g. BOX, CVFE method) and time discretization schemes (explicit, implicit). The two most common spatial discretization techniques are the Fully Upwind Box Method (BOX), which is a Finite-Volume formulation with piecewise linear shape functions including fully upwinding of the upstream mobilities, and a Control-Volume Finite-Element Method (CVFE), which is a mass-conservative formulation on a discrete patch including a first-order upwinding scheme. The time integration employs the Finite Difference Method, and the temporal discretization is carried out fully implicitly.
Further information is found in HELMIG (1997 [39]), BASTIAN et al. (1997 [6]), BREITING et al. (2002 [18]), HELMIG and CUNNINGHAM (2003 [41]) and HINKELMANN (2005 [42]).

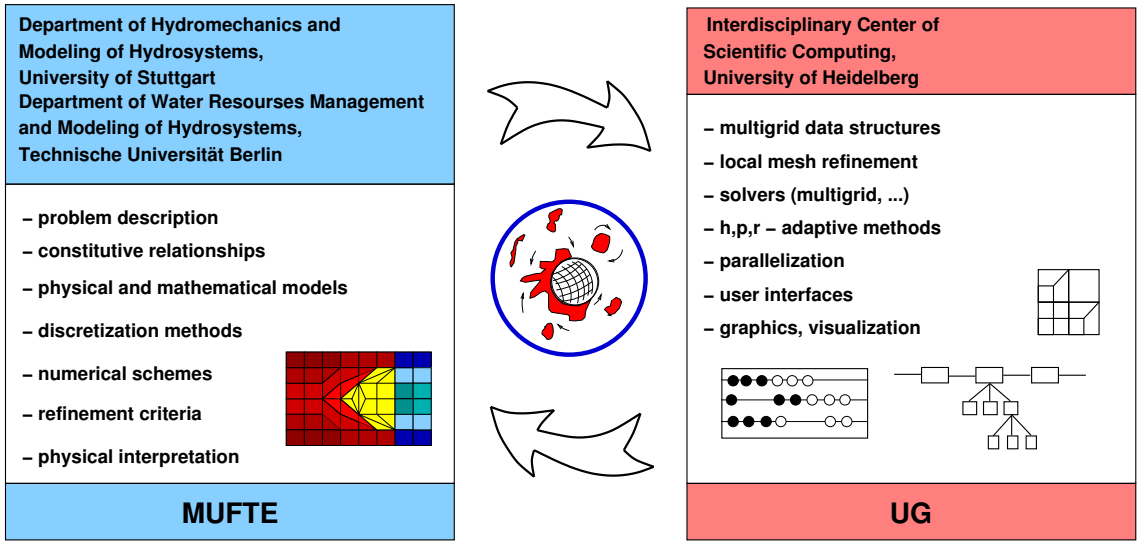

Figure 3.16: Numerical simulator MUFTE-UG

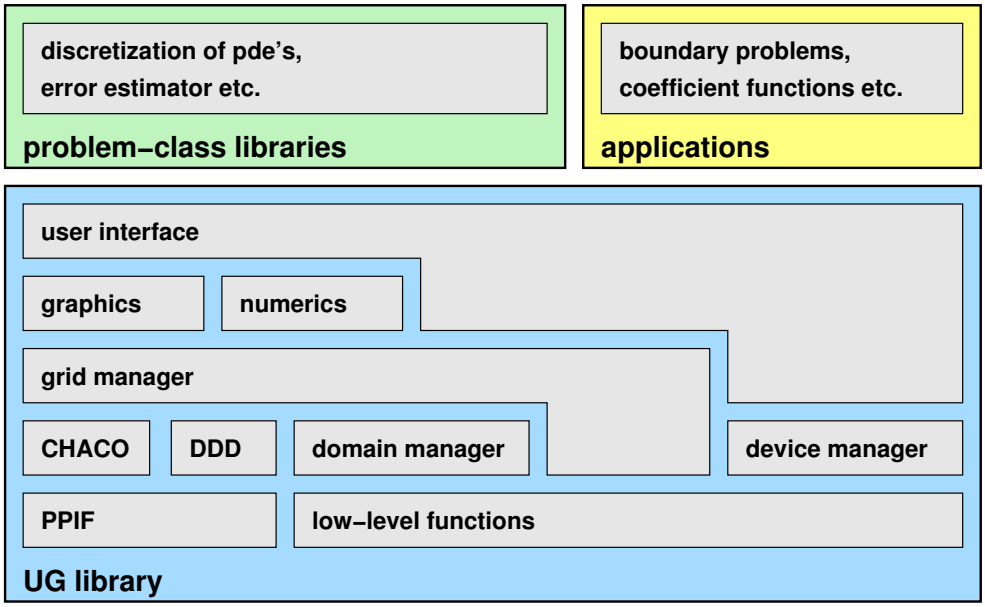

Figure 3.17: Structure of the UG toolbox (BASTIAN (1996 [5]))

UG is a toolbox for the solution of partial differential equations and it is currently used by a number of different groups in engineering research and application. UG provides the data structures and fast solvers based on parallel, adaptive Multigrid Methods. Special advantages of the UG toolbox are the data structures for unstructured grids, i.e. the ability to deal with complex geometries and boundaries in two and three dimensions, functional parallelization, i.e. especially suitable for MIMD parallel computers, adaptive local-grid refinement in order to minimize the degrees of freedom for a desired accuracy and robust Multigrid solvers for linear and non-linear problems. UG has several pre- and postprocessing tools which are also suitable for parallel computers, e.g. online graphics.
As shown in figure 3.17, UG is divided into three major parts: the *UG library, problem-class libraries* and *applications*. The UG library is independent of the partial differential equation, and it contains geometric and algebraic data structures, refinement and coarsening techniques, numerical algorithms, visualization techniques as well as a user interface. The problem class libraries provide discretization methods as well as error estimators and indicators. Finally, the applications describe the system set-up, i.e. the geometry, physical parameters and their functional relationships as well as the initial and boundary conditions. A simulation run is steered by a script file. More detailed information can be found in the literature mentioned above and in several manuals which can be downloaded from the UG homepage ([96]).
The overview of the modeling system of MUFTE-UG with pre- and postprocessor as well as interfaces is shown in Figure 3.18.

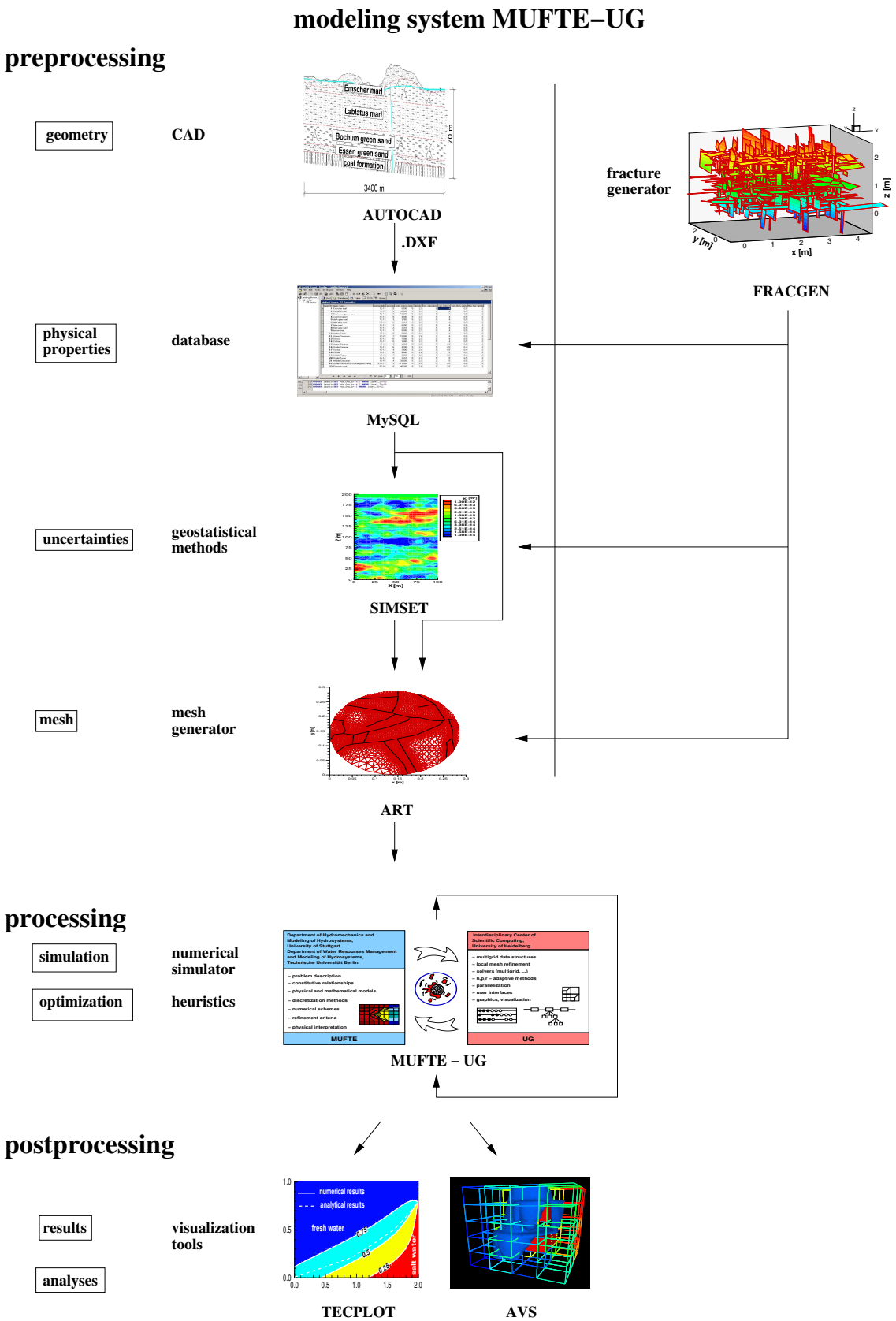

Figure 3.18: Modeling system MUFTE-UG with its pre- and postprocessors (HINKELMANN (2005 [42]))

3.3.6 Pre- and Post-Processing

3.3.6.1 Mesh Generation

After the geometric and physical information has been prepared, a mesh of the computational domain must be generated. The most basic form of mesh classification is based upon the connectivity of the mesh: *structured* or *unstructured*.
Strictly speaking, a structured mesh can be recognized by all interior nodes of the mesh having an equal number of adjacent elements. Structured means that, in 2D, each inner node has a connection to 4 neighboring nodes and to 4 rectangular elements and, in 3D, each inner node has a connection to 6 neighboring nodes and to 8 bricks elements. This mesh is suitable for 'simple' domains.
For complex domains and boundaries as well as spatial parameter distributions, *unstructured meshes* are recommended, i.e. triangles or quadrilateral in 2D and hexahedra in 3D. In the unstructured meshes, the node valence requirement is relaxed allowing any number of elements to meet at a single node. Triangle and tetrahedral meshes are most commonly thought of when referring to unstructured meshing, although quadrilateral and hexahedral meshes can also be unstructured. Because the triangle mesh is more flexible to adapt especially for complex domains. Most of the commonly used unstructured mesh generation techniques are based upon the properties of the *Delaunay triangulation*, the *Advancing Front Method* or *block-structured methods* (see FUCHS (1999 [34])). Unstructured meshes are especially suitable for the Finite Element and Finite Volume Method.

In this study, the unstructured meshes with triangular element in 2D are used with helps of the software ART (developed by FUCHS (1999 [34])). ART is the abbreviation for Almost Regular Triangulation which is based on the Delaunay triangulation method. It generates high-quality triangles or tetrahedral with regular mesh structure and enables area-wise higher mesh resolutions according to a user-defined density function. ART has been extended to discrete fractured systems; for fractures as elements of lower dimensions (e.g. 1D fractures in a 2D matrix) and for fractures as elements of equal dimensions (e.g. 2D fractures in 2D matrix). Figure 3.19 shows the process and the data input files which are used in ART program.

3.3.6.2 Visualization

After the numerical simulation, the computed data are presented and analyzed in the postprocessing. Postprocessing of simulation results is performed in order to extract the desired information from computed flow field. In 1D, the function values are connected

by straight lines. In 2D, the results of scalars, such as the water level, concentrations or saturations, are presented with isoline or isoarea plots. The visualization module of UG was designed in a scalable way, so that large parallel simulations can be visualized in an efficient way. It employs the hierarchical data structure and is parallelized, thus avoiding unnecessary calculations in the process. Output can be drawn to the screen or to PostScript or Portable Pixmap (PPM) files (as well as to a native picture format). For more sophisticated visualization it is possible to write data in several visualization program formats: OpenDX/ Data Explorer, TecPlot, GRAPE and AVS. The visualization tool which has been used for this study is the TECPLOT system.

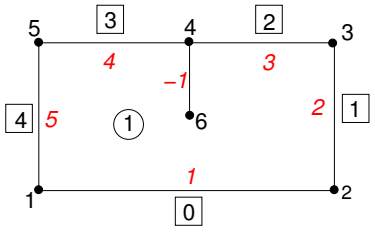

Control file: **default**

```
% Parameter for Delaunay_2D

type 2D                 % type of net: 2D or 2D
boudary input.bnd       % "domain" description
finename  input         % net data
density 0.02            % density of net
density_function 0      % density function


gen_net 6               % mesh with optimisation level 6
save_net                % save net to file
```

Density function for fracture: **dens.func**

```
−1:  0.005
```

Data input file: **input.bnd**

```
%%Version 3.0
%%VertexNumber: 6
%%EdgeNumber: 6
%%FaceNumber: 1
%%ElementNumber: 0
%%DO NOT CHANGE LINES ABOVE !!!!
%%Net: Vertices <–> Edge <–> Faces <–> Elements
%%Vertices: x y z
 0.00  0.00  0.00
 1.00  0.00  0.00
 1.00  0.50  0.00
 0.50  0.50  0.00
 0.00  0.50  0.00
 0.50  0.25  0.00
 $
%%Edges (Indices to List of Points)
 1:   0  1
 2:   1  2
 3:   2  3
 4:   3  4
 5:   4  0
 −1:  3  5
 $
%%Faces (Indices to List of Points)
 1: 0 1 2 3 4
 $
```

Figure 3.19: Data input for ART

3.4 Introduction to Geostatistical Methods

Most of the natural phenomena are variable in space and time. Time series analysis is one of the first fields where variability has been considered and described with stochastic methods. These methods were extended and further developed to analyse spatial variability. These spatial methods form the discipline called *geostatistics* (BARDOSSY (2004 [3]), YEH (2006 [108])).
What is Geostatistics? There are many definitions proposed in articles and texbooks. For example:
"Geostatistics: study of phenomena that vary in space and/or time" (DEUTSCH (2002 [27])).
"Geostatistics can be regarded as a collection of numerical techniques that deal with the characterization of spatial attributes, employing primarily random models in a manner similar to the way in which time series analysis characterizes temporal data" (OLEA (1999 [63])).
The word *geostatistics* is from the two parts, *geo* and *statistics*, similarly to geophysics or geochemistry. It is used with different meanings (see BARDOSSY (2004 [3])):

- as a collection of all stastical and probabilistical methods applied in geosciences or
- as another name for the theory of regionalized variables.

Compared to the classic approaches which examine the statistical distribution of sample data, geostatistics incorporates both the statistical distribution of sample data and the spatial correlation between the sample data. Because of this difference, many earth science problems are more effectively addressed using geostatistical methods.
Geostatistical methods were initially applied to mining engineering, but later found interesting applications in many other fields such as subsurface hydrology, meteorology, environmental sciences, agriculture, even structural engineering.
Before appling geostatistical methods to analyse the two-phase flow processes in porous media with a case study in chapter 6. Several basic definitions will be introduced in the following.

3.4.1 Stationary Processes

In geostatistics, the parameters of the governing equations are assumed to be *random spatial functions*. A *regionalized variable* is the realization of a random function. This means that for each point u in the d dimensional space, the value of the parameter being interested in, $z(u)$ is one realization of the random function $Z(u)$.

A stationary process is a random process in which none of its statistical properties varies with time. The random process consists of random variables at the location u in time and has all the properties of random variables, such as mean and variance.
A random process is classified as *strictly stationary* (or *strong stationary*) if its joint distributions are identical regardless of the separation vector h. The probability distribution of random variables with same configuration of points does not change:

$$P\left(Z(u_1), Z(u_1), ..., Z(u_n)\right) = P\left(Z(u_1+h), Z(u_1+h), ..., Z(u_n+h)\right) \tag{3.61}$$

Second-order stationary is a weaker form of the strictly stationary process. A random process is second-order stationary if the expected value of random function $Z(u)$ is constant over the whole domain D and the covariance of two random variables corresponding to two locations depends only on the vector h seperating two points:

$$E\left[Z(u)\right] = m \quad \text{for} \quad u \in D \tag{3.62}$$

$$E\left[(Z(u+h)-m)(Z(u)-m)\right] = Cov(h) \quad \text{for} \quad u, u+h \in D \tag{3.63}$$

The function $Cov(h)$ is called *covariance function.*
A random process is *intrinsic stationary* if the expected value of random fuction $Z(u)$ is constant over the whole domain D and the variance of the increment corresponding to two different locations depends only on the vector h seperating two points:

$$E\left[Z(u)\right] = m \quad \text{for} \quad u \in D \tag{3.64}$$

$$Var\left[Z(u+h)-Z(u)\right] = E\left[(Z(u+h)-Z(u))^2\right] = 2\gamma(h) \quad \text{for} \quad u, u+h \in D \tag{3.65}$$

The function $\gamma(h)$ is called *variogram* (also *semi-variogram* because of the 'half' in front of the equation):

$$\gamma(h) = \frac{1}{2}\text{Var}\left[Z(u+h)-Z(u)\right] \tag{3.66}$$

$$\gamma(h) = \frac{1}{2}E\left[(Z(u+h)-Z(u))^2\right] \tag{3.67}$$

$$= \frac{1}{2}\left(E\left[(Z(u+h))^2\right] - 2E\left[Z(u+h)Z(u)\right] + E\left[(Z(u))^2\right]\right) \tag{3.68}$$

$$\tag{3.69}$$

If the random process Z is second-oder stationary, the variogram can be related to the covariance:

$$\gamma(h) = Cov(0) - Cov(h) \tag{3.70}$$

3.4.2 Variogram Analysis

The variogram defined in Equation 3.67 and 3.68 is based on the ensemble concept. To derive a variogram from a data set, again, the ergodicity assumption must be invoked, and the variogram is called an *experimental variogram* or *empirical variogram*.
The experimental variogram $\gamma(h)$ can be defined as following function:

$$\gamma(h) = \frac{1}{2N(h)} \sum_{i=1}^{N(h)} \left(Z(u_i + h) - Z(u_i)\right)^2 \tag{3.71}$$

Here $Z(u_i)$ is the sample value at point u_i, h is distance or lag between observations, $N(h)$ is the number of data pairs of locations separated by the distance h.
In general, experimental variograms of a space data set are estimated from observed data using equation 3.71 in a discrete form. The experimental variogram generally fluctuates, in particular at large separation distances where the number of data pairs becomes small. For the sake of kriging (or stochastic simulation), the experimental variogram is replaced with an acceptable variogram model. An experimental variogram is often fitted with a continuous *theoretical variogram model* and the spatial structure of the data set is then described by the name of the theoretical model and its associated model parameters. Figure 3.20 gives an illustration of an experimental and theoretical variogram.
The constraint of the intrinsic hypothesis is satisfied when a variogram function is a positive-definite function. The variogram models imply that the adjacent data are more correlated than the remote data, which means the correlation decreases when the separating distance h increases. If the separating distance h is larger than a *range*, the data are no longer correlated and reach a plateau which is called a *sill*. There are many positive definite variograms available, using h to represent the distance, a to represent the (practical) range, and C to represent the sill. Some of those commonly used are introduced below. For comparison of the different variogram models, the curves of the four above variogram models with the same variance/sill and the same range are shown in Figure 3.21.

- Nugget model:

$$\gamma(h) = \begin{cases} C & \text{if} \quad h > 0 \\ 0 & \text{if} \quad h = 0 \end{cases} \tag{3.72}$$

  The nugget model represents the discontinuity at the origin due to small-scale variation. The abrupt change of the variogram from 0 (at $h = 0$) to C (at $h > 0$) indicates the variability of the variable over small scales or the measurement error. On its own it would represent a purely random variable, with no spatial correlation (see Figure 3.21).

- Spherical variogram model:

$$\gamma(h) = \begin{cases} C\left(\frac{3h}{2a} - \frac{1}{2}\left(\frac{h}{a}\right)^3\right) & \text{if} \quad h \leq a \\ C & \text{if} \quad h > a \end{cases} \tag{3.73}$$

  The spherical variogram model actually reaches the specified sill value, C, at the specified range, a (see Figure 3.21). In some articles, the model belongs to the group of *bounded models* (variance reaches a sill at some range).

- Exponential variogram model:

$$\gamma(h) = C\left(1 - e^{\frac{-h}{a}}\right) \quad \text{for} \quad a > 0 \tag{3.74}$$

Unlike the spherical variogram model, the exponential model has no well-defined range. The model line comes asymptotically to the sill. The practical range is the value of $3a$ where the variogram reaches 95% of the the sill value (see Figure 3.21).

- Gaussian variogram model:

$$\gamma(h) = C\left(1 - e^{\frac{-h^2}{a^2}}\right) \quad \text{for} \quad a > 0 \tag{3.75}$$

The Gaussian variogram model, with its parabolic behavior at the origin, represents very smoothly varying properties. The effective range is $\sqrt{3}a$ and slope at the origin is 0. This model differs from the exponential model at small angles, variances are close to zero in a 'halo' around each point (see Figure 3.21). In some articles, the exponential and Gaussian variogram model belong to the group of *bounded asymptotic models* (variance approaches a sill at some effective range).

Each of the theoretical variogram models as well as the covariance models represents some type of heterogeneity pattern (perhaps, geologic depositional environment). In fact, only subtle differences exist between spherical, exponential, and Gaussian variogram models. More importantly, to accurately select a correct model for a data set, a very densely sampled data set is required. As a densely sampled data set becomes available, a deterministic approach is resorted in many situations as well. Therefore, the simple model such as the exponential model is highly desirable and it is widely used (YEH (2006 [108])). In this study, the object that we have been dealing with is subsurface simulations with properties, i.e. permeability field, fracture field. The exponential variogram model is chosen. The model has been applied for simulations of the permeability field in a natural slope and the detailed processes are discussed in section 6.4.

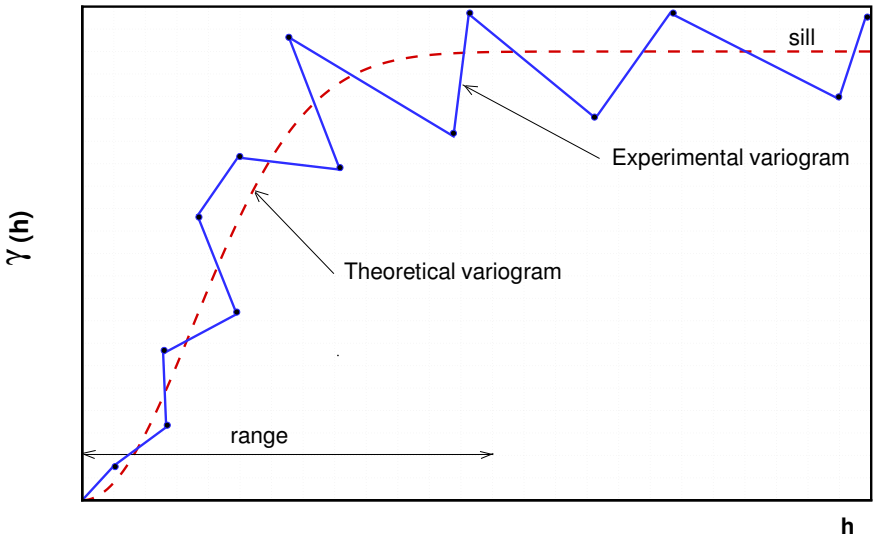

Figure 3.20: An illustration of an experimental variogram and theoretical variogram

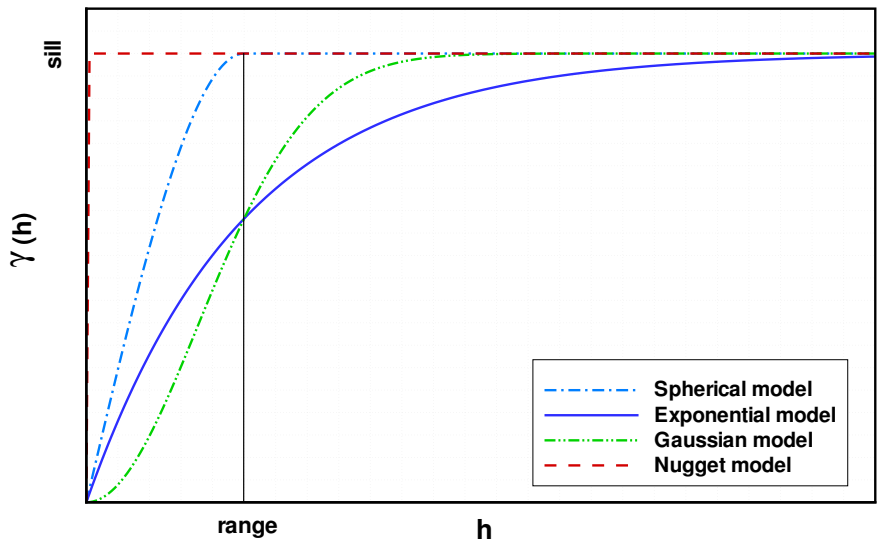

Figure 3.21: Theoretical variogram models: Nugget model, Spherical model, Gaussian model and Exponential model

Chapter 4

Water Infiltration Processes in a Vertical Fault Zone

4.1 Introduction

Porous media with fault zones can be very complex. In natural systems, porous media may have many fractures inside. To compare the different model concepts, first a very simple and academic case is investigated dealing with two-phase flow processes in porous media with a vertical fault zone. This example is set up to assess the differences between three different model concepts: *2D fracture model concept*, *1D fracture model concept* and *fracture with pipe model concept* (see section 2.4).
Normally, the saturated/unsaturated water flow in porous media is mathematically described by the Richards equation (see section 1.2). For such infiltration processes, this model concept would determine very similar results. Here, an active gas phase is of minor importance compared to the two-phase flow model concept chosen here (see section 3.2). A detailed disscusion is presented in PHAM VAN and HINKELMANN (2005 [71]), PHAM VAN et al (2006 [72]), PHAM VAN and HINKELMANN (2007 [73]).

4.2 Model Concepts

4.2.1 2D Fracture Model Concept

Fractured porous medium is defined by two subdomains with different properties, the fracture and the matrix. This system is characterized by a high permeability within the fracture and a low permeability within the matrix. The 2D fracture model concept takes the fracture and the matrix into account as elements of the same dimension. Here, the fracture is set as the two-dimensional element in the two-dimensional domain. Therefore,

the mesh is highly resolved in the fracture as well as in its close surroundings (see Figure 4.1).

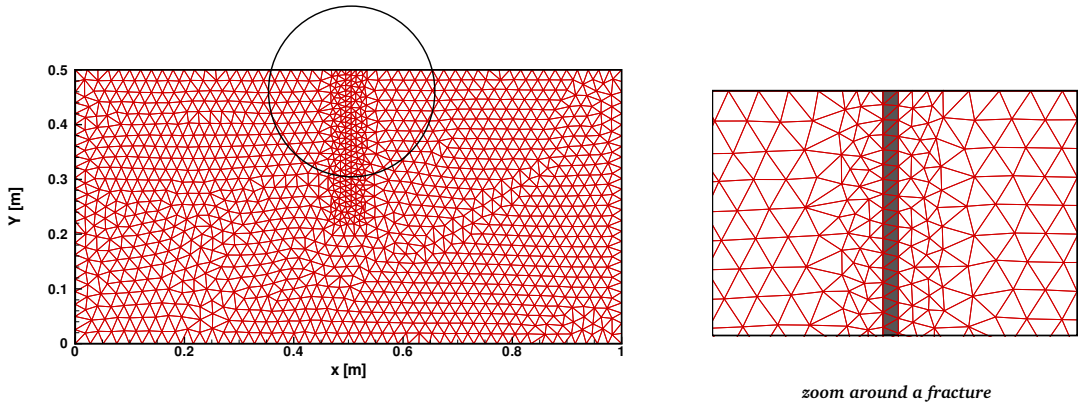

Figure 4.1: Mesh for the 2D fracture model concept (left), zoom around a fracture (right)

4.2.2 1D Fracture Model Concept

On meso- and large scales, the 2D fracture model concept cannot be used in a larger domain due to the limitations of the CPU time. The 1D fracture model concept is based on the combined model approach, i.e. fractures are considered as elements of lower dimension, for example as one-dimensional elements in a two-dimensional domain. Generally, the mesh resolution of the fracture-matrix space is coarser compared to the 2D fracture model concept (see Figure 4.2). However, to compare both model concepts, approximately the same mesh resolution is chosen here with 2641nodes.

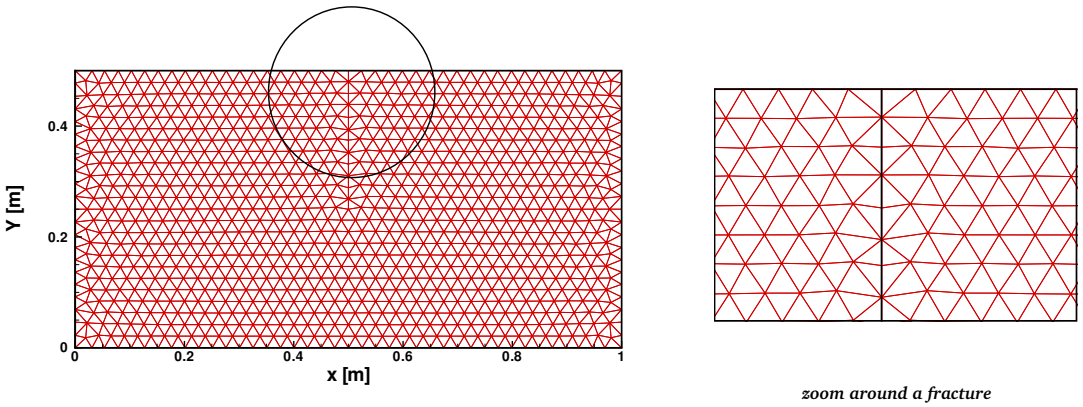

Figure 4.2: Mesh for the 1D fracture model concept (left), zoom around a fracture (right)

4.2.3 Fracture with Pipe Model Concept

As the fracture permeability is much higher than the matrix, the flow velocities in fractures are also much higher. The fractures or macropores in the soil are commonly referred to as 'soil pipes' and concentrated subsurface flow of water in these natural soil pipes is called 'pipeflow' (e.g. BEVEN and GERMANN (1982 [12]), UCHIDA et al. (2001[95])). To set off the fracture model and illustrate the flow mechanism, a so-called 'pipe model' is introduced for simulation (see Figure 4.3). In this simple concept, the fracture is idealised as an open pipe. The water pressure in the pipe must be computed or estimated and it is prescribed as a Dirichlet boundary condition along the pipe wall.

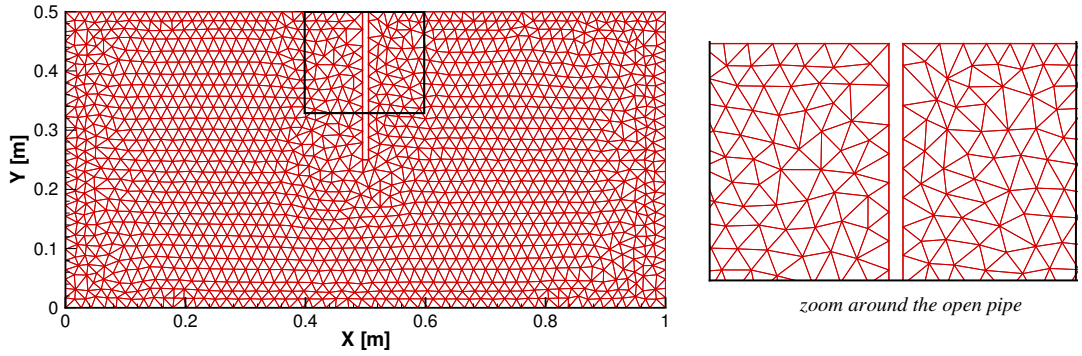

Figure 4.3: Mesh for pipe model concept (left), zoom around the pipe (right)

4.3 Numerical Simulation

4.3.1 Model Setup

The rectangular domain of 1m x 0.5m shown in Figure 4.1, 4.2 and 4.3 is chosen for the simulations. The setup includes one vertical fracture inside the domain. The fracture is located along the line from (x=0.5m , y=0.25m) to (x=0.5m , y=0.5m). Water infiltration processes are investigated in the system with the Dirichlet boundary condition (bc) on the top. The water height is set to 1cm equivalent to pressure of 100100Pa. This is an idealization of a heavy rainfall resulting in runoff with a 1cm water level. The other sides of the domain are closed (Neumann no flow bc) (see Figure 4.4). The domain has the permeability $K_m = 10^{-12}m^2$ and the porosity $\phi = 0.57$, and the fracture has the permeability $K_f = 10^{-9}m^2$, the porosity $\phi = 0.9$ and the fracture width $b = 1cm$. The constitutive relationships of Brooks-Corey are chosen in this simulation with the parameters $\lambda^m = 2$, $p_d^m = 2000Pa$ in matrix and $\lambda^f = 2$, $p_d^f = 63Pa$ in the fracture

based on Leverett scaling function (see section 3.2). Initially, the gas saturation is set to $S_{n0} = 0.9$. The other parameters in the domain are set as follows:

$\rho_w = 1000\ [kg/m^3]$	$\rho_n = \frac{p_n}{RT}[kg/m^3]$
$\mu_w = 10^{-3}\ [Pas]$	$\mu_g = 1.65 \cdot 10^{-5}\ [Pas]$
$S^m_{wr} = 0.1$	$S^f_{wr} = 0.1$
$S^m_{nr} = 0.01$	$S^f_{nr} = 0.01$

Table 4.1: Parameters set up in the domain

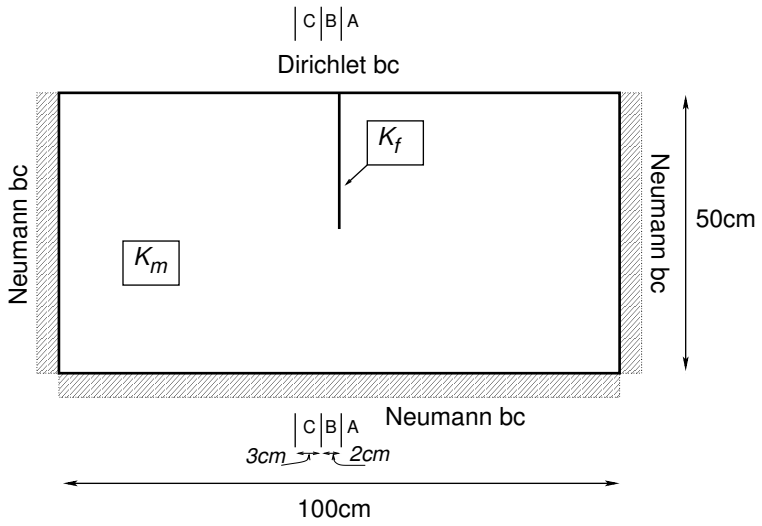

Figure 4.4: Sketch of the domain with one vertical fracture

4.3.2 Simulation Results

To examine the infiltration processes, three cross sections are considered in the system: cut A-A lies directly in the axis of the fracture, cut B-B has a distance of 2cm and cut C-C of 5cm from the fracture axis (see Figure 4.4). Figure 4.5 and Figure 4.6 show the water saturation fields and water saturation distributions at different time steps in the domain with the 2D fracture and the 1D fracture model concepts, respectively. For detailed investigation, the water saturation distributions along the cut A-A, cut B-B and cut C-C are drawn in these figures. From the results several conclusions can be drawn out as following:

Firstly, due to a very high permeability in the fracture, the water movement in the fracture is much faster than in the matrix. As can be seen in Figure 4.5 and 4.6 at the time step t =30s that the water has already reached the bottom of the fracture.

The fracture geometry has a notable influence on the simulation results. If the fracture thickness increases, the faster water front occurs in the domain.
In the simulation, the flow in the fracture follows the validity of the Darcy law (see more in section 2.3). The permeability of the fracture is chosen as $K_f = 10^{-9}m^2$ and it is three orders of magnitudes higher compared to the permeability in the matrix. When the fracture permeability is higher, the validity of Darcy law can be violated. If the permeability of fracture increases to larger than $K_f = 9 \cdot 10^{-6}m^2$, numerical problems can occur.
The results show an overall very good agreement between two model concepts: 2D fracture model concept and 1D fracture model concept. Theoretically, the domain with the 2D fracture model concept needs longer CPU simulation time conpared to the 1D fracture model concept because of the finer mesh surrouding the fracture. For the small scale, the difference is small. Therefore, both model concepts (2D and 1D fracture) are suitable for this scale.
In some cases, the fractures or macropores in the soil are commonly referred to as soil pipes and for this case, the fracture can be idealised as an open pipe (see more in section 2.4). As the simple example, the Dirictlet boundary condition (bc) is set along the pipe wall. Two examples are set up for simulation here: water pressure is prescribed as a *hydrostatic bc* and a *atmospheric bc* in the pipe (see Figure 4.8).
The first example is chosen as a reference case: water pressure is prescribed as the hydrostatic pressure bc along the pipe wall. The pipe is filled up with water. Figure 4.7 shows the water saturations computed using the pipe model concept after $t = 30s$, $t = 10min$ and $t = 40min$. Big differences can be observed in the simulation results compared to the domain with 1D and 2D fracture model concepts. They are illustrated in Figure 4.9, Figure 4.10 and Figure 4.11 in detail. The results show a faster water infiltration process into the system compared to the 1D and 2D fracture model concepts. The water flow is over-estimated with open pipe model concept. The reason for these differences can be explained inside the model itself. Using pipe model concept as reference case, the water pressure is prescribed as a hydrostatic bc and the fracture (as an open pipe) is always full with water and the capillarity is not included in this case. There are no flux limitations in the fracture and the gas can not escape from the system.
Second example for the pipe model concept is the ideal case that the water pressure is prescribed as the atmospheric bc in the pipe (Figure 4.8). That means the water pressure along the pipe wall is set as atmospheric pressure $p_w = 1 \cdot 10^5 Pa$. For this case, the result is quite different because the flow in the fracture is under-estimated. The comparison of three above cases is shown in Figure 4.12.

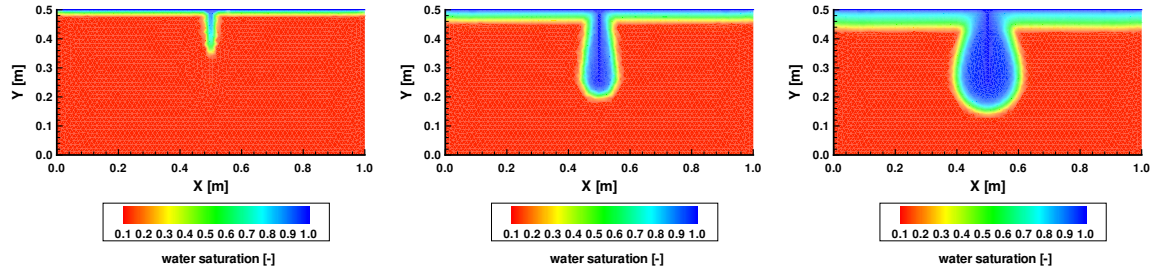

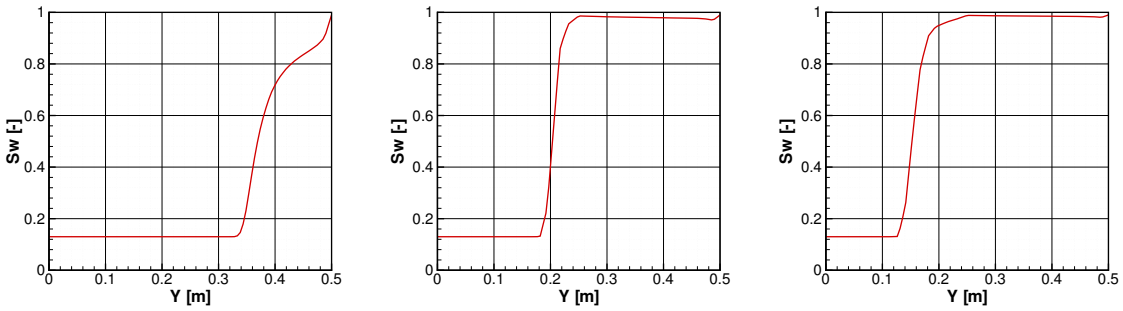

cut A-A, t=30s cut A-A, t=10min cut A-A, t=40min

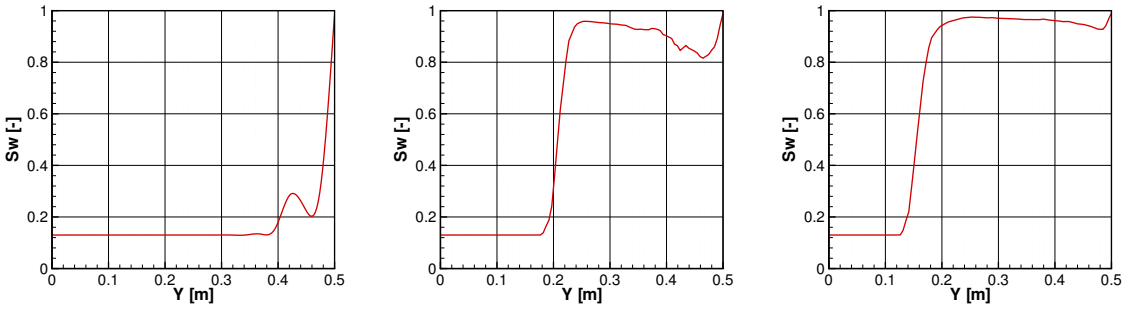

cut B-B, t=30s cut B-B, t=10min cut B-B, t=40min

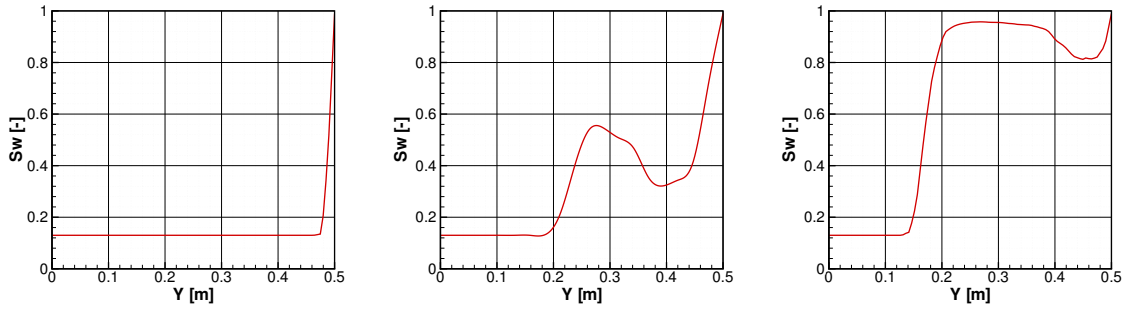

cut C-C, t=30s cut C-C, t=10min cut C-C, t=40min

Figure 4.5: Water saturation $S_w[-]$ computed with the 2D fracture model concept

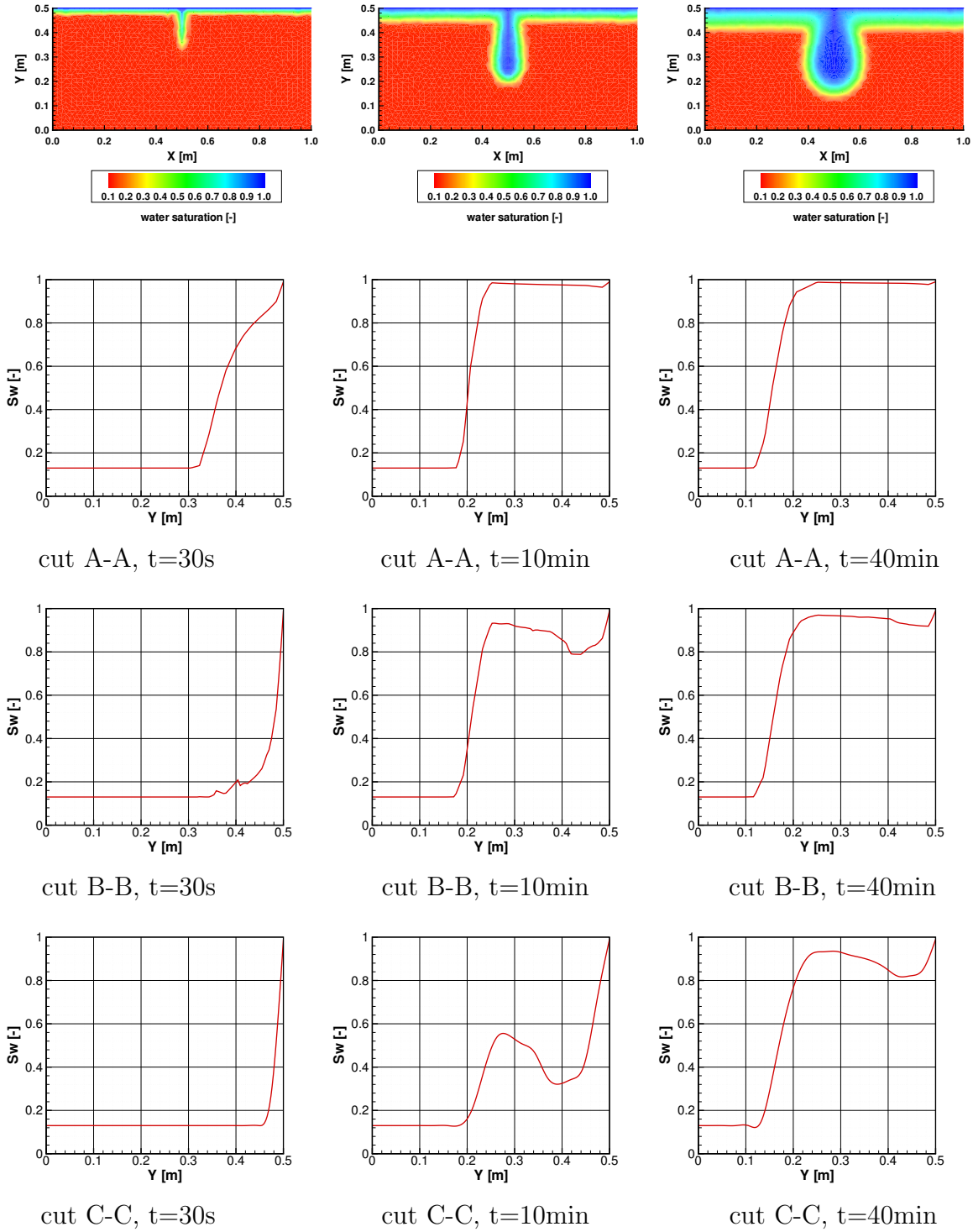

Figure 4.6: Water saturation $S_w[-]$ computed with the 1D fracture model concept

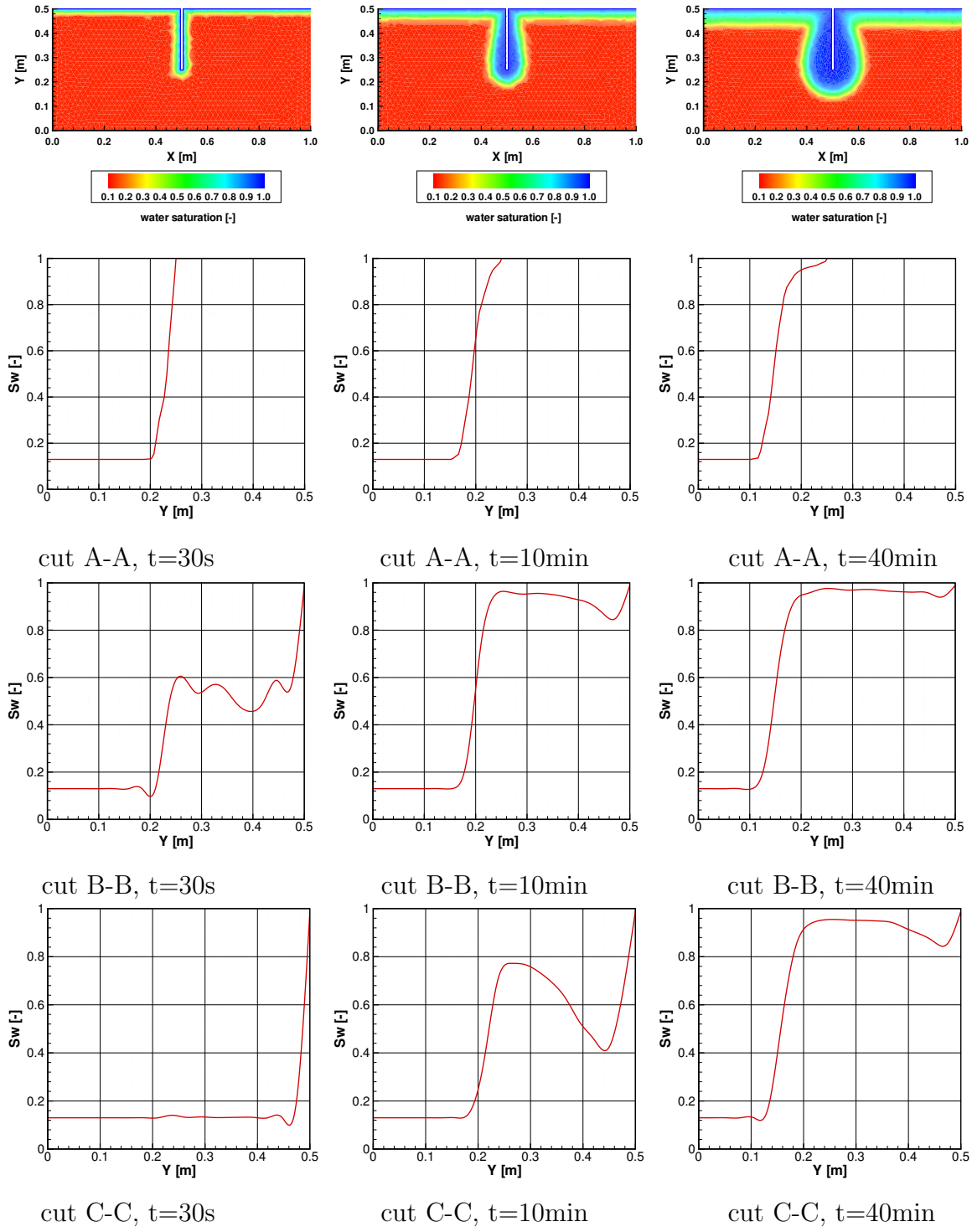

Figure 4.7: Water saturation $S_w[-]$ computed with pipe model concept after t=30s (left), t=10min (middle), t=40min (right)

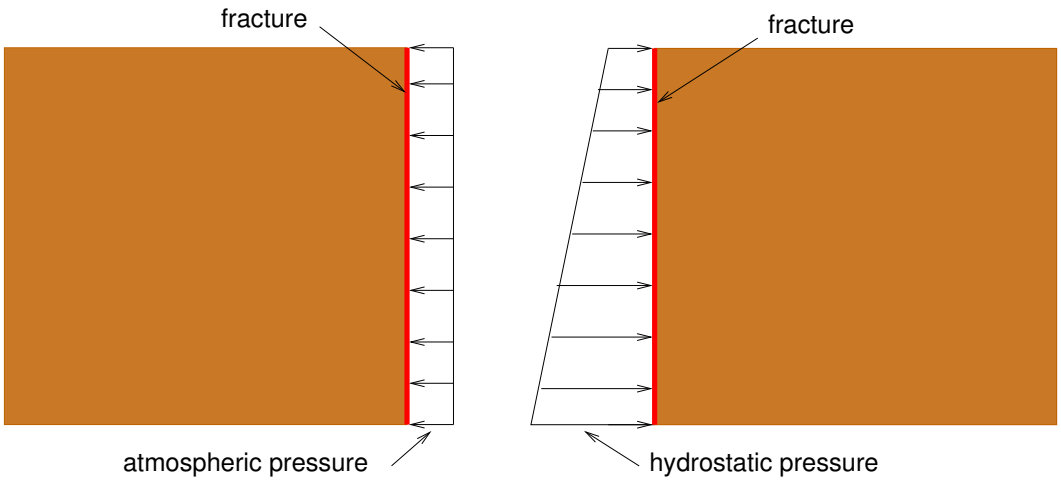

Figure 4.8: Schematic view of a fracture as a pipe model concept: (left) pipe with atmospheric pressure bc, (right) pipe as hydrostatic pressure bc

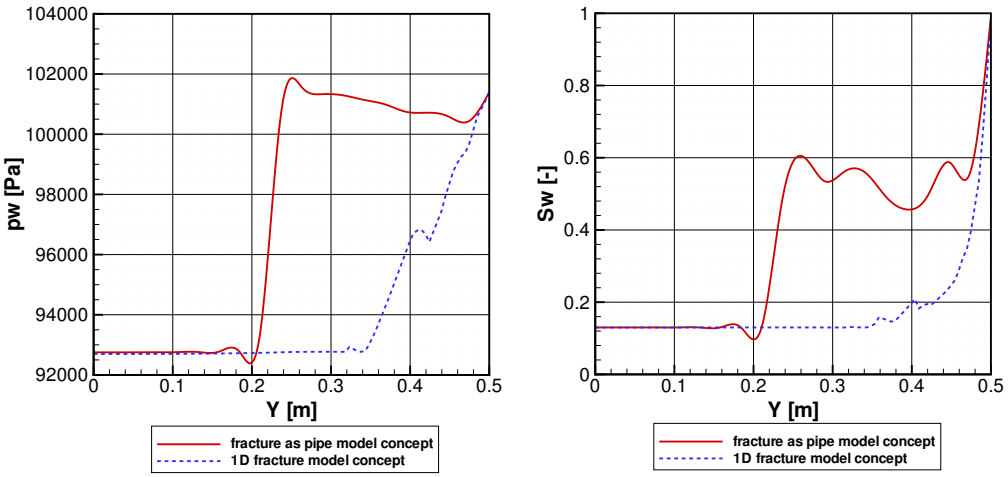

Figure 4.9: Water pressure $p_w[Pa]$ (left) and water saturation distribution $S_w[-]$ (right) along cut B-B after t = 30s computed by the 1D fracture model concept and fracture as pipe model concept

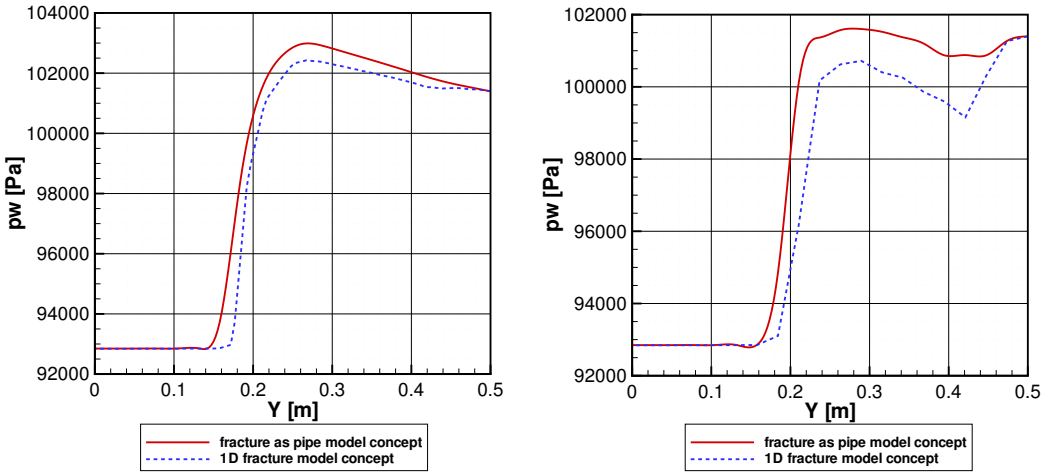

Figure 4.10: Water pressure distribution $p_w[Pa]$ along cut B-B (left) and cut C-C (right) after t = 10min computed by the 1D fracture model concept and fracture as pipe model concept

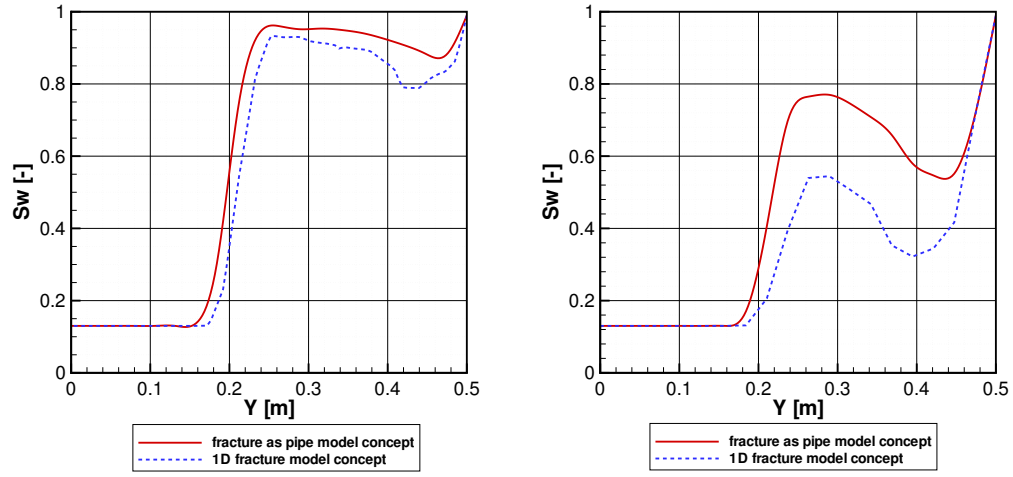

Figure 4.11: Water saturation distribution $S_w[-]$ along cut B-B (left) and cut C-C (right) after t = 10min computed by the 1D fracture model concept and fracture as pipe model concept

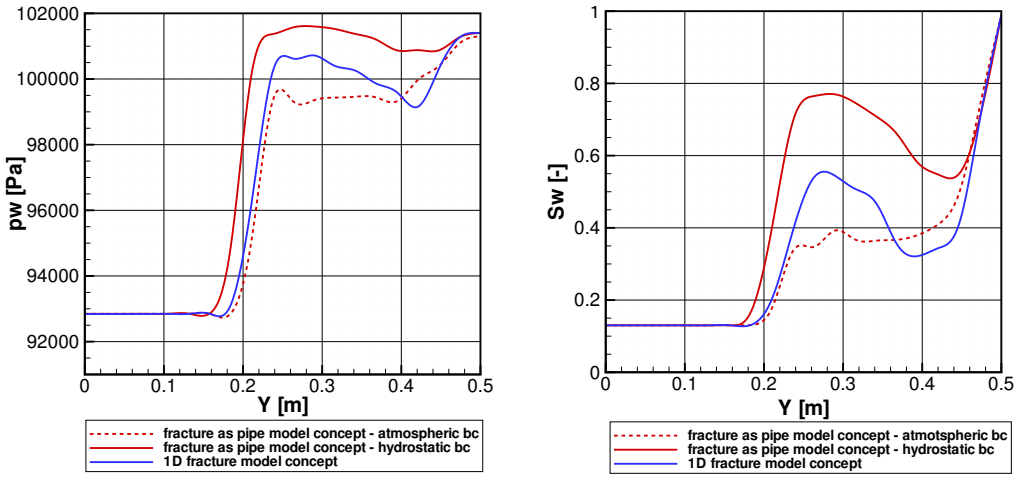

Figure 4.12: Comparison of the water pressure $p_w[Pa]$ (left) and water saturation distribution $S_w[-]$ (right) along cut C-C in cases of fracture as pipe model concepts and 1D fracture model concept

4.4 Conclusions

In this chapter, the two-phase flow processes are investigated on a small scale domain with a vertical fault zone (fracture). Three different model concepts are used for numerical simulation: *2D fracture model concept*, *1D fracture model concept* and *fracture with pipe model concept*.

In the domain with the 2D fracture model concept, a fault zone is discretized as a two-dimensional element in the two-dimensional domain and the mesh is highly resolved in the fault zone as well as in its close surroundings. Contrastly, in the domain with the 1D fracture model concept, the fault zone is discretized as a one-dimensional element in a two-dimensional domain and the mesh resolution of the fracture-matrix space is coarser compared to the domain with 2D fracture model concept. In the domain with a fracture as pipe model concept, the fault zone is idealised as an open pipe and a Dirichlet boundary condition is set up along the pipe wall. For this example, two cases are used for investigation: water pressure is prescribed as a hydrostatic bc and as an atmospheric bc in the pipe.

After applying the different model concepts for two-phase flow simulation, the results have been analysed and compared to each other. Due to a very high permeability in the fracture, the water movement in the fracture is much faster than in the matrix and the fracture geometry has a notable influence on the simulation results. The results show an overall very good agreement between two model concepts: 2D fracture model concept and 1D fracture model concept. Theoretically, the domain with the 2D fracture model concept

needs longer CPU simulation time compared to the 1D fracture model concept because of the finer mesh surrouding the fracture. In this small-scale example, the difference is small. Therefore, both model concepts (2D and 1D fracture) are suitable for this scale. In the domain with a fracture using the pipe model concept, different results can be seen compared to the previous model concepts. The water infiltration process is over-estimatimated in the domain with the hydrostatic bc along the pipe wall. Even though, in the domain with the atmospheric bc in the pipe wall, the water infiltration process is under-estimatimated. In such cases, pipe model concepts are not suitable.

Chapter 5

Seepage Processes through a Dike with a Fault Zone

5.1 Problem Description

A large part of the world population lives close to oceans, seas, lakes and rivers, of course they need dikes. That is why dikes play an important role for the protection of human life and goods. In long history, the failures of dikes causes big damages for human lives and goods. The causes and failure mechanisms of the dikes are quite complex. Figure 5.1 shows the failure mechanisms that can occur in dikes (see e.g. VRIJING (1994 [100]), OUMERACI and SCHÜTTRUMPF (1999 [64]), KORTENHAUS et al. (2002 [51]), VAN BAAR (2005 [97])).

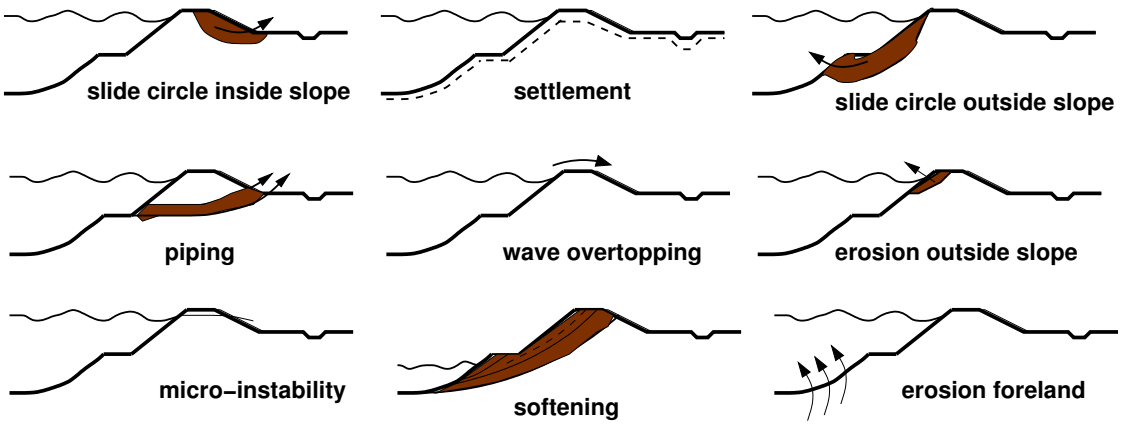

Figure 5.1: Dike failure mechanisms (VRIJING (1994 [100]))

A dike failure is often the result of different effects during a high-water level event. One of the failure mechanisms is overflow or wave overtopping (Figure 5.2). With this failure

mechanism, the dike collapses because large quantities of water run over the top of the dike or because the waves break over the dike. During high floods, dikes are stressed by an increasing water level. The water percolates through the dike body and may cause instabilities due to processes of suffusion and erosion.
Figure 5.3 shows the model concept of the overtopping dike (see PAUL et al. (2000 [67]), PAUL (2003 [65]) and HINKELMANN et al. (2005 [43])). In this case, the surface wave is coupled with the flow in the porous medium along the common interface via the pressure. The pressure field coming from the surface waves can be computed by a wave model or it can be taken from experimental or field data.

Figure 5.2: Water overtopping event at a dike (left), breaking dike (right)

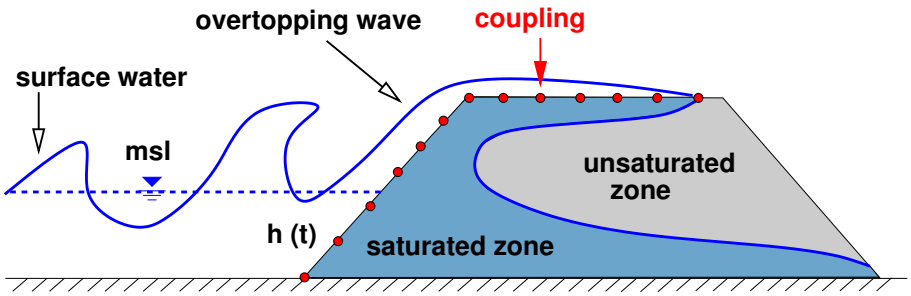

Figure 5.3: Model concept of overtopping dike (after PAUL et al. (2000 [67]))

Statistics from the International Commission on Large Dams (ICOLD 1995) show that dike problems and failures are often related to internal erosion in one way or another. The existing fault zones in dikes such as macropores, void spaces or inhomogeneities caused by animals, roots of dead plants or construction measures can increase these processes (Figure 5.4). Due to the pressure of the water the sealing layer of clay behind the dike, if present, first uplifts (becomes raised). This allows the “piping” to take place, in which the sand is washed away and the dike subsides (collapses). With this mechanism, the dike collapses due to sand being washed away from under the dike.

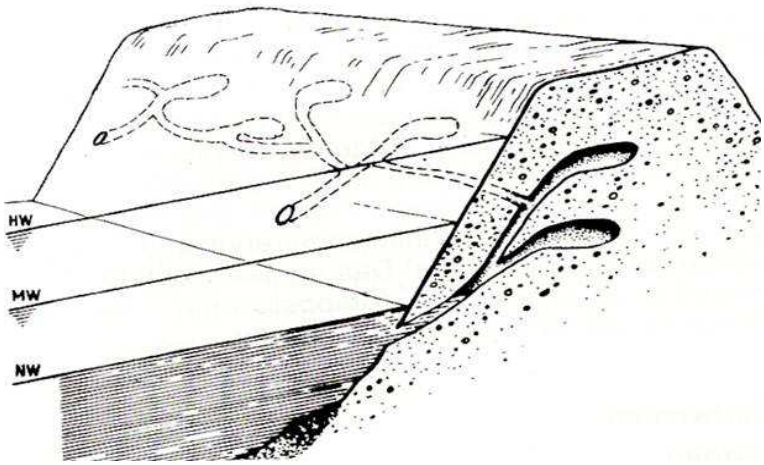

Figure 5.4: A typical dike model with fault zones or piping inside

Normally, problems with a "simple" free-surface in the dike system can be treated with a groundwater flow model which determines the free water surface iteratively. This is, for example, the case for seepage problems when the water level on the seaside is higher than on the landside (see WIBBELER (1995 [107]), HASELSTEINER (2007 [37])). However, the influences of capillarity and variable initial water saturation in unsaturated zones in dikes are not accounted for in such a model.
The flow processes in dike systems can be modeled as the flow of soil water in unsaturated zone using the Richards equation (see section 1.2). This model is based on the implicit assumption that the soil water freely flows through the porous medium: A change of water content goes together with a change of gas content and therefore with the flow of the gas. The air phase essentially remains at a constant pressure, equal to atmospheric; the system is then reduced to the consideration of the water phase only. This assumption is feasible since the density of air is about 1% of that of water for small to medium water saturations. Under certain circumstances, however, larger packages of gas may be trapped within fairly wet soil. Then, the extremely small relative permeability of gas at high water saturations makes it difficult for the gas to escape. When overflowing occurs in dikes, the shape of the free-surface might be very complex (Figure 5.3) and regions with entrapped air may occur which can be pressed out at the landside boundary (D'ELISO et al. (2006 [29])). To overcome the above problems and to work with a more general tool which is also capable of simulating active gas flow in partially saturated soils, the two-phase flow model concept for porous media is generally recommended and chosen for analyzing the water infiltration processes in the dikes with fault zones.

The different model concepts for the fault zone have been applied in the small scale domain described in the chapter 4. The model concepts should be further investigated and compared to controlled laboratory experiments before being transfered to larger scales. The following work aims to discuss issues such as the evaluation of numerical model introduced in chapter 3, the reliability of different approaches from the numerical and the experimental point of view. For these purposes, a two-phase flow model concept is applied in the laboratory scale. Here, a dike on a laboratory scale is used for simulation. The results from numerical simulations are compared to laboratory experiments performed in the Chair of Hydraulic Engineering, Technische Universität Berlin, Germany (see PLESCHER and HAMM (2005 [79]), MINACK (2005 [59]), HINKELMANN et al. (2005 [43])). The experiments include a homogeneous sand dike and one with a horizontal fault zone at different locations.

Detailed information about this work is also given in ROUALT et al. (2006 [82]), PHAM VAN and HINKELMANN (2008 [74]), PHAM VAN et al. (2008 [75])

5.2 Laboratory Experiments

As part of a research project on dike monitoring, a physical model of a dike was built at the Chair of Hydraulic Engineering, Technische Universität Berlin. A dike with a scale 1:8 had dimensions of 0.6m height, 4.0m length and 0.4m width (Figure 5.5). The installation was made on smooth PVC bed and glass walls. The inflow to the dike experiment (on the seaside) was controlled by a gate and a pump was set up here to measure the water discharge (Figure 5.6). The experiment is conducted with a quartz sand with grain size diameters ranging from 0.06 to 3.0mm (see Figure 5.9). The material for the experiments used here has a measured hydraulic conductivity $K_f = 0.95 \cdot 10^{-4} m/s$, density $\rho = 1.78 kg/m^3$ and initial moisture $w = 11.5\%$ and porosity $\phi = 0.49$. The fault zone in the dike was made out of a system of several highly porous pipes being perforated to a porosity of 0.5 to allow the water to enter from all directions. The fault has a $2cm$ thickness and it is located on the seaside or the landside of the dike.
The model was equipped with several sensors to automatically acquire the experimental data. The electrical method has been used for measurements on the physical model. To measure the seepage processes, a system of electrical gauges was set up along the dike (see Figure 5.7 and Figure 5.8). The discharge Q through the dike was also measured during the experiment.

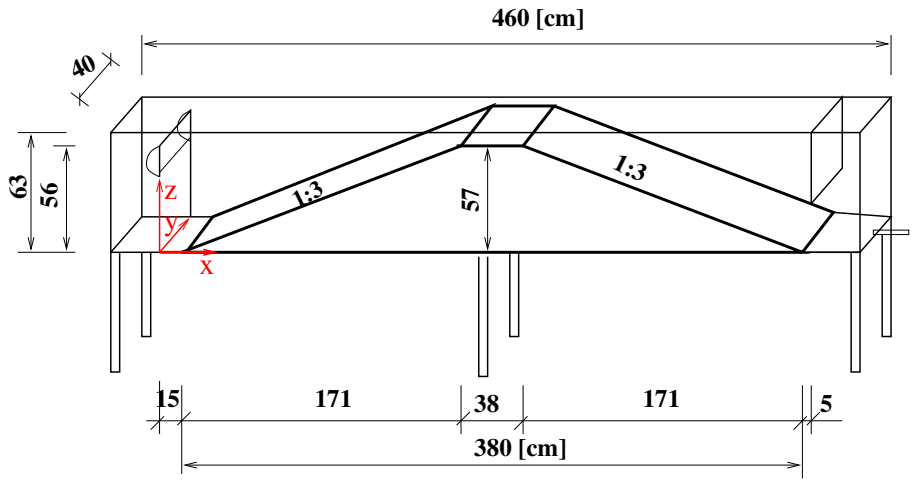

Figure 5.5: Schematic experimental setup

Figure 5.6: View on the experimental dike

Figure 5.7: Water level gauges in the dike

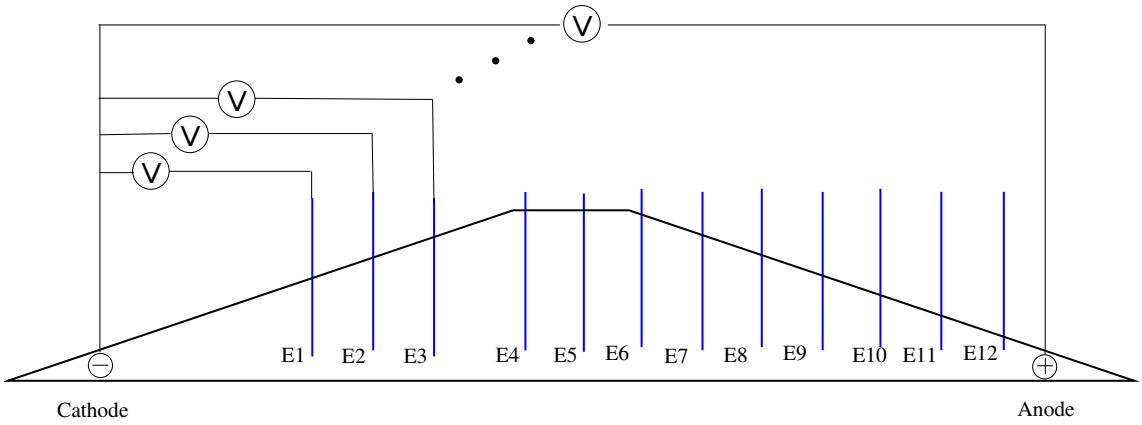

Figure 5.8: Installation of electrodes in the dikes

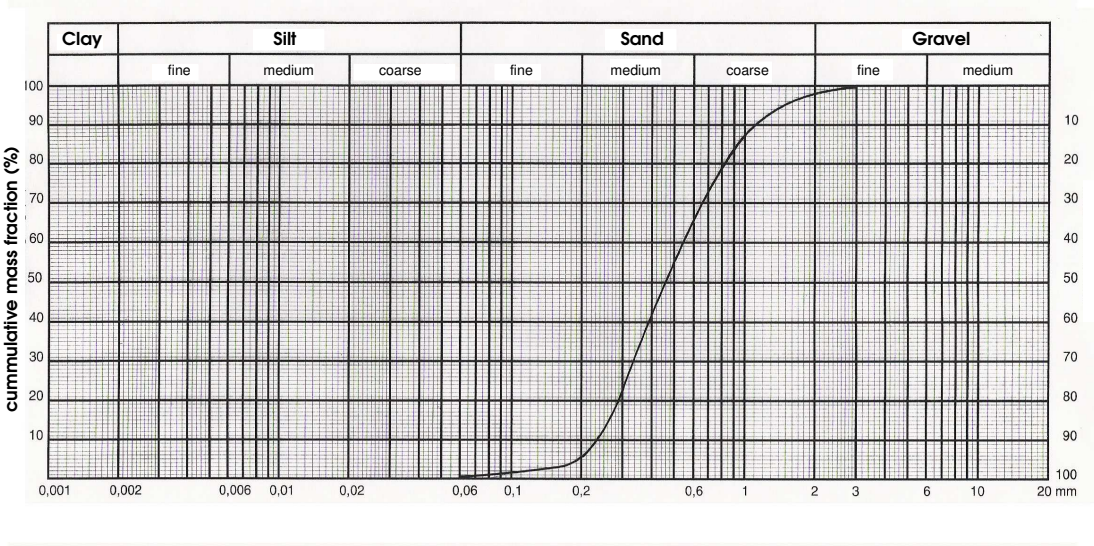

Figure 5.9: Grain size distribution of the dike material

Several experiments were performed with the dike. The purposes are investigating the water infiltration processes in the dike under different conditions. The inflow in the tests involved in most of the cases has been controlled by the gate in upstream. Therefore, the upstream water level is increased during the time. The results are shown in Figure 5.11.
First experiments were carried out with a homogeneous dike. On the seaside of the dike, a discharge was pumped until the water level reaches to $h = 0.48m$ at time $t = 1h25min$ (see Figure 5.10). The water front evolution in this case is given in Figure 5.11a. The seepage lines for different time steps can be seen in the results. The steady state occurred after about $t = 2h30min$.
Similar experiments were carried out with different locations of the fault zone in the dike (on the seaside and the landside). Figure 5.11b presents the water front evolution with a fault zone on the seaside. The time for steady state is about $t = 1h55min$. Figure 5.11c shows the water front evolution in the dike with a fault zone on the landside. For this case, the steady state occurred approximately after $t = 2h20min$. Because of fault zone influences, erosion was observed in the downstream of dike from time step $t = 1h25min$.

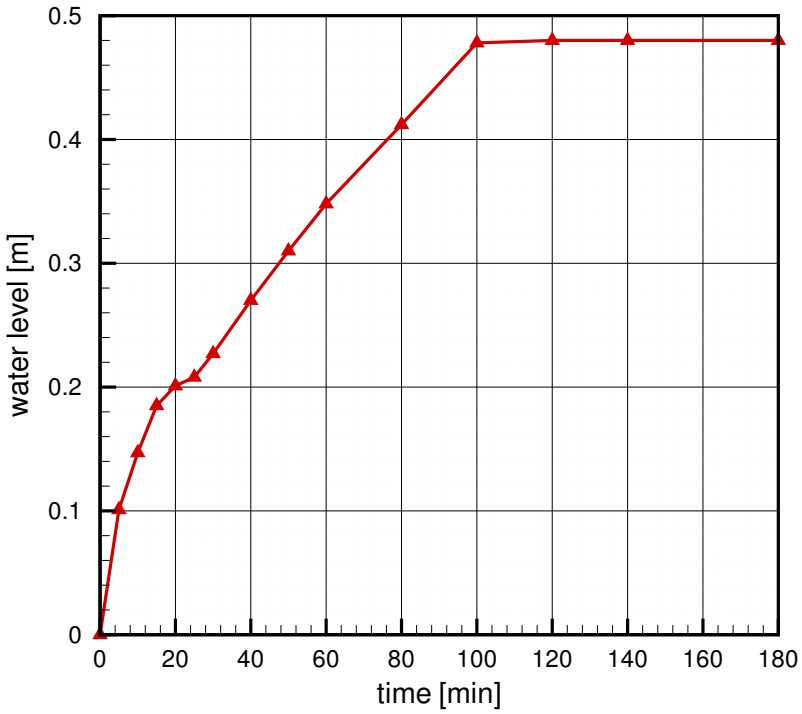

Figure 5.10: Increasing water level for seaside boundary condition

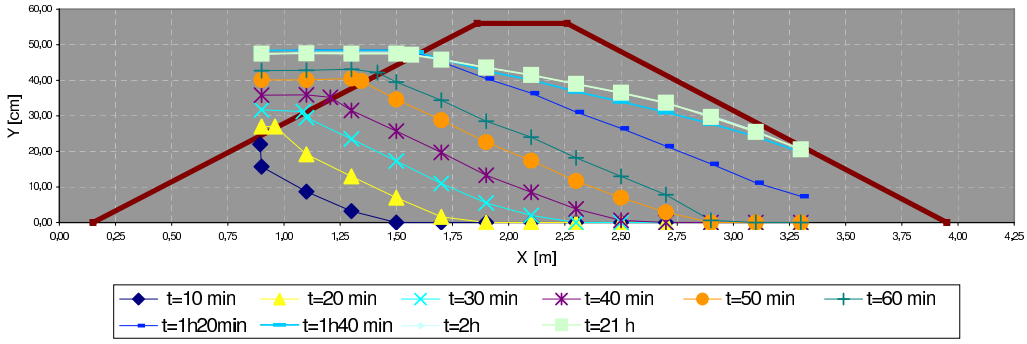

(a)

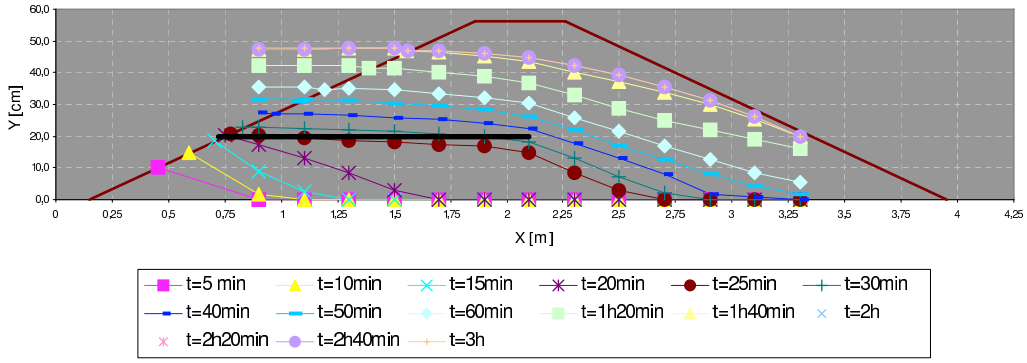

(b)

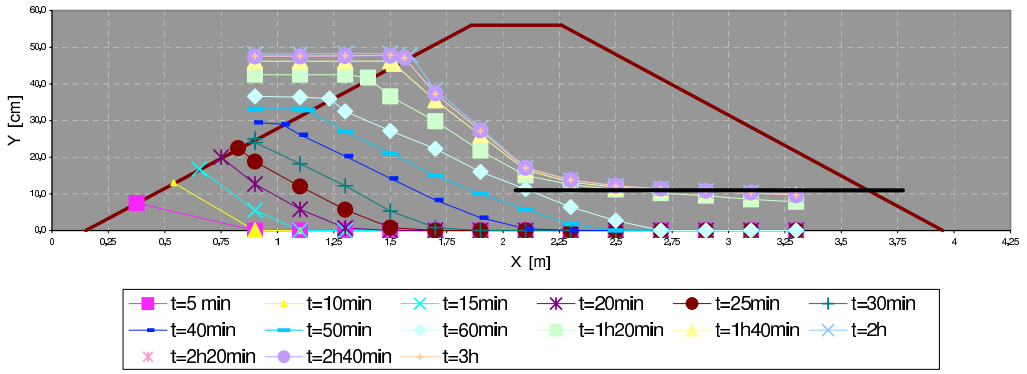

(c)

Figure 5.11: Experimental results in the dike: (a) homogeneous case, (b) dike with a fault zone on the seaside and (c) dike with a fault zone on the landside

5.3 Numerical Simulations

5.3.1 System and Parameters

For numerical simulations, the dike system shown in Figure 5.5 has been chosen. Four different cases are investigated: *homogeneous dike, dike with 2D fault zone model concept, dike with 1D fault zone model concept* and *dike with fault zone with pipe model concept.* The results are compared to the experimental results of section 5.2. Initially, the saturation of water S_w in the model domain is equal to 0.22 corresponding to the measured water content $w = 0.115$ (see section 5.2) and the gas pressure p_w is set to be atmospheric.
On the seaside, time dependent Dirichlet boundary conditions (bc) are applied for the water and gas phase. The maximal water level reaches to $h = 0.48m$ after time $t = 1h25min$ in the experiments (see Figure 5.10). Therefore, the water level can be calculated as a function of the time variable. The following lines show the implementation of the time dependent boundary conditions (bc) and their values for one boundary segment in the MUFTE code (given in the c-file (*.c).

```
time = in[IN_T];
waterlv=(((sqrt(576 + 960*((t-startt*60.0*60.0)/60)))-24)/480);
bndType[OUT_BNDTYP_pw] = DIRICHLET;
bndType[OUT_BNDTYP_Sn] = DIRICHLET;
pw = 1.013e5 +(Rhow * grav * (waterlv-h));
Sn = 0.0;
```

On the bottom, the Neumann no flow boundary condition is set up. The other sides of the dike are atmospheric Dirichlet boundary conditions.
In the homogeneous case, the dike has the permeability $K = 0.95 \cdot 10^{-11} m^2$, corresponding to the measured hydraulic conductivity $K_f = 0.95 \cdot 10^{-4} m/s$, and it has the porosity $\phi = 0.49$. The fluid properties of water are $\rho_w = 10^3 kg/m^3$, $\mu_w = 10^{-3} Pas$ and of air are $\rho_g = 1.2 kg/m^3$, $\mu_w = 1.8 \cdot 10^{-5} Pas$. Based on measurements with a similar sand carried out by SHETA (1999 [86]), the constitutive relationships of Brooks-Corey are chosen with the parameters $\lambda = 2.0$, $p_d = 350 Pa$. Residual water and gas (air) saturations are set to $S_{wr} = 0.01$, $S_{gr} = 0.05$.
In the heterogeneous cases (dike with fault zone), the permeability in the fault zone is set to $K^f = 1 \cdot 10^{-9} m^2$, the porosity of the fault zone $\phi^f = 0.9$ and the fault zone thickness $b = 2cm$. The Brooks-Corey parameters are calculated by the Leverett function (see LEVERETT (1941 [53]), SHETA (1999 [86]) and PHAM VAN (2004 [68])):

$$J = p_d \sqrt{\frac{K}{\phi}} \tag{5.1}$$

By scaling the entry pressure p_d and neglecting the effect of porosity ϕ, the entry pressure in the fault zone p_d^f can be determined as follows:

$$p_d^f = p_d^m \sqrt{\frac{K^m}{K^f}} \tag{5.2}$$

Therefore, in the fault zone, the Brooks-Corey parameters were set to $\lambda^f = 2.0$, $p_d^f = 35Pa$ ($\lambda^m = 2.0$, $p_d^m = 350Pa$ in the matrix).
For the hererogeneous cases, different model concepts are chosen (in chapter 4): 2D fault zone model concept, 1D fault zone model concept and fault zone with pipe model concept. In the dike with 2D fault zone model concept, the fault zone was treated as a 2D porous medium. It is characterized by a higher permeability compared to the matrix. The mesh is highly resolved in the fault zone as well as in its close surroundings (Figure 5.12 (upper part) and Figure 5.13).
In the dike with 1D fault zone model concept, to overcome the problem with highly resolved meshes in and around the fault zone, a fault zone in the dike can be discretized as elements of lower dimension (a one-dimensional fault zone in a two-dimensional domain) (see Figure 5.12 (middle part)).
In the case of dike with fault zone with pipe model concept, a 2cm opening on the seaside is chosen (see the mesh in Figure 5.12 (lower part)). As a simple approach, a hydrostatic pressure was set as Dirichlet bc along the pipe wall.

5.3.2 Homogeneous Dike

The comparisons of the experimental and numerical results for water infiltration processes in the dike at different time steps are given in Figure 5.14 at $t = 60min$ and in Figure 5.15 at $t = 1h20min$. The results show an overall good agreement. Due to the small entry pressure p_d in the model, the influences of the capillarity are small in the numerical results. The system reaches steady state after $t = 2h10min$ (Figure 5.16 (upper)). In a two-phase flow system, the so-called 'free flow boundary condition' problem can occur, i.e. the seepage line cannot reach the outflow boundary. This comes from the circumstance that atmospheric pressure and residual water saturation is prescribed as Dirichlet boundary condition along the boundary which is later the outflow boundary and switching the type of boundary condition is generally not foreseen in a two-phase flow model. To overcome this problem, the dike is artificially extended by a zone of much higher permeability, here the permeability of the extended domain is chosen to be $K_{ex} = 1 \cdot 10^{-9} m^2$. A reasonable agreement between computed and measured seepage lines as well as discharges for steady state was observed in Figure 5.16 (below). The simulated discharge is $Q_{num} = 0.37l/s$ which reasonally agrees with the measured discharge $Q_{ex} = 0.40l/s$.

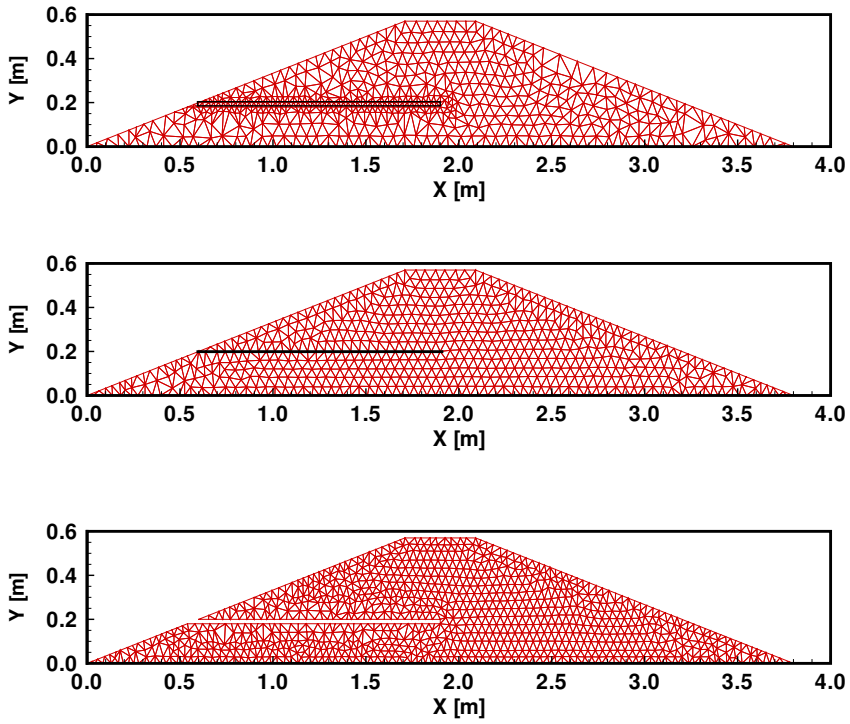

Figure 5.12: Mesh of the domain: (upper) dike with 2D fault zone on the seaside, (middle) dike with 1D fault zone on the seaside, (lower) dike with fault zone as a pipe on the seaside

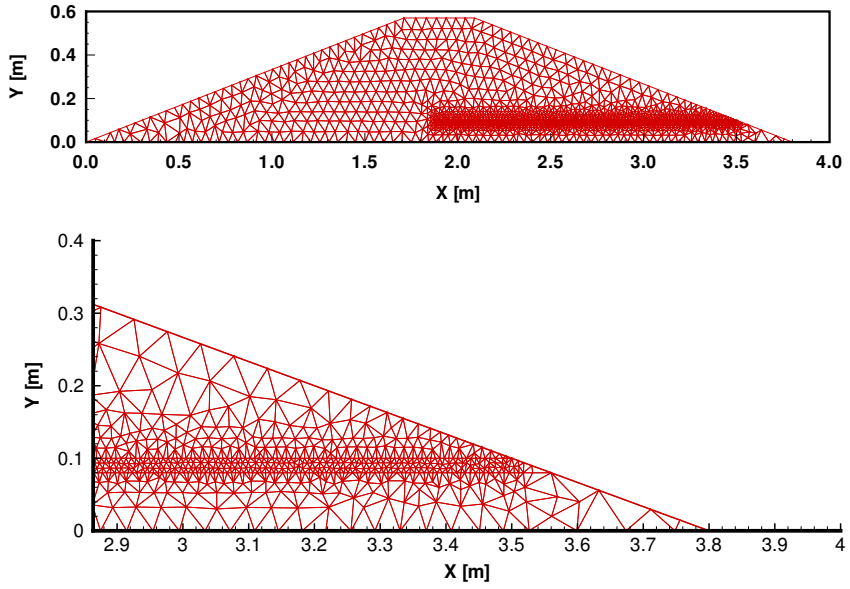

Figure 5.13: Mesh of the domain: (upper) dike with 2D fault zone on the landside, (lower) zoom around the fault zone

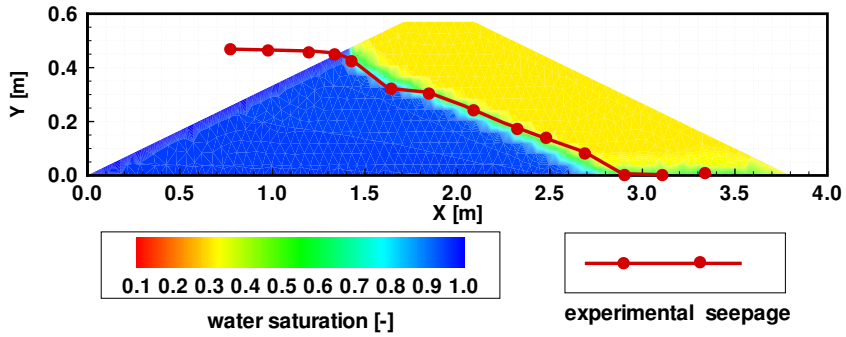

Figure 5.14: Water seepage through the homogeneous dike after t = 60min, comparison of experimental and numerical results

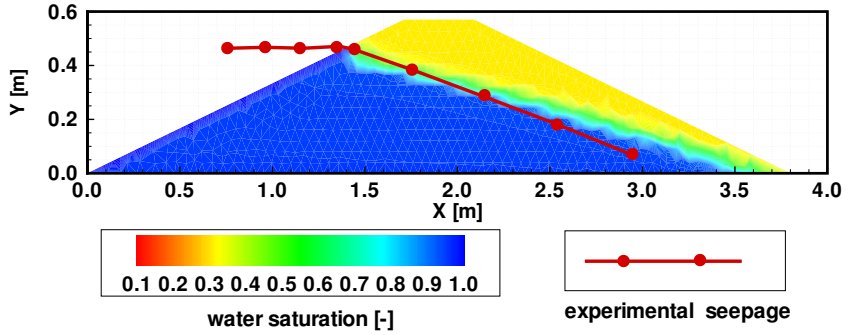

Figure 5.15: Water seepage through the homogeneous dike after t = 1h20min, comparison of experimental and numerical results

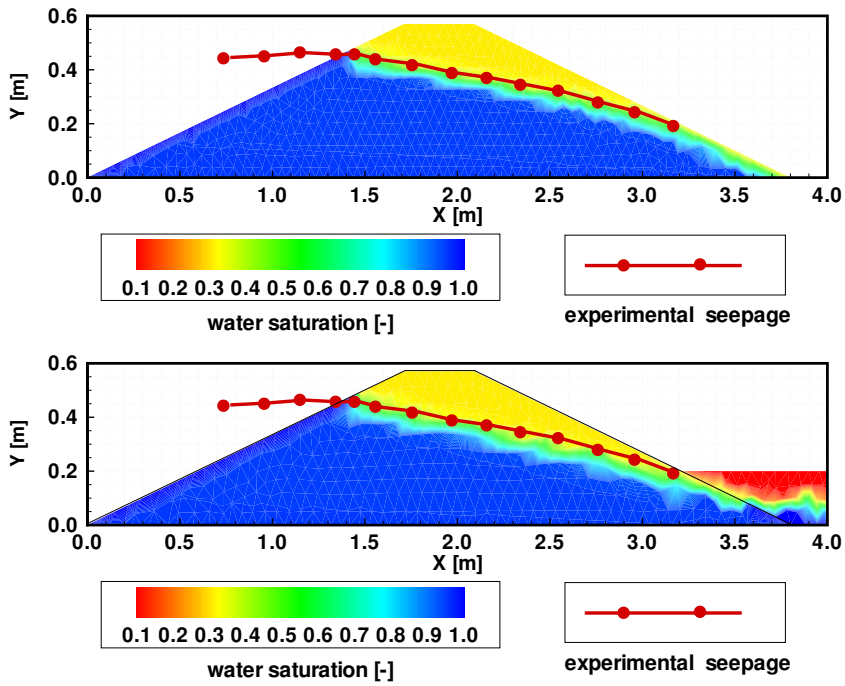

Figure 5.16: Steady state process in the homogeneous dike after t = 2h10min: (upper) no extended domain, (below) extended domain

5.3.3 Dike with Fault Zone

In this case, a fault zone is set up in two different directions of the dike: on the seaside and on the landside. Three model concepts have been chosen for numerical simulation: *2D fault zone model concept* and *1D fault zone model concept* and *fault zone with pipe model concept*.

Figure 5.17 compares the water infiltration processes in the dike with a fault zone on the seaside given by water saturation distributions at time step $t = 60min$ in the experiment and in the numerical simulations for the different model concepts. Due to the much higher permeability of the fault zone, the water front moves much faster through this domain compared to the background material. A very good agreement between the simulation results in two model concepts (2D fault zone model concept, 1D fault zone model concept) and experimental results was obtained, see Figure 5.17a, 5.17b and 5.17c after $t = 60min$. For the 2D fault zone model concept (equi-dimensional fault zone), the fault zone has a small thickness and the much finer mesh surrouding the fault zone is needed for spatial discretization. Therefore, the 2D fault zone model concept requires longer CPU time compared to the 1D fault zone model concept (lower-dimensional fault zone). For the

Finite Volume Methods, the number of unknowns is equal to the number of nodes in the grids, so that the system with 1D fault zone is easier to solve and requires less iterations than the system with 2D fault zone model concept. The computations reached steady state after $t = 2h$ in case of the dike with fault zone on the seaside while this occured after $t = 1h55min$ in the experiment. A good agreement between simulated and measured seepage lines was also observed in this case and similar computed water discharge $Q = 0.53l/s$ are obtained compared to the discharge $Q = 0.49l/s$ in the experiment.

In the following, the system with the fault zone on the landside is investigated. Figure 5.18 shows the comparison of the experimental and the numerical results for the different model concepts in this case at the time step $t = 1h20min$. The computations reached steady state after $t = 1h55min$ while the experiment was somewhat slower with $t = 2hmin$. A reasonable agreement between computed and measured seepage line was observed in Figure 5.19. Overall, the experiments are somewhat slower compared to the numerical simulations. An improvement could only be achieved when the dike permeability would be reduced. However, the dike permeability was a measured value and let to good agreements in the previous cases. The simulated discharge was $Q_{num} = 1.14l/s$ and the measured discharge was $Q_{ex} = 1.05l/s$ and they are much bigger compared to the steady state discharge $0.4l/s$ in the homogeneous case. Here, the influences of the fault zone on the infiltration processes is clearly illustrated.

In the numerical simulation, the permeability of the fault zone is defined to follow the validity of Darcy law. The permeability of the fault zone is chosen as $K_f = 10^{-9}m^2$ and is about two times order of magnitudes higher compared to the permeability of the matrix. When the permeability of the fault zone is higher, the validity of Darcy law can be violated. If the permeability of the fault zone increases to larger than $K_f = 4 \cdot 10^{-5}m^2$, numerical problems occur.

In the dike with fault zone as pipe model concept, the fault zone is idelized as a horizontal open pipe. From the beginning, the pipe is filled up water, the hydrostatic pressure is set as the Dirichtlet boundary condition along the pipe wall. An over-estimation of water occurs in the system. The results show that the water infiltration processes are faster than in previous cases (in system with 2D fault zone and 1D fault zone)(see Figure 5.17d) and the steady state condition is reached earlier at the time $t = 1h30min$.

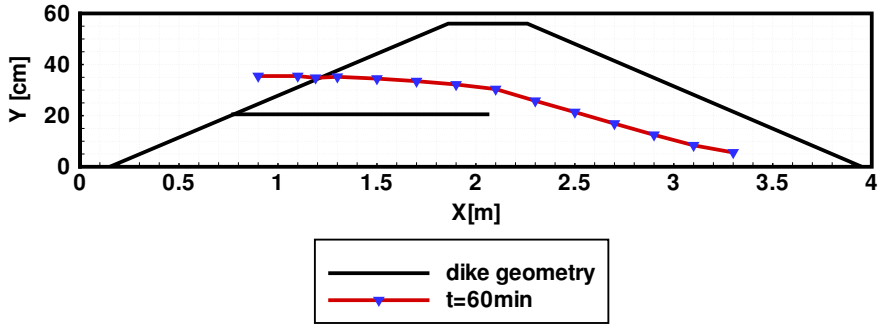

(a)

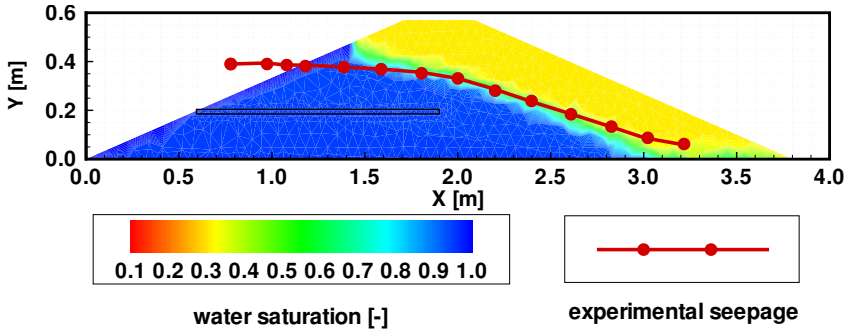

(b)

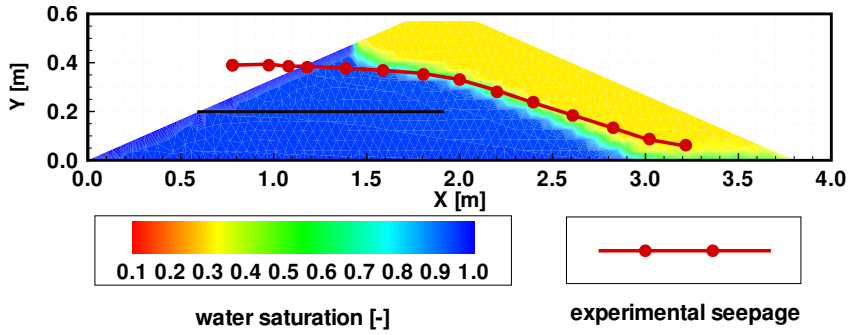

(c)

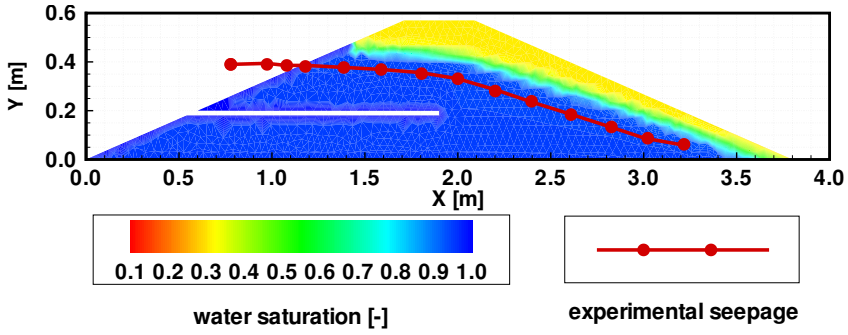

(d)

Figure 5.17: Water seepage through the dike with a fault zone on the seaside after t = 60min: (a) experimental result, (b) numerical result in a dike with 2D fault zone, (c) numerical result in a dike with 1D fault zone, (d) numerical result in a dike with fault zone as a pipe

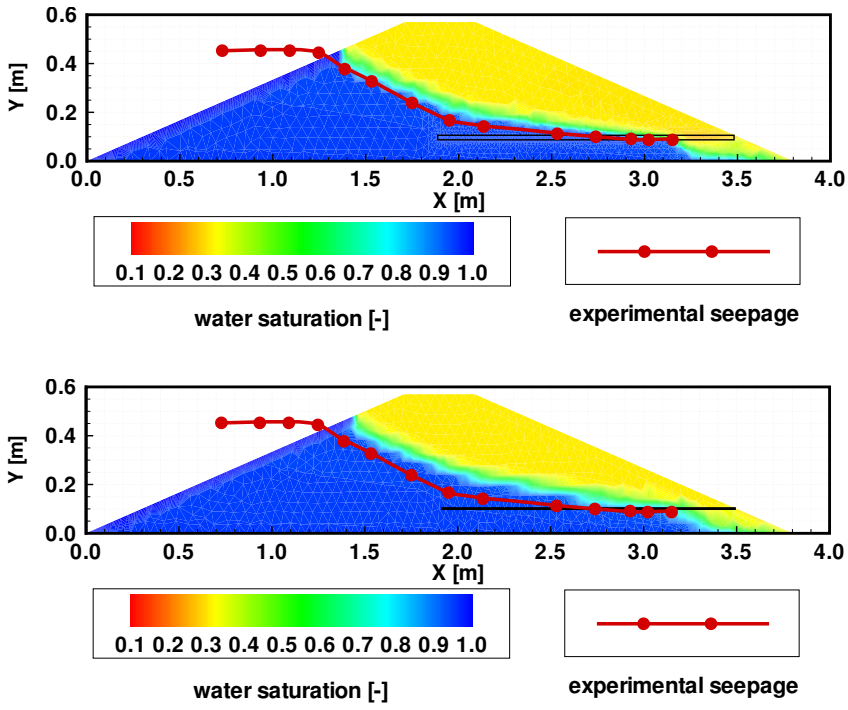

Figure 5.18: Water seepage in the dike with a fault zone on the landside after t = 1h20min: (a) numerical result with 2D fault zone, (b) numerical result with 1D fault zone

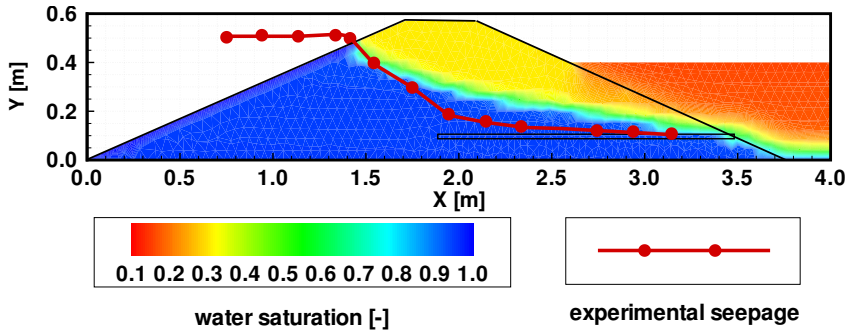

Figure 5.19: Steady state process in the dike with a fault zone after t = 1h55min

5.4 Conclusions

In this chapter, modeling of the two-phase flow in porous media is applied to a laboratory scale domain. A dike with fault zones on different sides is chosen for both, experimental and numerical simulations. Here, the fault zone is set in horizontal direction in the dike. First, the experimental simulation of the dike is carried out to investigate the seepage processes. The electrical method has been used for measurements on the physical model. The seepage processes in the dike are investigated by numerical simulation. The results have been compared with the experimental results.

For the homogeneous dike, due to the small entry pressure p_d, the influences of the capillarity in the numerical results are small. The seepage line and the water discharge through the dike are calculated in the numerical simulation. The results show an overall good agreement between the experimental and numerical simulations. Here, to deal with the free flow boundary condition problem in the simulation, the domain should be extended in the numerical simulation.

For the dike with the fault zone, the fault zone is set up in both landside and seaside of the dike for the numerical simulation. Three different model concepts are also used: *2D fault zone model concept* and *1D fault zone model concept* and *fault zone with pipe model concept*.

The seepage lines as well as water discharge are computed in the numerical simulations. The numerical results show mostly a very good agreement for two models concepts (2D fault zone model concept, 1D fault zone model concept) and the experimental simulations. The 2D fault zone model concept and 1D fault zone model concept are suitable for numerical model in this case. The results show an over-estimation of water infiltration processes for the pipe model concept. Therefore, this model concept is not recommended for further investigations.

Chapter 6

Water Infiltration in a Natural Slope

6.1 Problem Description

Landslides occur almost every year in many regions of the world, more or less, small or large. They are one of the most dangerous natural hazards in mountainous regions that have a severe impact on the welfare of societies. A landslide is the sliding movement of masses of loosened rock and soil down a hillside or slope. Landslide causes depend on rock type, precipitation, seismic shaking, land development and zoning practices, soil composition, moisture, and slope steepness. In some mountain areas, extreme rainfall situations, e.g. heavy rainfall or long periods of rainfall are the main reasons for the slope failures. One mechanism that leads to slope failures is that the negative pore-pressure starts to increase when water start to infiltrate into the unsaturated zone. The loss of negative pore-pressure decreases the shear strength of the soil below the mobilised shear strength along the potential slip surface (RAHARDJO et al. (2002 [80])).
Many researches show that infiltration and the preferential flow through macropores in unsaturated zone are also major factors influencing stability in shallow slopes. (e.g. BOOGARD (2001 [13]), RAHARDJO et al. (2005 [81]), LINDENMAIER et al. (2005 [55]), VAN ASCH (1999 [98])). Figure 6.1 shows the schematic view of water infiltration processes in a hillslope. Under these conditions, fast infiltration may result in large volumes of water entering what was initially an unsaturated soil slope. The infiltration may let the soil become fully saturated. The saturation of soil materials increases the weight of slope materials which then leads to greater gravitational force. This large amount of water in the soil can reduce the cohesive bonds between individual soil particles resulting in the reduction of the internal strength of the hillslope enough to trigger the failure (CHO and LEE (2000 [25])). In more complex landslide types with deeper failure zones, a rising and falling groundwater table leads to changes in the stress field (VAN ASCH (1999 [98]).

In this chapter a natural slope case study from an interdisciplinary Research Unit sponsored by the Deutsche Forschungsgemeinschaft (German Research Foundation, DFG) is chosen to investigate the effect of rainfall induced infiltration into a slope composed of unsaturated soils. The two-phase flow model has been chosen for analysing the water infiltration processes in the natural Heumoes slope, Austria. The 2D fault zone model concept (combined model approach, see section 2.4) which was carefully investigated and compared with other concepts on smaller scales in chapter 4 and 5 has been applied here for macropore in the hillslope.
Further information about the infiltration studies is given in PHAM VAN et al. (2004 [69]), PHAM VAN et al. (2004 [70]), PHAM VAN and HINKELMANN (2008 [74]), STADLER et al. (2008 [93]).

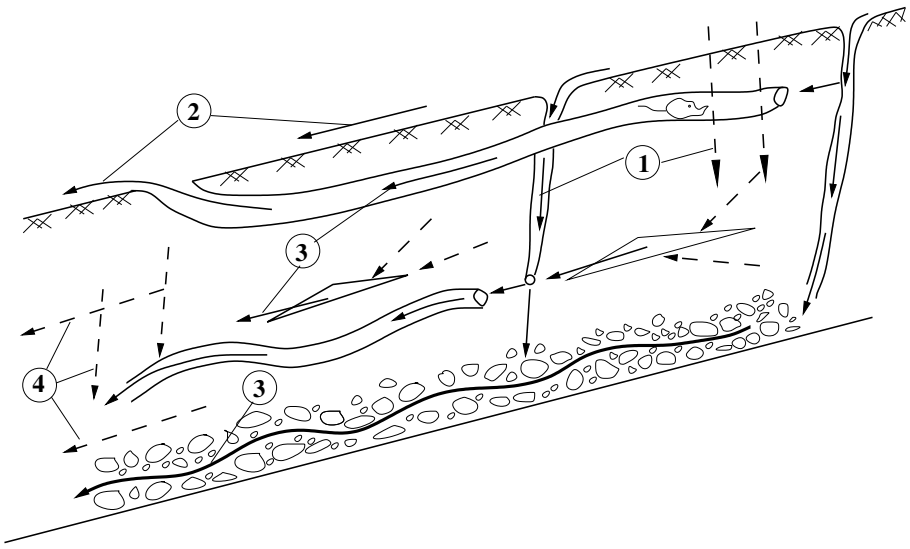

Figure 6.1: Schematic view of water infiltration processes in a hillslope: (1): Infiltration in micro- and macropores; (2): Overland flow; (3): Preferential flow; (4): Flow in micropores (flow in matrix) (BRONSTERT (1994 [15]))

6.2 Natural Slope and Research Unit

The development of the movement of large hillslopes until failure is the result of complex interactions of hydrological, subsurface-hydraulic and soil-mechanical processes ranging over large space and time scales. As no reliable simulation methods exist today for such purposes, an interdisciplinary Research Unit sponsored by the DFG named “Coupling of Flow and Deformation Processes for Modeling the Movement of Natural Slopes -

Großshang" has been launched for these purposes. Five groups from the Technische Universität Berlin, Technische Universität München, Universität Stuttgart and Universität Karlsruhe (TH) participated in the project (HINKELMAN and ZEHE (2007 [45])).
In this Research Unit, new solutions are suggested which bring together improved process models with coupling, averaging and upscaling methods while combining deterministic and stochastic approaches to take the complexity of the processes as well as the available data on the different scales into account. The tools which have been developed should first be verified using controlled experiments (benchmarks) before being transferred to a concrete field case for which a very good data set already exists. To improve the predictions on the initiation of slope movements, a simulation tool which combines the coupled flow and derformation processes has also been developed in this project.
The Research Unit consists of 5 sub-projects (see Figure 6.2). The work in this chapter is a part of the sub-project 2. In this sub-project, the numerical simulation of two-phase flow processes in the subsurface is applied particularly on a natural hillslope area. Based on a model concept for multi-dimensional two-phase flow in fractured porous media, suitable process models and coupling methods for the interaction of surface runoff, infiltration, especially preferential flow, and multi-dimensional flow in the subsurface will be developed and validated by means of infiltration experiments. For these purposes, three model concepts are further developed and compared: combined model approach, coupling porous medium with a 1D pipe and a double-continuum approach (see section 2.4). Based on the experiments the results will be transferred to the field case. The coupling to the deformation processes will be carried out and remediation measures will be investigated. For the collaboration within the research units, a central internet-based information system will be set up to also serve as a platform for software-technical model couplings in the range of possibilities.
The natural slope Heumoes is a slow-moving alpine slope in Vorarlberg Alps (Austria) which is chosen as case study in this research. The slope is located in the eastern Vorarlberg Alps, $10km$ east of city of Dornbirn and $0.5km$ south of the village of Ebnit (Figure 6.3). The Heumoes slope belongs to the head of a very steep mountainous catchment which is drained by the Ebnit and Dornbirn rivers. The extension of the slope is about $1800m$ in east-west and $500m$ in north-south direction. Several buildings, a small vacation village and a skiing lift are situated on the slope. Two small slides occurred in the over-steepened slope, the larger one must have occurred before 1965. In the year 2000, one of the buildings was torn down due to its instability (Figure 6.4). Measurements on the Heumoes slope showed that the high infiltration rates on the upper part of the slope are supported by a complex network of macropores and soil-pipes (LINDENMAIER et al. (2005 [55])).

DEPENHAL and SCHMITT (2003 [26]) have measured the movements of the slope by using GPS measurement methods (Figure 6.5). The monitoring detected slowly creeping movements and their velocity variations contribute to the prediction of future risks. The results of the vertical movements showed considerably smaller displacements than the respective horizontal movements.

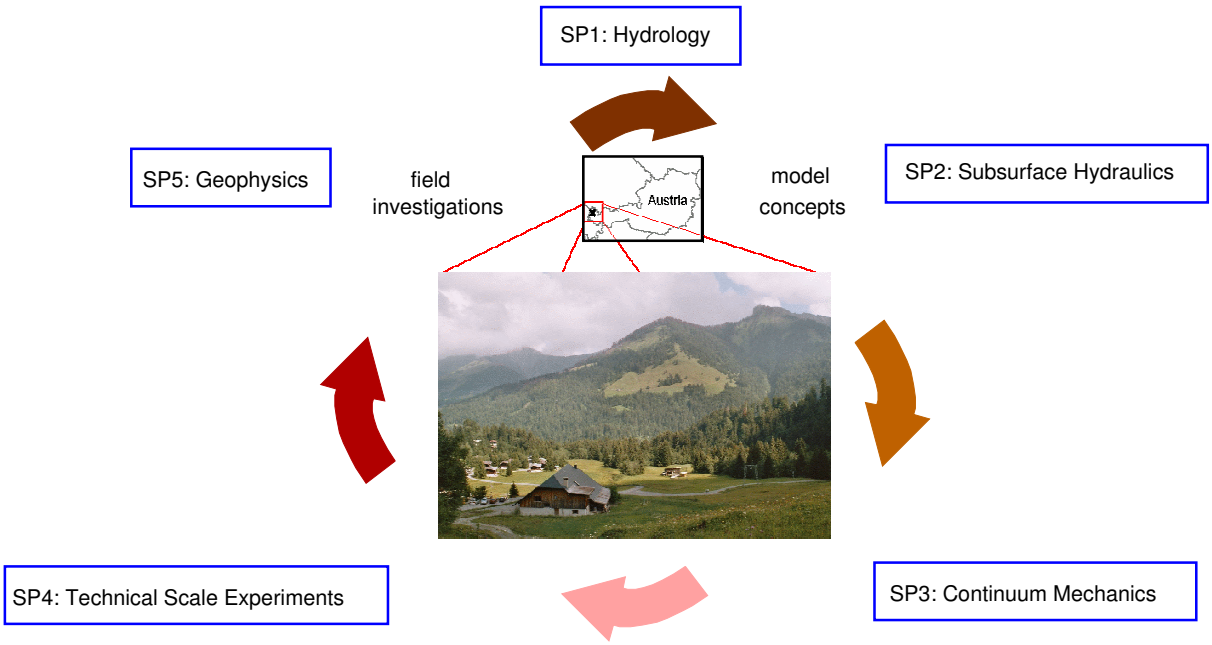

Figure 6.2: Research working group distribution

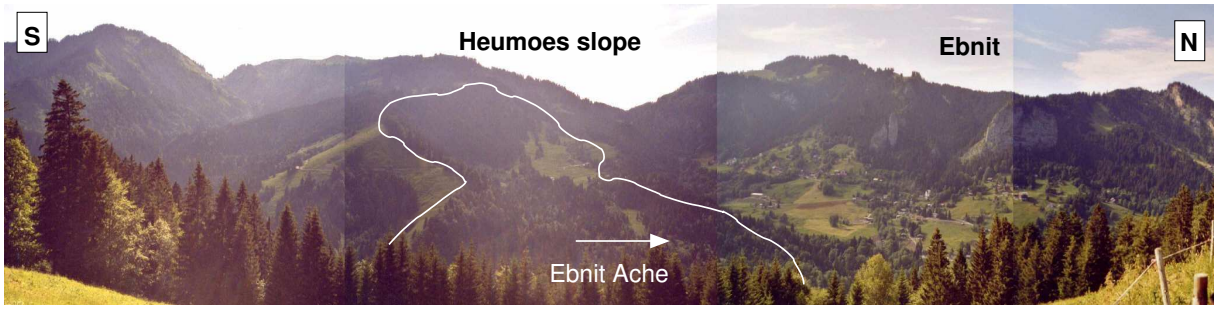

Figure 6.3: View on the village Ebnit and the adjacent Heumoes slope, the white line represents the catchment boundaries, the meadow on the right site is the moving hillslope body. The view is towards the west, the drainage is towards the north (LINDENMAIER (2007 [56]))

Figure 6.4: Location of the Heumoes slope (left), and failure at "Hohe Kugel" (right)

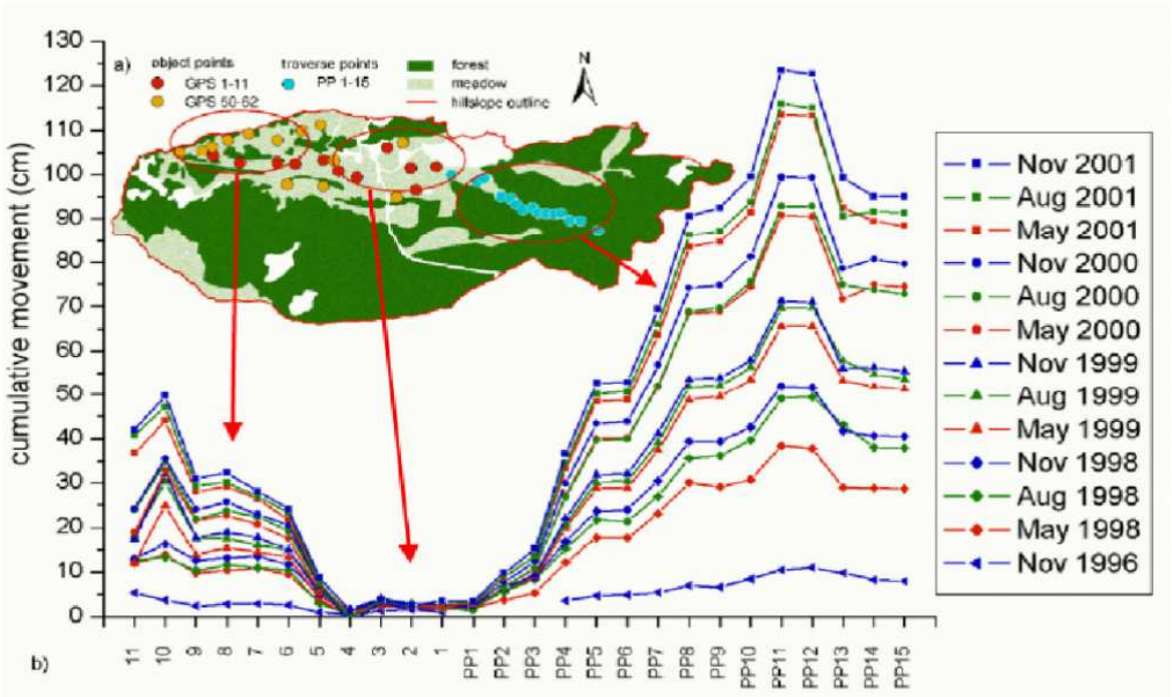

Figure 6.5: (a) Map of GPS points with zones of similar movement behaviour on the Heumoes slope; (b) Absolute deformation distance of GPS and terrestrial points for each epoch (DEPENHAL and SCHMITT (2003 [26]))

6.3 Numerical Simulations

As mentioned before in section 6.2, in the Research Unit the approach to develop appropriate tools combines bottom up modeling with top down modeling. Bottom up models are based on highly complex approaches for multiphase flow and interactions between the fluid and the solid phase, including macropore flow which is crucial at the natural site. These tools where in a first step validated based on sound benchmark experiments. Top down modeling includes on one hand a physically based hydrological simulation tool that successfully reproduced the complete water balance of a part of the Heumoes slope. And second a tool to simulate large scale movements as well as accumulations of masses in parts of the slope.

For better undestanding and visualising the water infiltration processes on Heumoes slope which has been chosen as a case study, the numerical simulation is useful. Normally, the model can be used as the model of flow of soil water in unsaturated zone using the Richards equation. This model is based on assumption that the air phase essentially remains at a constant pressure, equal to atmospheric; the system is then reduced to the consideration of the water phase only (see section 1.2). In the system here, the gas phase is important and should be included in the simulation because high gas pressures can occurr in a layered aquifer (see Figure 6.6), especially if subdomain 3 has a low permeability. Therefore, a two-phase flow model has been applied. The implemented two-phase flow model concept assumes a fixed soil-matrix. The model concept does not include soil processes like swelling and shrinking or deformations.

An idealized natural slope which has a geometry as shown in Figure 6.6 is chosen for simulations in this study (the mesh in Figure 6.7). The slope has a length of about 29m and a height of 14.5m and consists of two main different types of soils (fine and coarse). The soil properties used for simulation are typical for those from the Heumoes slope. The lower part including subdomain 1 and subdomain 3 consists of coarse sand compared to the upper part (subdomain 2) with fine sand. The constitutive relationships of Brooks-Corey are used in this simulation. All soil parameters are summarised in Table 6.1. Preferential flow in the macropores is represented using combined model concept (i.e. 1D fracture model concept). Macropores are modeled as as elements. Three macropores were set up in the system each having a width $b = 1cm$, a permeability $K^f = 10^{-9}m^2$ and a porosity $\phi = 0.9$.

In order to simplify the problem, the heavy rainfall is idealized as runoff with $1cm$ water level on the slope. That means a Dirictlet boundary condition is set on the top of the slope and the water height is set to $1cm$ equivalent to a pressure of 100100Pa. At the

bottom of the domain a Neumann no flow boundary condition describes a non permeable rock layer. As initial condition, the saturation of the wetting phase is set to $S_w = 0.2$ in the whole domain. The other parameters are discribed in the Table 6.1.

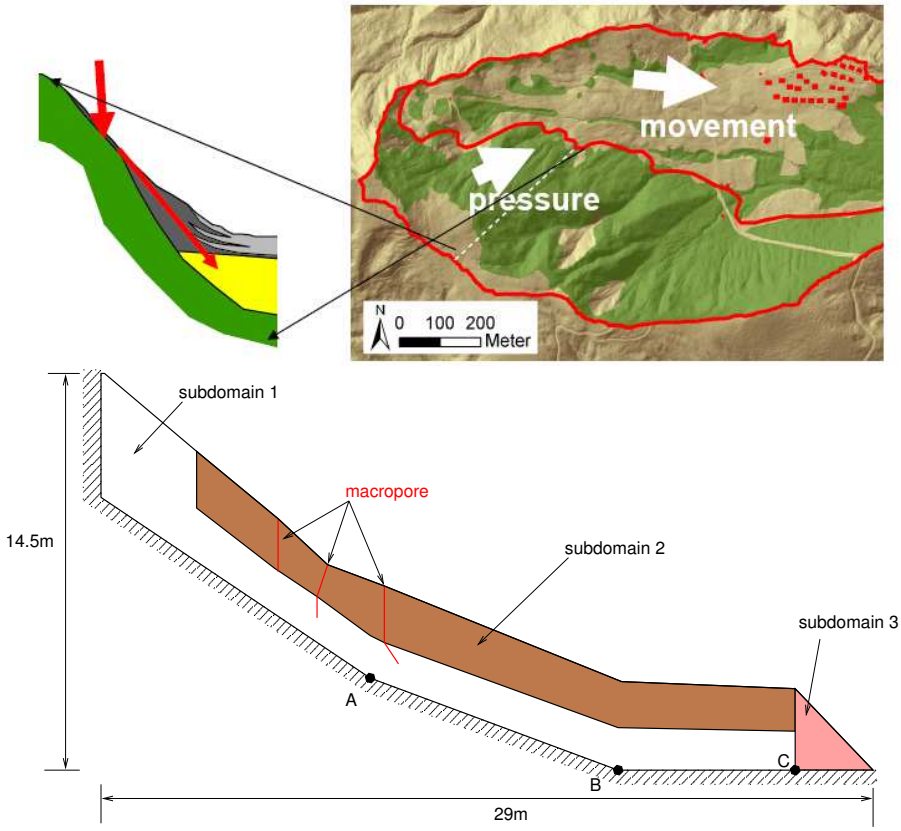

Figure 6.6: Idealized and schematic view of the natural slope (LINDENMAIER (2007 [56]))

Parameters	**Fine Sand**	**Coarse Sand**
K $[m^2]$	$9.05 \cdot 10^{-15}$	$3.1 \cdot 10^{-11}$
S_{wr} [-]	0.18	0.15
S_{nr} [-]	0.01	0.01
p_d [Pa] (Brooks-Corey)	2400.0	700.0
λ [-] (Brooks-Corey)	3.5	2.3
ϕ [-]	0.43	0.36

Table 6.1: Soil Properties

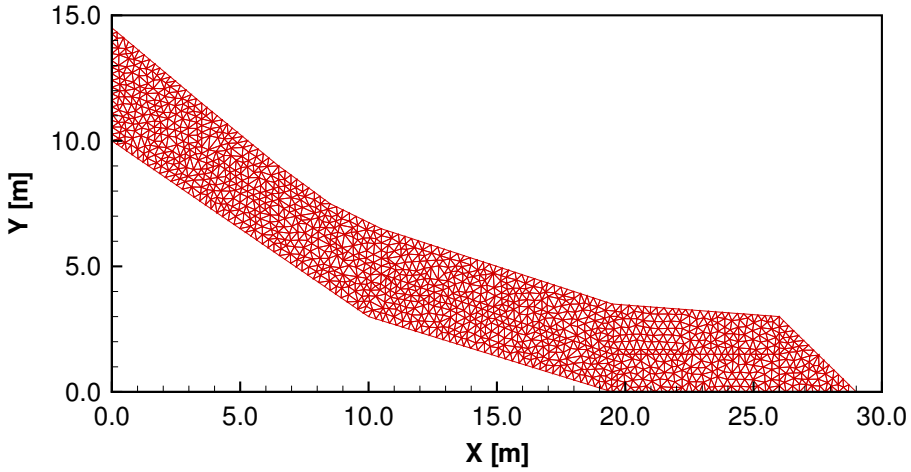

Figure 6.7: Mesh of the domain used for numerical simulation

In the first case, the two-phase flow model is applied to the domain without macropores. A slope is structured in two layers with 3 subdomains like in Figure 6.6. The lower layer consists of 2 subdomains (subdomain 1 and and subdomain 3) with the same properties (coarse sand). The upper layer is the subdomain 2 which consists of fine sand material. Figure 6.8 presents the water pressure fields for different time steps ($t_1 = 3h, t_2 = 5h, t_3 = 7h$ and $t_4 = 15h$) indicating the water infiltration by the increasing pressure over time. Figure 6.9 shows the diagram describing the water pressure profiles at the 3 points A, B and C at the bottom of the slope (see Figure 6.6). From the results, it is clear that the water pressure in the deeper soil-layers (in A, B) increases stronger due to the low permeable layer above. This is one main factor influencing the slope instability. When the water pressure increases, driving forces can increase and with the high pore pressure, the internal strength (shear resistance) of slopes is reduced.

Measurements in previous researches (i.e. LINDENMAIER (2007 [56])) show that the soil in the Heumoes slope is highly heterogeneous. The macropores play a dominant role in the soils, enhancing the heterogeneity of the soil and influencing the subsurface hydraulics. In this area, former root holes from marsh plants are the most dominant circular macropores. These macropores have diameters of around 0.3 to $1.0cm$.
In the second case, the numerical simulation is done in a slope with macropores. To simplify the problems, preferential flow in the slope is represented by the flow in three macropores (see Figure 6.6).
Figure 6.10 shows the water pressure fields in the case of the slope with macropores (at

time step $t_1 = 3h, t_2 = 5h, t_3 = 7h$ and $t_4 = 15h$). Due to the macropores, the whole infiltration processes is speeded up, if it is compared to Figure 6.8. However, the maximum pressures are a little bit smaller with the macropores.
The diagram describing the water pressure profiles at the 3 points A, B and C in the bottom of the macro-porous slope is illustrated in Figure 6.11. In principal, the same results as mentioned above are obtained, if Figure 6.11 is compared to Figure 6.9.
A comparison of the water saturation fields without and with macropore is given in Figure 6.12 also showing the acceleration of the infiltration due to the macropores, i.e. the soil becomes much ealier saturated. Figure 6.13 illustrates the comparison of the results in detail at the points A, B and C in the slope. At point A, the saturation reaches the maximal value (saturated soil) after early time $t = 20min$. With the influences of the macropores, the water pressure increases to the around 140000Pa, while it increases up 150000Pa in the case without macropores.
The numerical results principally agree with the observation in the field (in reseaches of LINDENMAYER (2007 [56]), DEPENHAL and SCHMITT (2003 [26]))) and WIENHÖFER (2008 [105]).

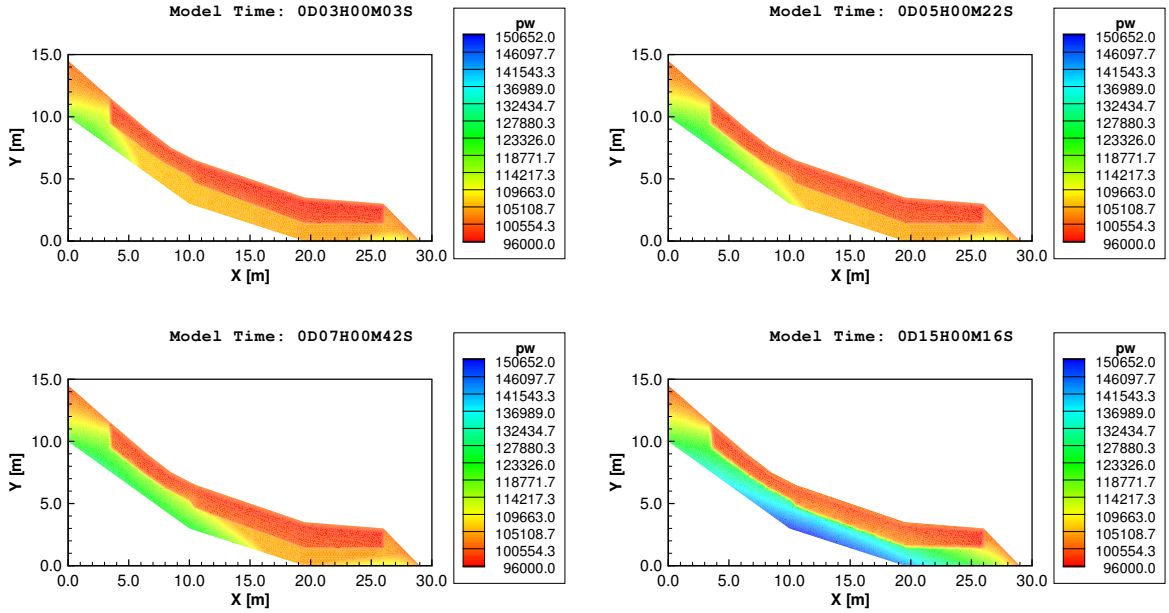

Figure 6.8: Water pressure $p_w[Pa]$ in the two-layer slope at different time steps

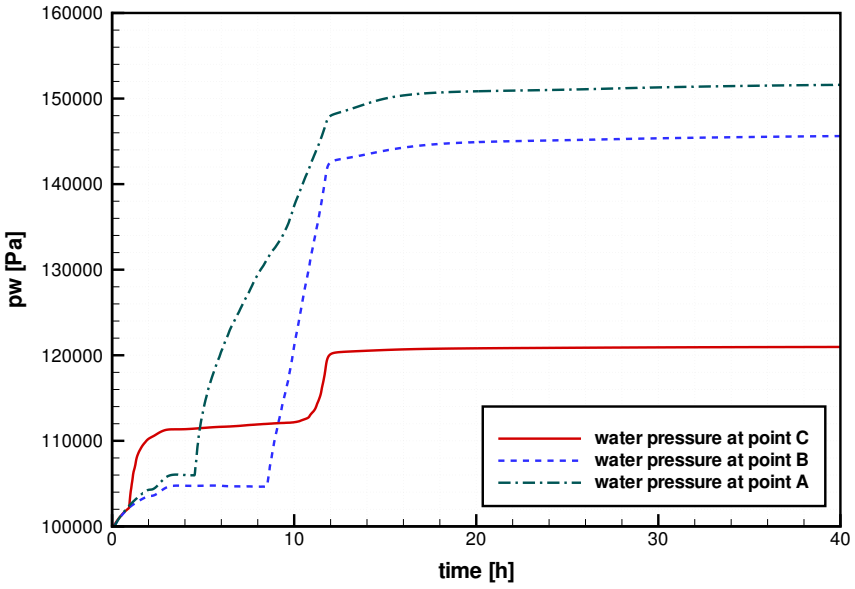

Figure 6.9: Water pressure at point A, B and C in the two-layer slope

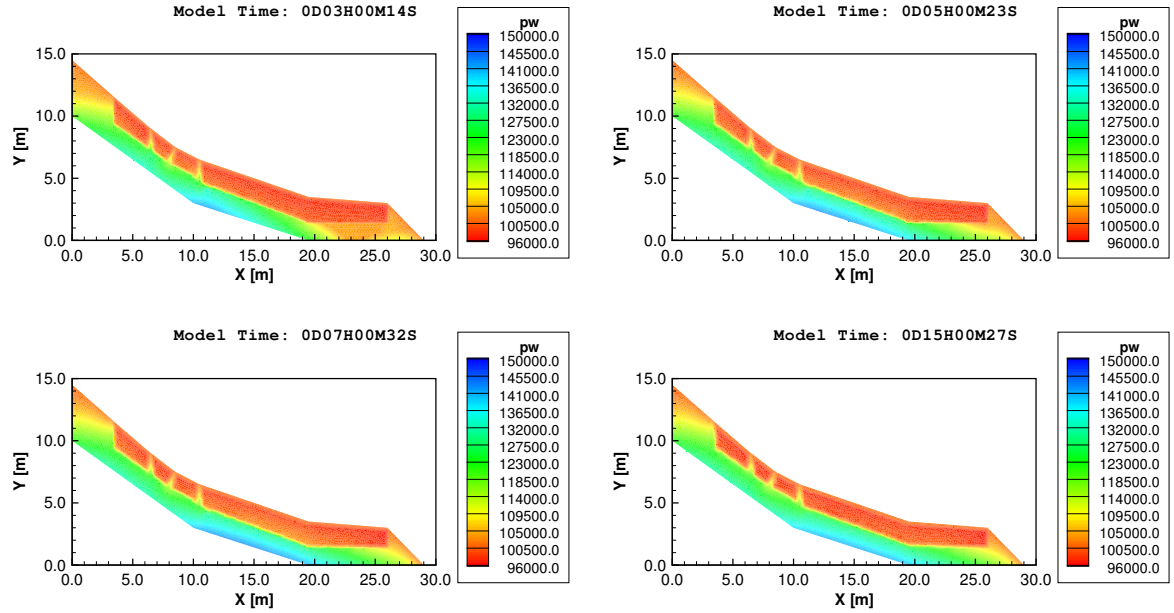

Figure 6.10: Water pressure $p_w[Pa]$ in the slope with macropores at different time steps

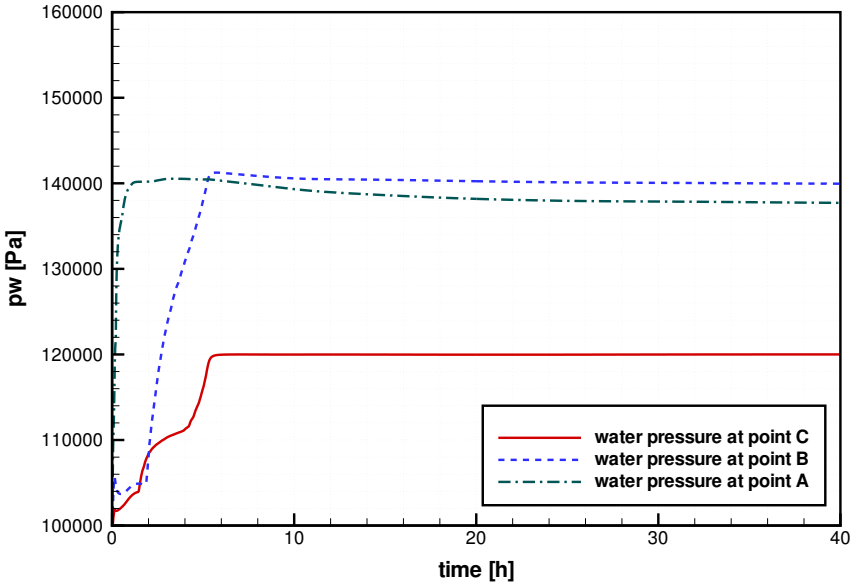

Figure 6.11: Water pressure at point A, B and C in the slope with macropores

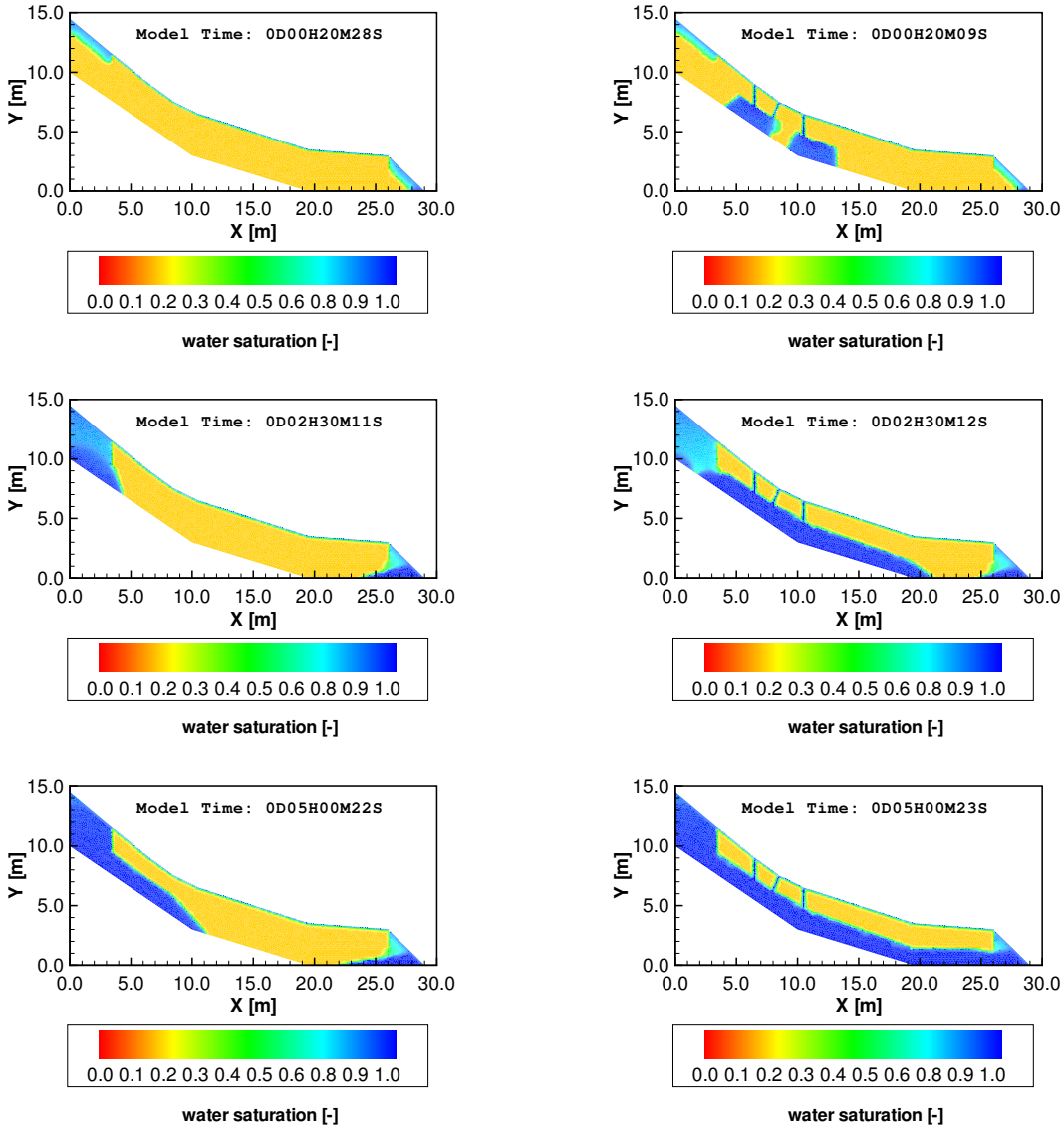

Figure 6.12: Water saturation fields in the slope without macropores (left) and with macropores (right)

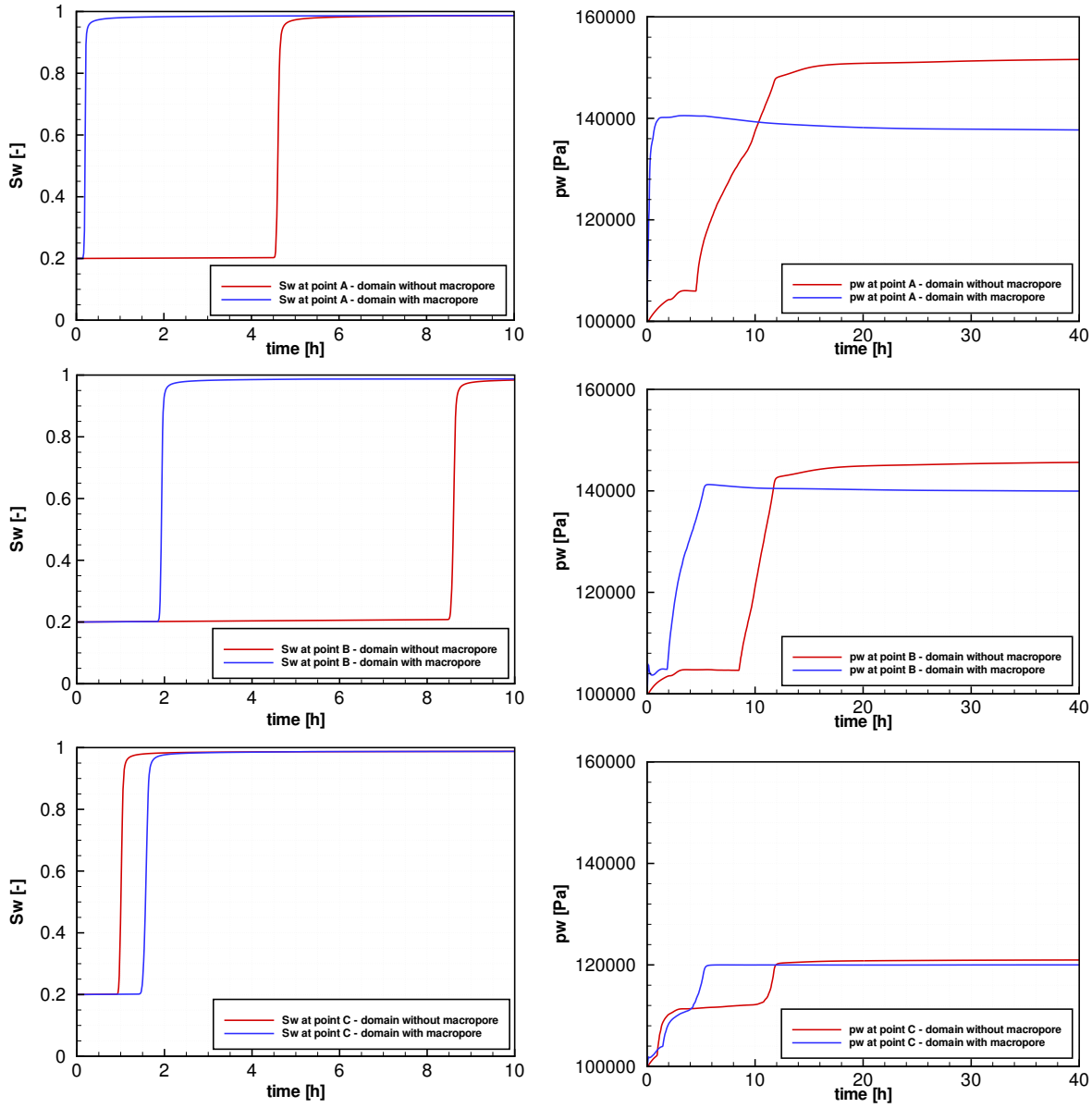

Figure 6.13: Comparison of water saturation and water pressure in points A, B and C

6.4 A Slope with Small-scale Heterogeneities

Numerical simulation of flow and transport in subsurface is always associated with uncertainties. In the nature, the soil structure is highly heterogeneous and small-scale heterogeneities whose spatial distribution is generally unknown can influence the flow and transport processes significantly, especially in two- and multiphase systems.
In this section, the influences of the heterogeneities in a natural slope (Heumoes slope) which is shown in Figure 6.6 are investigated. The small-scale heterogeneties in the natural slope domain are represented by the permeability field. First, the geostatistical method is used to compute the pemeability field of the domain. Then, the two-phase flow model is applied for numerical simulation of water infitration processes in the slope.
Geostatistic methods provide information about the spatial variability of a considered property for given a mean value, variance and correlation length. Several variogram models have been introduced in section 3.4 and some models can be used to determine geostastical permeability distributions (see BARDOSSY (1992 [2])). Here, the exponential variogram model is used.
An *exponential variogram function* $\gamma(h)$ is characterized by the *variance* C, the *correlation length* cl and the *nugget effect* ne (see the Figure 6.14). This function is written in the following formula:

$$\gamma(h) = C\left(1 - e^{\frac{-h}{a}}\right) + ne \tag{6.1}$$

The variance C for a permeability field considered at location i is computed with the arithmetic average K_m as follows:

$$C = \frac{1}{n}\sum_{i=1}^{n}(K_i - K_m)^2 \tag{6.2}$$

$$K_m = \frac{1}{n}\sum_{i=1}^{n} K_i \tag{6.3}$$

The length cl is the range that one random variable can affect the other random variable in neighboring points, often called *correlation length*. If the distance between two points is larger than the correlation length, they are not correlated. To take layering effect into account, the correlation length in the horizontal direction can be chosen to be greater than that in the vertical direction. Often, the horizontal correlation length is 5 to 10 times larger than the vertical one. The correlation length cl is assumed to be the practical range value $3a$ where the variogram reaches 95% of the the sill value in the variogram model.
Nugget ne (a nonzero variogram at the origin) is used to force a variogram to be discontinuous near the origin. The nugget effect is often neglected in environment water.

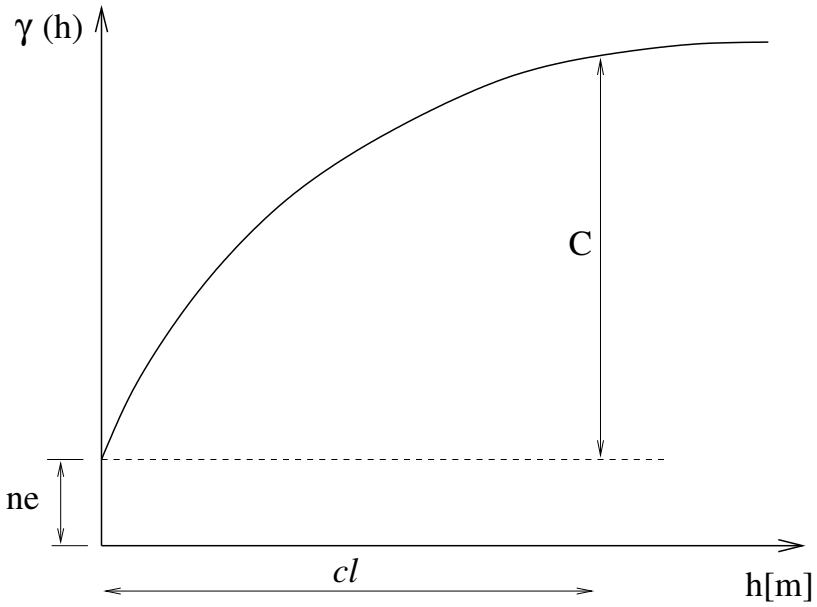

Figure 6.14: Exponential variogram

In this study the anisotropy ratio *an* comes from the anisotropic term when the correlation scales of a stochastic process in x, y, and z directions are different. Anisotropy ratio reflects the ratio of the vertical to the horizontal correlation length. Figure 6.15 shows an illustration of the difference between the statistically isotropic process and the statistically anisotropic process.
For two- and multiphase systems, it is mentioned that the entry pressure distribution p_d in a geostatistically varied field can be determined according to the Leverett function (see LEVERETT (1941 [53])):

$$J = p_d \sqrt{\frac{K}{\phi}} \tag{6.4}$$

If the average permeability K_m, the porosity ϕ_m and the entry pressure p_d of a homogeneous system are known, the entry pressure at location i in the geostatistically varied field can be computed as:

$$p_{di} = p_d \sqrt{\frac{K_m \phi_i}{K_i \phi_m}} \tag{6.5}$$

Neglecting the effect of porosity, the equation 6.5 leads to:

$$p_{di} = p_d \sqrt{\frac{K_m}{K_i}} \tag{6.6}$$

The geostatistic method is implemented in the statistical simulator SIMSET (see BARDOSSY (1992 [2])). The SIMSET tool is using the *Turning Band Method* simulation for generating geostatistical permeability fields. In the turning band method, 1D simulations are performed on lines turned around a center point and these 1D simulations are merged into 2D or 3D simulations. In other words, a point in the 2D or 3D space is projected onto these lines at first, then 1D simulation are carried out on those lines and the sum of the results of the 1D simulations yields the value in the 2D or 3D space. Different covariance structures or variograms have to be chosen.
In this example, the exponential variogram with no nugget effect is applied. A correlation length, a variance and an anisotropy ratio (correlation length in z-direction, x-direction) have to be assigned.

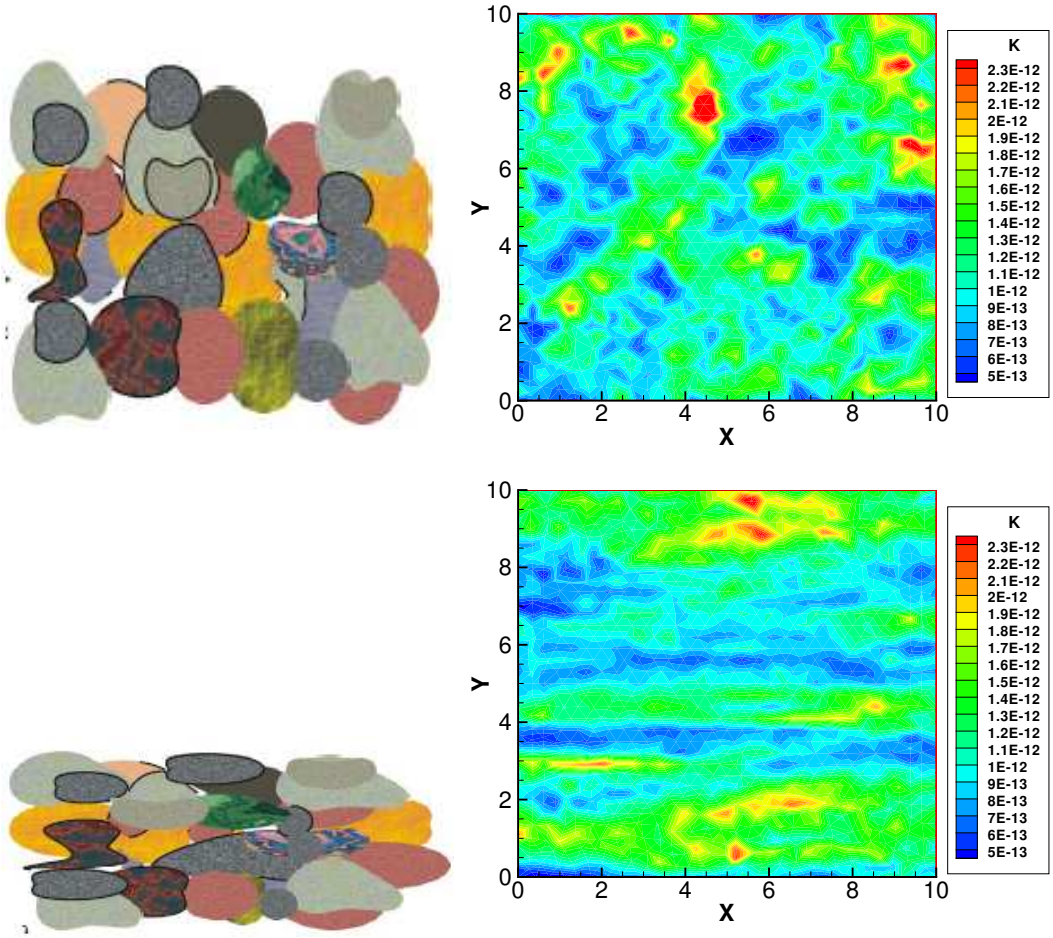

Figure 6.15: An illustration of the statistically isotropic process (above) and statistically anisotropic process (lower)

As the first case, pemeability fields are generated in a homogeneous slope with a mean value $K_m = 10^{-12}m^2$. In the framework of the Research Unit, experiments have been carried out in the Heumos slope to measure the hydraulic conductivities (see WIENHÖFER (2008 [106])). The test has been done in about 40 boreholes. Based on these data, the variance can be estimated using equation 6.2 and 6.3. The correlation length *cl*, varicance *C*, and anisotropy ratio *an* are chosen to 0.5, 0.8 and 0.2 respectively. The case of *cl0.5 C0.8 an0.2* is implied as the standard case. Here, the notation, for example, *cl0.5 C0.8 an0.2* means, that the variogram has a correlation length of 0.5m, a variance of 0.8, and an anisotropy ratio of 0.2.

The influences due to the changes of the correlation lengths, variances and anisotropy ratios are investigated by using the SIMSET model. Figure 6.16 shows the permeability fields with different geostatistical parameters. From the simulation, several tendencies were deduced:

- When the variance of the variogram decreases, in the example from $C = 0.8$ to $C = 0.2$, the permeability field becomes more homogeneous. This problem is similar if the correlation length is changed. A low correlation length signifies greater randomness in the spatial distribution of a quantity, while a high correlation length leads to a distinct spatial structure of clusters of similar values (like large blobs of ink). The influences due to the changes of of variances seem to be relatively higher compared to the correlation lengths.

- When the constant values of correlation length and variance are taken, the anisotropy is changed, the permeability field is changed, too. The differences come from the definition of the anisotropic process. If the correlation scales of a stochastic process in x, y, and z directions are different, the process then is said to be statistically anisotropic. The system is considered as being made of many inclusions of elliptic shapes. In reality, because of geologic deposition processes, geologic materials are often spread over larger horizontal extents than the vertical. Therefore, statistical anisotropy is a common and legitimate spatial structure of geologic heterogeneity.

After generating the permeability field, the two-phase flow model in MUFTE-UG program system is applied for the numerical simulation to demonstrate the influences of small-scale heterogeneities on the water infiltration processes in the slope. The model and parameters are the same as in section 6.3 (without macropore). The Brooks-Corey model is applied for both, the capillary pressure- and the relative permeability-saturation relations with parameters depending on the permeability fields which are calculated in SIMSET. The

entry pressure is strongly dependent on the permeability, which is considered applying equation 6.6 with the mean values of the entry pressure $p_d = 1000Pa$ and the form parameter $\lambda = 2$.

Figure 6.17 shows the comparison of water saturation fields between the homogeneous slope (left) with $K = 10^{-12}m^2$ and the small-scale heterogeneus slope with different geostatistical parameters (right) at the time $t = 29h$. More or less strong influences of heteregeneities are observed. The influences due to the changes of variances seem to be relatively higher compared to those of correlation lengths. A detailed comparison of the water pressure and saturation at point A, B, C the homogeneous slope and the slope with small-scale heterogeneitiess using the reference case (corelation length $cl = 0.5$, variance $C = 0.8$, anitropy ratio $an = 0.2$) is presented in Figure 6.18. These results show more or less strong influences of heteregeneities on the water infiltration processes.

If the domain consists of several subdomains (i.e. the case of a two-layer slope), the permeability fields can also be generated. The result is shown in Figure 6.19.

Figure 6.20 shows the effect of the entry pressure on the saturation distribution for the slope using the reference case. Here, the capillary pressure is dominant. The water can approach quickly into the regions with higher entry pressure. The results clearly show that a high saturation of water in the hillslope corresponds to high capillary pressures (not close to the top boundary condition).

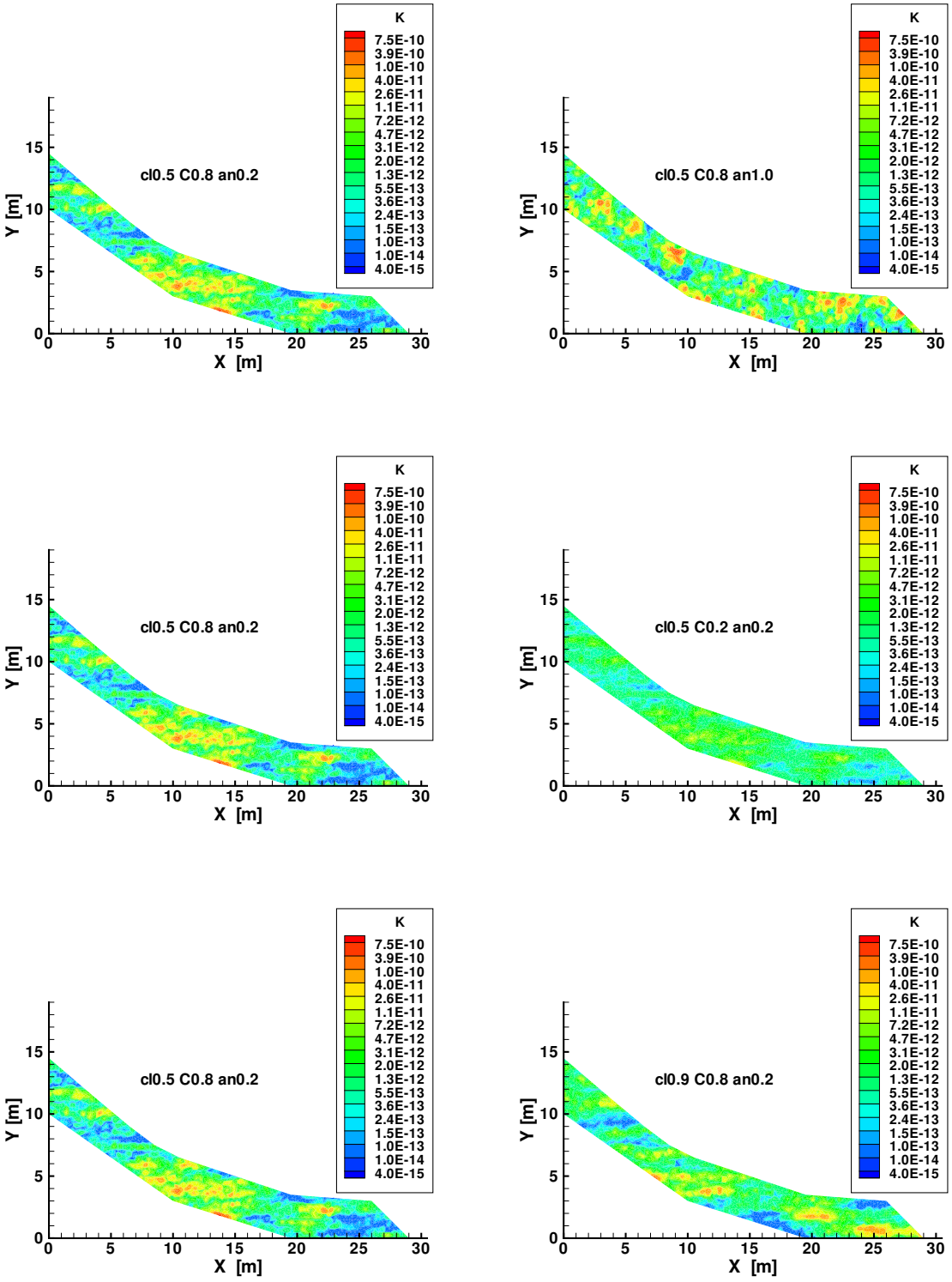

Figure 6.16: Permeability fields $K[m^2]$ with different geostatistical parameters

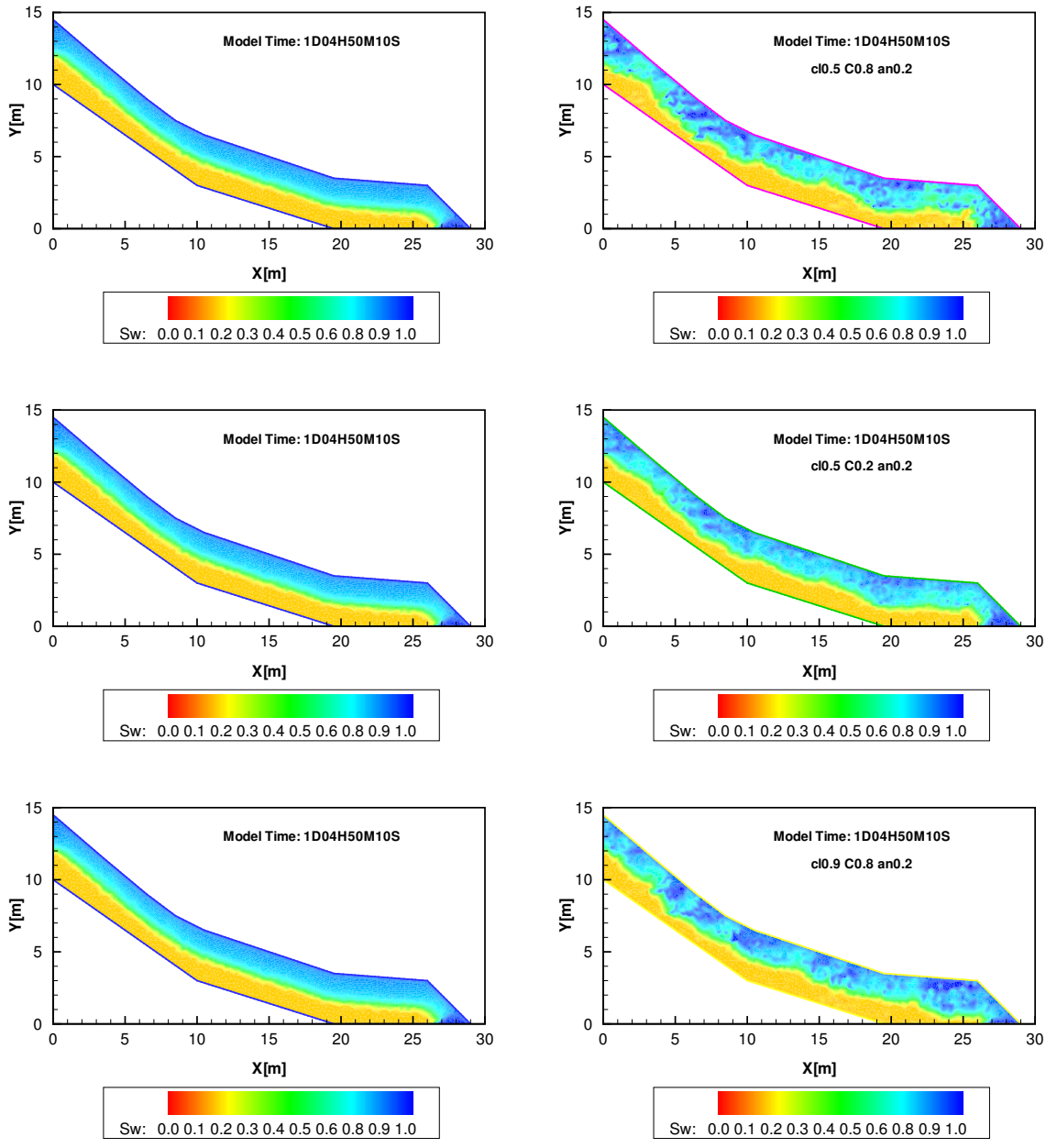

Figure 6.17: Comparison of water saturation distributions $S_w[-]$ between homogeneous slope (left) and small-scale hetererogeneous slope (right)

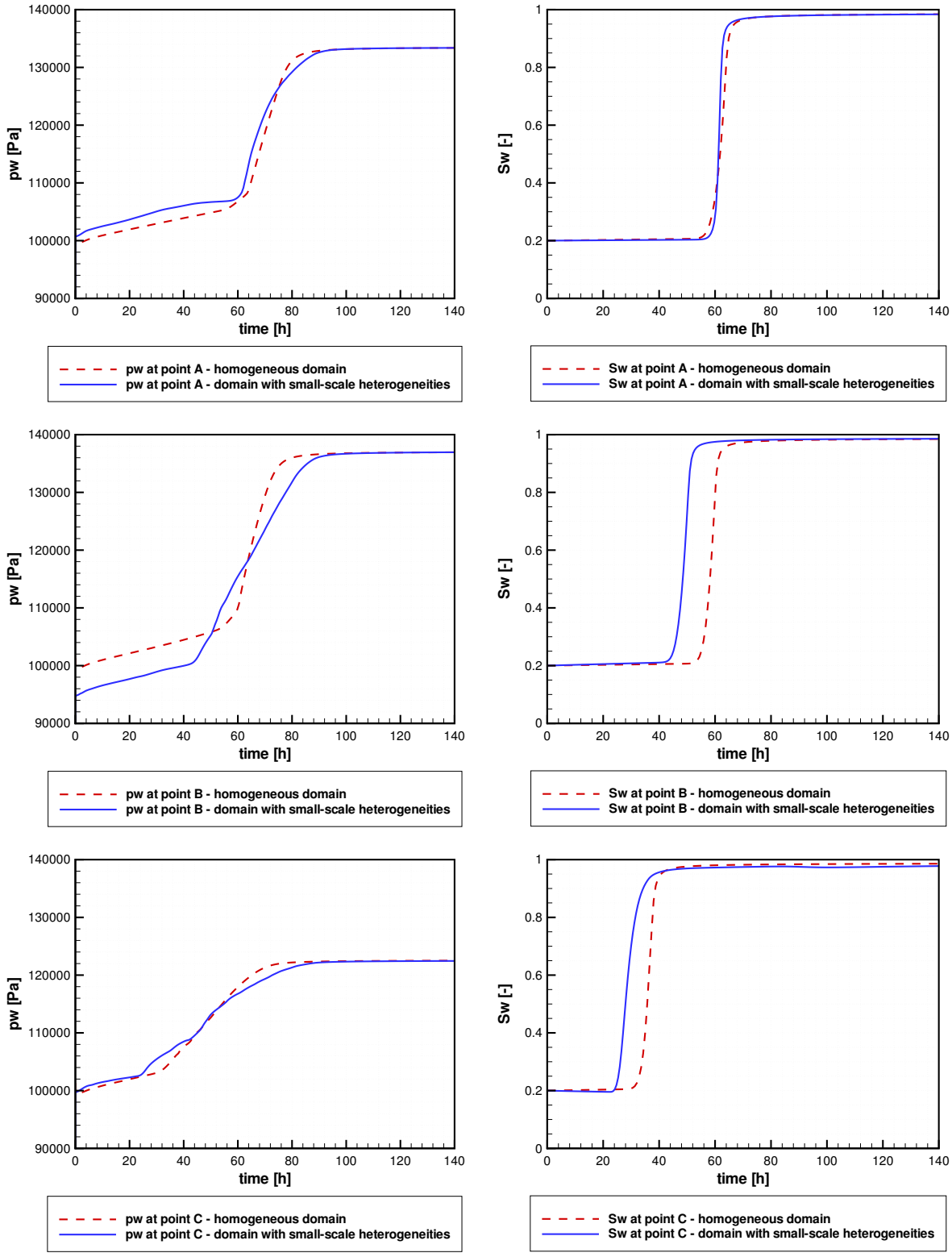

Figure 6.18: Comparison of water pressure and water saturation at point A, B, C between homogeneous slope and the slope with small-scale hetererogeneities using the reference case

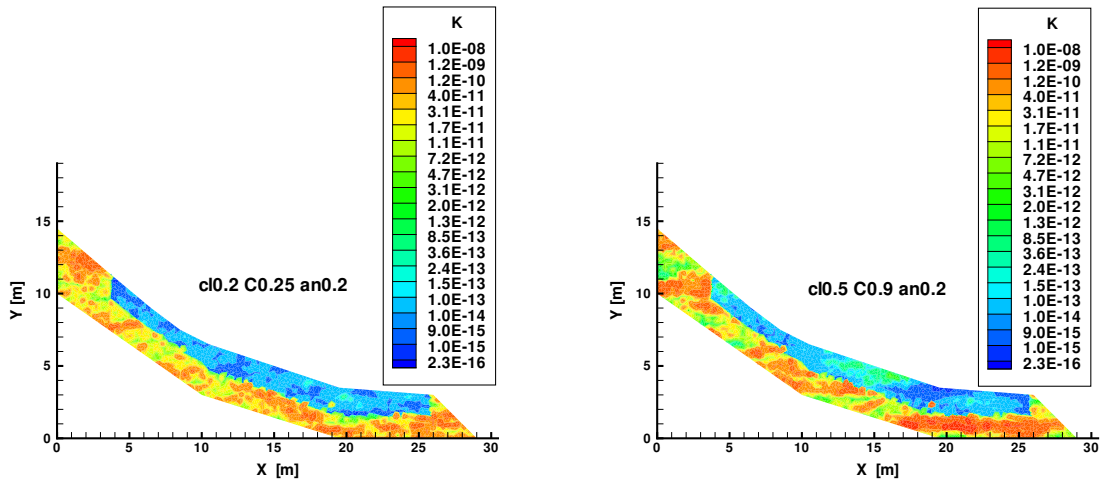

Figure 6.19: Permeability fields $K[m^2]$ with different geostatistical parameters, 2-layer domain

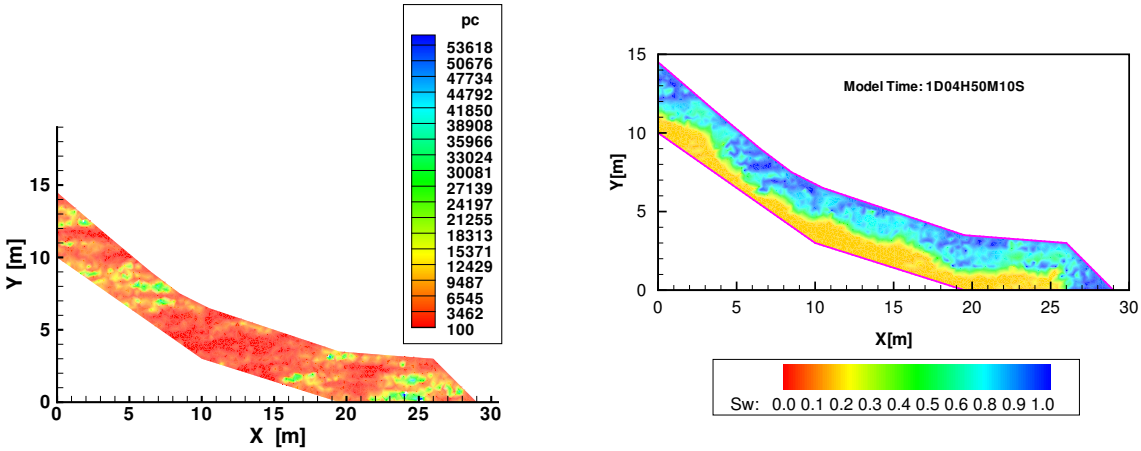

Figure 6.20: Effect of entry pressure on the saturation distribution; left: capillary pressure $p_c[Pa]$, right: water saturation $S_w[-]$ in reference case

6.5 Conclusions

In this chapter, the modeling of two-phase flow has been applied to a small field scale for numerical simulations. A slope which is idealised from a natural hillslope in Vorarlberg Alps area is chosen as a case study. The slope belongs to the head of a very steep mountainous catchment which is slow-moving and highly heterogeneous. Measurements on the slope showed that the high infiltration rates on the upper part of the slope are supported by a complex network of macropores and thus trigger deformations.

In the previous chapters, the two-phase flow model with different approaches for accounting for fault zones has been applied and analysed on the small and laboratory scale. The results have shown a very good agreement between two model concepts for fractures: 2D fracture model concept and 1D fracture model concept and they are similar to the experimental results. Thefore, the 1D fracture model concept for two-phase flow is chosen for simulation in this example.
The numerical simulations show the very strong influence of macropores on the water infiltration process in the slope. Because of the macropores, the infiltration is considerably speeded up concerning the water pressure and water saturation. However, the maximum pressure in the system is somewhat smaller compared to a system without macropores. The pressure increase is one main factor influencing the slope stability. The principal effects which have been numerically simulated qualitatively agree with observations in the field.

The numerical simulation of two-phase flow is also applied to a slope with small-scale heterogeneities which are represented by the permeability field. Here, the permeability field of the slope is generated by a geostatistical method. In the calculations, comparative studies are carried out and analysed varying different parameters like correlation lengths, variances, and anisotropies. Based on the parameter study, a reference case has been chosen for simulation. The numerical simulations indicate a more or less strong influence of small-scale heterogeneities on the saturation and pressure fields in the slope.

Chapter 7

Summary and Outlook

7.1 Summary

Multiphase models for the simulation of processes in the subsurface are widely used in different fields of technical applications. They link various fields from hydrogeology, hydraulic engineering, thermodynamics, computer science and mathematics. Characteristic for such models is that they consider flow of more than one fluid phase (e.g. water, gas, oil, alcohol). One major difficulty in numerical simulation of multiphase flow in subsurface arises from the possibly strongly heterogeneous and anisotropic porous media. In the subsurface, the typical heterogeneous porous media are often porous media with fault zones including fractured porous media and macroporous media.

The description of multiphase flow in porous media with fault zones becomes a challenging problem, because of the multiple scales involved and because of the non-linearity of the governing equations. With the presence of heterogeneties (e.g fault zones), the difficulty of the simulation stems from this non-linearity, from the sharp contrast of the matrix and fault zone properties and from the random character of the medium geometry.

Nowadays, there are several numerical codes for modeling of flow in subsurface system. For the modeling of flow and transport in porous media with fault zones including fractured porous media and macroporous media, numerical problems can occur because of the strong heterogeneities. For macroporous media which consist of many macropores, there is 'no' proven concept for numerically simulating two-phase flow processes.

In this study, a numerical model for two-phase flow including the gas and water phase in porous media with fault zones is chosen for relatively new fields of application, seepage processes through dikes with fault zones and water infiltration in natural slopes with macropores.

The overall objective of this work is to make applications and comparisons of different model concepts for the simulation of two-phase flow processes in porous media with fault

zones. Based on the mathematical model which describes the model concepts, the numerical model is applied for simulation. The numerical simulation is investigated in different applications from small scales to large scales. A comparative study using the results from the numerical simulations is carried out in order to reveal possibilities and limitations of the different approaches and provide knowledge related to the potential for investigation of two-phase flow in heterogeneous structures. In oder to check the numerical model, laboratory experiments have been used for comparisons. Overall, the work contributes to an improved process understanding.
Different model concepts for flow in porous media with fault zones are decribed in Chapter 2. The physical fundamentals used for the model are introduced in Chapter 3. Chapter 3 also explains the mathematical model including the governing equations, constitutive relationships, several formulations and the numerical model of two-phase flow in porous media with fault zones. The short description of the model can be summaried as following:

- The two-phase model is applied considering the water and gas phase. Here, different components are not included. The temperature change is negligible and thus isothermal conditions are assumed. The gas phase is considered to be compressible and the ideal gas law is assumed to be valid.

- For mathematical modeling, two-phase flow in porous media with fault zones is described by the balance equations for mass and for momentum (the generalized Darcy Law). Additionally, two constitutive relationships are required: Brooks-Corey and Van Genuchten. Several formulations for the primary variables have been introduced in the thesis, although the pressure-saturation formulation is chosen. For the flow in the fault zones, the validity of Darcy's law is assumed. This is a crucial point when the Reynolds number becomes larger than 10.

- The numerical model used in this work is supplied within the program system MUFTE-UG. The Fully Upwind Box Method is applied for the spatial discretization of the equations of the mathematical model. A fully implicit Euler scheme is used for the time discretization.

- A Newton-Raphson algorithm is applied to handle the non-linearities of the system of the discretized equations and the linearized equations are solved with the BiCGSTAB Method with Multigrid preconditioning.

- Dealing with the problem of small-scale heterogeneities, geostatistical methods are introduced. An overview of these methods is given and several theoretical variogram models are explained. The exponential variogram model is chosen for the simulations here.

Generally, the choice of model concept for modeling of flow processes in porous media with fault zones is strongly depending on the characteristics of problems being considered, for example, the scales of the problem. The modeling of two-phase flow in porous media with fault zones has been applied to domains with different scales (small scale, laboratory scale and small field scale). For each problem, different model concepts are compared and applied for numerical simulations.
Three different model concepts were used for the numerical simulations: *2D fracture model concept*, *1D fracture model concept* and *fracture with pipe model concept*.

- In the approach with 2D fracture model concept, a fault zone is discretized as a two-dimensional element in the two-dimensional domain and the mesh is highly resoluted in the fault zone as well as in its close surroundings.
- Contrastly, in the approach with the 1D fracture model concept, the fault zone is discretized as a one-dimensional element in a two-dimensional domain and the mesh resolution of the fracture-matrix space is coarser compared to the domain with 2D fracture model concept. This is also called combined approach.
- In the approach with a fracture as pipe model concept, the fault zone is idealised as an open pipe and a Dirichlet boundary condition is set up along the pipe wall assuming hydrostatic or atmospheric pressure distributions.

Firstly, an application is carried out in a small scale domain. It is presented in Chapter 4. Water infiltration processes in a single vertical fracture are analysed. The above-mentioned three different model concepts for two-phase flow are used for the numerical simulations. The results show an overall very good agreement between two model concepts: 2D fracture model concept and 1D fracture model concept. The pipe model concept is not suitable in this case.

The second application is done in a laboratory scale domain and it is presented in Chapter 5. Seepage processes through a dike are investigated for systems with one horizontal fault zone on different locations. Here, the three different model concepts for two-phase flow are also applied for the numerical simulation. To check the model concepts, experiments from the laboratory were compared to the numerical simulations. Seepage proceses in the dike can be quantified by both, experimental and numerical simulations. The 2D fracture model concept and 1D fracture model concept are suitable for numerical model in this case, as a good agreement between the experimental and numerical results was obtained. However, the results show an over-estimation of the seepage processes for the pipe model concept. Therefore, this model concept is not further recommended.

The last application is carried out in a small field scale domain. It is presented in Chapter 6. A slope which is idealised from the natural hillslope in Vorarlberg Alps area is chosen as a case study for the simulation. Based on the last applications, the 1D fracture model concept is chosen for numerical simulation of two-phase flow proceses in the slope with macropores. The results show the considerable influences of the preferential flow in macropores on the water infiltration processes in the slope. Due to the property of macropores, the infiltration is strongly speeded up. However, the maximum water pressure in the system is somewhat smaller due to the macropores. The pressure increase in lower parts of the layered aquifer is one main factor influencing the slope stability. The numerical results are in principal argreement with observations in the field.
In case of a slope with small-scale heterogeneities, geostatistical methods are used to generate permeability fields. Comparative studies have been carried out and analysed for cases with different parameters like correlation lengths, variances, and anisotropies. The simulation results illustrate a more or less strong influence of small-scale heterogeneities on the saturation and pressure fields of the slope.

7.2 Outlook

- The research work presents the applications of different model concepts for simulation of two-phase flow processes in porous media with fault zones. The model concepts are applied only in 2D domains. In some examples, e.g. dike problems, a 3D discretization should be used for simulation to better describe the fault zone in future. Moreover, in the thesis work, the over-estimation of flow occured for the 2D domain with pipe model concept. This process is even stronger expected in 3D. Therefore, the pipe model concept is not suitable for macropore infiltration. Overall, improved model concepts based on controlled experiments should be developed in the future.

- As mentioned the choice of model concepts for the modeling of flow processes in porous media with fault zones is strongly depending on the characteristics of problems being considered, for example, scales of the problems. Model concepts with combined approach have been applied for different problems on different scales (small, laboratory and small field scale). When going to the larger field scale in the future with complex geometries and parameter fields, a double-continuum model concept should be used.

- In the framework of the Research Unit “Großshang”, the Heumoes slope which has been chosen as a case study belongs to the head of a very steep mountainous

catchment and contains a large number of macropores. To describe the macropore network, geostatistical methods should be applied in the future.

- Coupling methods must be developed in the future which link surface runoff with subsurface hydraulics and soil deformation processes.
- Additionally, intensive geophysical investigations must be carried out to describe the geometry and the spatial parameter fields in detail. Field measurements will also be used to calibrate and validate the models. This hind of models can support vulneralbility and risk assessments for such alpine region in the future.

Bibliography

[1] Mortensen, A.P. (2001): *Preferential Flow Phenomenomena in Partially -Saturated Porous Media*, Ph.D Thesis, Environment and Resources DTU, Technical University of Denmark

[2] Bardossy, A. (1992): *Geostatistical Methods: Recent Developments and Applications in Surface and Subsurface Hydrology*, UNESCO, Paris

[3] Bardossy, A. (2004): *Introduction to Geostatistics*, Class Notes for WAREM Program, Institute of Hydraulic Engineering, University of Stuttgart

[4] Barlag, C. (1997): *Adaptive Methoden zur Modellierung von Stofftransport im Kluftgestein*, Dissertation, Report No. 52/1997, Institut für Strömungsmechanik und Elektronisches Rechnen im Bauwesen, Universität Hannover

[5] Bastian, P. (1996): *Parallele Adaptive Mehrgitterverfahren*, Teubner Skripte zur Numerik, B. G. Teubner, Stuttgart

[6] Bastian, P., Birken, K., Johannsen, K., Lang, S., Neuss, N., RentzReichert, H. and Wieners, C. (1996): *UG – a flexible software toolbox for solving partial differential equations*, Computing and Visualization in Science, 1(1), pp. 27-40

[7] Bastian, P. (1999): *Numerical Computation of Multiphase Flow in Porous Media*, Habilitation, Technische Fakultät der Christian-Albrechts-Universität Kiel

[8] Bastian, P., Chen, Z., Ewing, R., Helmig, R., Jakobs, H. and Reichenberger, V. (2000): *Numerical Simulation of Multiphase Flow in Fractured Porous Media*, in Chen, Z., Ewing, R. and Shi, Z.C. (eds.): Lecture Notes in Physics, Springer, pp. 52-71

[9] Bear, J. (1972): *Dynamics of Fluids in Porous Media*, American Elsevier, New York

[10] Bear, J. (1993): *Modeling flow and contaminant transport in fractured rocks, Chapter 1.1: Introduction*, In Flow and Contaminant Transport in Fractured Rock / Ed. by J.Bear, pages 110. Academic Press, San Diego, California, Academic Press

[11] Bielinski, A. (2007): *Numerical Simulation of CO2 Sequestration in Geological Formations*, Dissertation, Mitteilungsheft Nr. 155, Institut für Wasserbau, Universität Stuttgart

[12] Beven, K. and Germann, P. (1982): *Macropores and Water Flow in Soils*, Water Resources Research, 18, pp. 1311-1325

[13] Boogard, T. (2001): *Analysis of hydrological processes in unstable clayey slopes*, Nederlandse Geografische Studies, 287, Utrecht, 0169-4839.

[14] Bogdanov, I.I., Mourzenko, V.V., Thovert, J.F. and Adler, P.M. (2003): *Two-phase flow through fractured porous media*, Physical Review E 68, 026703

[15] Bronstert, A. (1994): *Modellierung der Abflussbildung und der Bodenwasserdynamik von Hängen*, Mitteilungen des Instituts für Hydrologie und Wasserwirtschaft, Nr. 46, Universität Karlsruhe

[16] Brush, D.J. and Thomson, N.R. (2003): *Flui Flow in Sythetic Rough-Walled Fracture: Navier-Strokes, Strokes, and Local Cubic Law Simulation*, Water Resources Research, 39 (4), 5.1-5.15

[17] Brutsaert, W. (1967): *Some methods of calculating unsaturated permeability*, Trans.ASAE, 10:400-404

[18] Breiting, T., Hinkelmann, R. and Helmig, R. (2002): *Modeling of Hydrosystems with MUFTE-UG: Multiphase Flow and Transport Processes in the Subsurface*, Fourth International Conference on Hydroinformatics, Iowa, USA

[19] Breiting, T., Hinkelmann, R. and Helmig, R. (2000): *Modellierung und Analyse von Mehrphasenprozessen zur Simulation von Methanausgasung im Untergrund*, Scientific Report, Institut für ComputerAnwendungen im Bauingenieurwesen, Technische Universität Braunschweig

[20] Barenblatt, G.I., Zheltov, I. P. and Kochina, I. N. (1960): *Basic concepts in the theory of seepage of homogeneous liquids in fissured rocks (strata)*, Journal of Applied Mathematical Mechanics (USSR), 24:1286-1303

[21] Brooks, R.H. and Corey, A.T. (1964): *Hydraulic Properties of Porous Media*, in Hydrol. Pap., Vol. 3, Fort Collins, Colorado State University

[22] Campbell, G. (1974): *A simple model for determining unsaturated hydraulic conductivity from moisture retention data*, Soil Sci., 117:311-314

[23] Class, H., Ebigbo, A. and Kopp, A. (2007): *Numerical modeling of CO2 storage in geological formations - recent developments and challenges*, 1. French-German Symposium on Geological Storage of CO2, Science Report No. 9, Geoforschungszentrum Potsdam, 51-58

[24] Burdine, N.T. (1953): *Relative Permeability Calculations from Pore-Size Distribution Data*, Technical Report, Petroleum Transactions, AIME

[25] Cho, S.E. and Lee, S.R (2001): *Instability of unsaturated soil slopes due to infiltration*, Computers and Geotechnics, 28: 185-208

[26] Depenthal, C. and Schmitt, G. (2003): *Monitoring of a landslide in Vorarlberg / Austria*, In: Stiros, S., Pytharouli, S. (Editor), Proceedings 11th International FIG Symposium on Deformation Measurements, May 25-28 2003, Santorini (Thera) Island, Greece, pp. 289-295

[27] Deutsch, C.V. (2002): *Geostatistical Reservoir Modeling*, Oxford University Press

[28] Dietrich, P., Helmig, R., Sauter, M., Hötzl, H., Köngeter, J. and Teutsch, G. (2005): *Flow and Transport in Fractured Porous Media*, Springer-Verlag, Berlin, Heidelberg, ISBN: 3-540-23270-2

[29] D'Eliso, C., Kortenhaus, A. and Oumeraci, H. (2006a): *Breaching of coastal dikes: Detailed breaching model*, Report Nr. 937, Leichtweiss-Institut für Wasserbau, Technische Universität Braunschweig

[30] Diodato, D.M. (1994): *A Compendium of Fracture Flow Models - 1994*, Center for Environmental Restoration Systems, Energy Systems Division, Argonne National Laboratory, USA, Available in: http://www.earthwardconsulting.com/library.htm

[31] Ebigbo, A., Bielinski, A., Kopp, A., Class, H. and Helmig, R. (2006): *Numerical Modeling of CO2 Sequestration with MUFTE-UG*, 16. International Conference on Computational Methods in Water Resources (18. - 22. Juni 2006, Copenhagen, Denmark)

[32] Ewing, R.E., and Spagnuolo, A.M. (2003): *Difficulties and uncertainty in mathematical/numerical modeling fluid flow in fractured media*, Fracture and In-situ Stress Characterization of Hydrocarbon Reservoirs, 209, Geological Society of London, London, England, pp. 187-200

[33] FEFLOW by DHI-WASY, DDD: http://www.wasy.de/

[34] Fuchs, A. (1999): *Optimierte Delaunay-Triangulierungen zur Vernetzung getrimmter NURBSs-Körper*, Dissertation, Shaker Verlag

[35] Van Genuchten, M.T. (1980): *A Closed-Form Equation for Predicting the Hydraulic Conductivity of Unsaturated Soils*, Soil Sci. Soc. Am. J., 44, pp. 892-898

[36] Forchheimer P. (1901): *Wasserbewegung durch Boden*, Zeitschrift des Vereins Deuscher Ingenieure, Vol. 49, pp. 1781-1788

[37] Haselsteiner, R. (2007): *Hochwasserschutzdeiche an Fließgewässern und ihre Durchsickerung*, Dissertation, Mitteilungsheft Nr. 111, Lehrstuhl und Versuchsanstalt für Wasserbau und Wasserwirtschaft, Technische Universität München

[38] Helmig, R. (1993): *Theorie und Numerik der Mehrphasenströmungen in geklüftet-porösen Medien*, Dissertation, Report No. 34/1993, Institut für Strömungsmechanik und Elektronisches Rechnen im Bauwesen, Universität Hannover

[39] Helmig, R. (1997): *Multiphase Flow and Transport Processes in the Subsurface - A Contribution to the Modeling of Hydrosystems*, Springer, Berlin, Heidelberg, New York

[40] Helmig, R., Class, H., Huber, R., Sheta, H., Ewing, J., Hinkelmann, R., Jakobs, H. and Bastian, P. (1998): *Architecture of the Modular Program System MUFTE-UG for Simulating Multiphase Flow and Transport Processes in Heterogeneous Porous Media*, Mathematische Geologie, Vol. 2, pp. 123-131

[41] Helmig, R. and Cunningham, A. (2002): *Multiphase Flow, Transport and Bioremediation in the Subsurface*, Course material of IAHR-EGW short course, Lehrstuhl für Hydromechanik und Hydrosystemmodellierung, Institut für Wasserbau, Universität Stuttgart in cooperation with the Center for Biofilm Engineering, Montana State University, Bozeman

[42] Hinkelmann, R. (2005): *Efficient Numerical Methods and Information - Processing Techniques for Modelling Hydro-and Environment Water*, Lecture Notes in Applied and Computational Mechanics, Vol. 1, Springer Berlin, Heidelberg, New York

[43] Hinkelmann, R. Busse, T. Roualt, P. and Nehrig, M. (2005): *Analysis of Water-Gas Flow Processes in Dike Systems with Fault Zones* , in Jun,B.-H., Lee,S.-J., Seo,I.W. and Choi,G.W. (eds.): Abstracts of XXXI IAHR Congress, Seoul, South Korea, Vol. I, pp. 550-551, (paper on CD), Korea Water Resources Association

[44] Hinkelmann, R., Kobayashi, K., Breiting, T. and Sheta, H. (2002): *Task: Risk Assessment of Methane Emission to the Surface in Post-Mining Areas*, in Kershaw,S. (ed.): Assessment of Hazardous Gas Emission to the Surface over Former Mined Areas, Research Annual Report of the ECSC project

[45] Hinkelmann, R. and Zehe, E. (2007): *Kopplung von Strömungs- und Transportprozessen für die Modellierung von Großhangbewegungen*, Hydrologie und Wasserbewirtschaftung(1): 51-54

[46] Hinkelmann, R., Stadler, L., Pham Van, S., Helmig, R., Germer, K. und Braun, J. (2007): *Simulation of water-gas flow processes in fractured-porous systems*, Computational Issues in the Geosciences, Santa Fe, New Mexico, USA

[47] Hoffmann, M. R. (2003): *Macroscopic Equations for Flow in Unsaturated Porous Media*, Dissertation, Wageningen Universiteit, Wageningen 2003, SBN 90-5808-893-6

[48] Kobayashi, K. (2004): *Optimization Methods for Multiphase Systems in the Subsurface - Application to Methane Migration in Coal Mining Areas*, Dissertation, Mitteilungen Heft 139, Institut für Wasserbau, Universität Stuttgart

[49] Kobus, H. and de Haar, U. (1995): *Perspektiven der Wasserforschung*, Deutsche Forschungsgemeinschaft

[50] Kolditz, O., Kaiser, R., Habbar, D., Rother, T. and Thorenz C. (1998): *ROCKFLOW -Theory and users' manual, release 3.4*, Institute of Fluid Mechanics and Computer Applications in Civil Engineering, University of Hannover, Gemany

[51] Kortenhaus, A., Oumeraci, H., Weissmann, R. and Richwien, W. (2002): *Failure Mode and Fault Tree Analysis for Sea and Estuary Dikes*, Proceedings 28th International Conference Coastal Engineering (ICCE), ASCE, Volume 2, Cardiff, U.K., pp. 2386-2398.

[52] Kröhn, K.P. (1991): *Simulation von Transportvorgängen im klüftigen Gestein mit der Methode der Finite Elemente*, Dissertation, Report No. 29/1991, Institut für Strömungsmechanik und Elektronisches Rechnen im Bauwesen, Universität Hannover

[53] Leverett, M.C. (1941): *Capillary Behavior in Porous Solids*, Transactions of the AIME, 142, pp. 152-169

[54] Lenhard, R., Parker, J., and Mishra, K. (1989): *On the correspondence between Brooks-Corey and Van Genuchten models*, Journal of Irrigation and Drainage Engineering, 115(4):744-751

[55] Lindenmaier, F., Zehe, E., Dittfurth, A. and Ihringer, J., (2005): *Process identification on a slow moving landslide*, Hydrological Processes, 19: 1635-1651

[56] Lindenmaier, F. (2007): *Hydrology of a large unstable hillslope at Ebnit, Vorarlberg - Identifying dominating processes and structures*, Ph.D Thesis, Mathematisch-Naturwissenschaftlichen Fakultät der Universität Potsdam

[57] Maurer, T. (1997): *Physikalisch begründete, zeitkontinuierliche Modellierung des Wassertransports in kleinen ländlichen Einzugsgebieten*, Dissertation, Mitteilungen Heft 61, Institut für Hydrologie und Wasserwirtschaft, Karlsruhe

[58] Mayer, J. (2008): *A Double-Continuum Approach for Two-Phase Flow in Macroporous Media: Parameter Study and Applications*, Fachgebiet für Wasserwirtschaft und Hydrosystemmodellierung, Technische Universität Berlin

[59] Minack, F. (2005): *Wirkung von Störstellen auf die Durchsickerung von Deichen*, Diplomarbeit, Fachgebiet für Wasserwirtschaft und Hydroinformatik, Technische Universität Berlin

[60] Mualem, Y. (1976): *A New Model for Predicting the Hydraulic Conductivity of Unsaturated Porous Media*, Water Resources Research, 12, pp. 513-522

[61] Niessner, J. und Helmig, R. (2006): *Multi-scale modeling of two-phase-two-component processes in heterogeneous porous media*, 16. International Conference on Computational Methods in Water Resources (18. - 22. Juni 2006, Copenhagen, Denmark)

[62] Ochs, S.O (2007): *Steam Injection into Saturated Porous Media - Process Analysis Including Experimental and Numerical Investigations*, Dissertation, Mitteilungsheft Heft 159, Institut für Wasserbau, Universität Stuttgart

[63] Olea, R.A. (1999): *Geostatistics for Engineers and Earth Scientists*, Kluwer Academic Publishers

[64] Oumeraci, H. and Schüttrumpf, H. (2006): *Review and Analysis of Failures Experienced by Sea and Estuary Dikes*, Res. Report, Leichtweiss-Institut für Wasserbau, Technische Universität Braunschweig

[65] Paul, M.(2003): *Simulation of Two-Phase Flow Processes in Porous Media with Adaptive Methods*, Dissertation, Mitteilungen Heft 120, Institut für Wasserbau, Universität Stuttgart

[66] Paul, M., Hinkelmann, R., Sheta, H. and Helmig, R. (1999): *Two-Phase Flow Modelling of Flood Defense Structures*, in Ehlers,W. (ed.): IUTAM Symposium on Theoretical and Numerical Methods in Continuum Mechanics of Porous Materials, Stuttgart, 1999, Kluwer Academic Publisher, Dordrecht, Boston, London, pp. 163-168

[67] Paul, M., Stauffer, F., Hinkelmann, R. and Helmig, R. (2000): *Calibration of a Water-Gas Flow Model for Dike Systems*, in Bentley,L.R., Sykes,J.F., Brebbia,C.A., Gray,W.C. and Pinder,G.F. (eds.): XIII International Conference on Computational Methods in Water Resources, A.A. Balkema, Rotterdam, Brookfield, pp. 201-208

[68] Pham Van, S. (2004): *Modeling of Two-Phase Flow in Porous Media - Parameter Studies on Water Infiltration Processes*, Master Thesis, Institut für Wasserbau, Universität Stuttgart

[69] Pham Van, S. (2004): *Modeling of Two-Phase Flow in Porous Media - Parameter Studies on Water Infiltration Processes in an Experimental Slope*, Young Water Research Journal, Vol. 1, pp. 58-64, YWAT, The Netherlands

[70] Pham Van, S., Busse, T. and Hinkelmann, R. (2004): *Modeling of Two-Phase Flow in Porous Media - Parameter Studies on Water Infiltration Processes*, 5. Workshop - Poröse Medien -, Eberhard Karls Universität Tübingen

[71] Pham Van, S. and Hinkelmann, R. (2005): *Development and Comparison of Different Model Concepts for Two-Phase Flow in Fractured-Porous Media - Application to Water Infiltration Processes in Hillslopes*. Progress Report, Fachgebiet Wasserwirtschaft und Hydroinformatik, Technische Universität Berlin

[72] Pham Van, S., Stadler, L. and Hinkelmann, R. (2006): *Comparison of a Micro-Scale and a Meso-Scale Model Concept for Two-Phase Flow in Fractured-Porous Media*, XVI International Conference on Computational Methods in Water Resources, Copenhagen, Denmark

[73] Pham Van, S. and Hinkelmann, R. (2007): *Development and Comparison of Different Model Concepts for Two-Phase Flow in Fractured-Porous Media*, Progress Report, Fachgebiet Wasserwirtschaft und Hydroinformatik, Technische Universität Berlin

[74] Pham Van, S. and Hinkelmann, R. (2008): *Development and Comparison of Different Model Concepts for Two-Phase Flow in Fractured-Porous Media*, Progress Report, Fachgebiet Wasserwirtschaft und Hydrosystemmodellierung, Technische Universität Berlin

[75] Pham Van, S., Hinkelmann, R. and Nehrig, M. (2008): *A Comparison of Model Concepts and Experiments for Seepage Processes through a Dike with Fault Zones*, in preparation for submission to an International Journal

[76] Pruess, K. (1991): *TOUGH 2, A General-Purpose Numerical Simulator for Multiphase Fluid and Heat Flow*, Lawrence Berkeley National Laboratory, University of California, USA

[77] Pruess, K. and Tsang, Y.W. (1990): *On Two-Phase Relative Permeability Capillary Pressure of Rough-Walled Rock Fractures*, Water Resources Research, 10

[78] Pruess, K. and Narasimhan, T.N. (1985): *A Practical Method for Modeling Fluid and Heat Flow in Fractured Porous Media*, Soc. Pet. Eng. J., 25, pp. 14-26

[79] Plescher, F and Hamm, F. (2005): *Schadenserkennung bei Deichen*, Diplomarbeit, Fachgebiet für Wasserwirtschaft und Hydroinformatik, Technische Universität Berlin

[80] Rahardjo, H., Tsaparas, I., Toll, D.G. and Leong, E.C. (2002): *Controlling parameters for rainfall-induced landslides*, Computer and Geotectics, 29: 1-27.

[81] Rahardjo, H., Lee, T.T., Leong, E.C. and Rezaur, R.B. (2005): *Response of a residual soil slope to rainfall*, Canadian Geotechnical Journal, 42: 340-351.

[82] Roualt, P., Nehrig, M., Pham Van, S. and Hinkelmann, R. (2006) : *Zerstörungsfreie experimentelle und numerische Untersuchungen zur Schwachstellenanalyse in Deichen*, Sicherung von Dämmen, Deichen und Stauanlagen - Handbuch für Theorie und Praxis, Vol. II, Eigenverlag des Instituts für Geotechnik und des Forschungsinstituts Wasser und Umwelt, Siegen. pp. 109-115

[83] Reichenberger, V., Jakobs, H., Bastian, P., Helmig, R. and Niessner, J. (2004): *Complex Gas-Water Processes in Discrete Fracture-Matrix Systems: Up-scaling, Mass-Conservative Discretization and Efficient Multilevel Solution*, Mitteilungen, Institut für Wasserbau, Universität Stuttgart, H.130, ISBN 3-933761-33-6

[84] Reichenberger, V., Jakobs, H., Bastian, P., and Helmig, R. (2006): *A Mixed-dimensional Finite Volume Method for Two-Phase Flow in Fractured Porous Media*, Adv. Water Resour., 29, pp. 1020-1036

[85] Richards, L.A. (1931): *Capillary Conduction of Liquid through Porous Medium*, Journal of Physics, Vol.1, pp. 318-333

[86] Sheta, H. (1999): *Simulation von Mehrphasenvorgängen in porösen Medien unter Einbeziehung von Hysterese-Effekten*, Dissertation, Mitteilungen Heft 100, Institut für Wasserbau, Universität Stuttgart

[87] Snow, D. (1965): *A parallel plate model of fractured permeable media*, Ph.D Dissertation, University of California, Berkeley-CA

[88] Silberhorn-Hemminger, A. (2002): *Modellierung von Kluftaquifersystemen: Geostatistische Analyse und deterministisch-stochastische Kluftgenerierung*, Dissertation, Mitteilungen Heft 114, Institut für Wasserbau, Universität Stuttgart

[89] Simunek, J., Van Genuchten, M.Th. and Sejna, M. 2008: *Development and applications of the HYDRUS and STANMOD software packages and related codes*, Vadose Zone J. 7:587-600

[90] Spiller, M. (2004): *Physical and Numerical Experiments of Flow and Transport in Heterogeneous Fractured Media: Single Fracture Flow at High Reynolds Number, and Reactive Particle Transport*, Dissertation, Mitteilungen Heft 143, Lehrstuhl und Institut für Wasserbau und Wasserwirtschaft, RWTH Aachen

[91] Stadler L., Germer K., Hinkelmann R., Färber A., and Braun J. (2008): *Studies on Infiltration Processes in a Soil Column with a Single Macropore*, Poster presentation at EGU General Assembly, Vienna

[92] Stadler, L., Mayer, J., Hinkelmann, R. and Helmig, R.(2008): *A double continuum approach for two-phase flow in porous media*, Abstract and oral presentation at Computational Method in Water Resources, XVII International Conference, San Francisco

[93] Stadler, L., Pham Van, S., Hinkelmann, R., Helmig, R. and Zehe, E. (2008): *Process Studies on Water Infiltration into Natural Slopes*, In preparation for submission to IAHS Journal

[94] Tsang, YW. and Tsang, CF Tang. (1987): *Channel model of flow through fractured media*, Water Resources Research, Vol. 23, pp. 467-479

[95] Uchida,T., Kosugi,K., and Mizuyama,T. (2001): *Effects of pipeflow on hydrological process and its relation to landslide: a review of pipeflow studies in forested headwater catchments*, Hydrological Processes, 15, 2151-2174

[96] UG, DDD: http://cox.iwr.uni-heidelberg.de/∼ug/index.html
Wittum,G., Bastian,P., Birken,K., Institut für Wissenschaftliches Rechnen, Universität Heidelberg

[97] Van Baars, S. (2005): *The Horizontal Failure Mechanism of the Wilnis Peat Dike*, Geotecnique, Thomas Telford, London, ISSN 0016-8505

[98] Van Asch, T.W.J., Buma, J. and van Beek, L.P.H. (1999): *A view on some hydrological triggering systems in landslides*, Geomorphology, 30: 25-32

[99] Van Duijn, C.J., Molenaar, J., and De Neef, M.J. (1995) *Effects of capillary forces on immiscible two-phase flow in heterogeneous porous media*, Transport in Porous Media, 21:71-93

[100] Vrijing, J.K. (1994): *Probalistic Design of Water-retaining Structures*, Delft Hydraulic Laboratory, The Netherlands

[101] Warren, J. E. and Root, P. J. (1963): *The behavior of naturally fractured reservoirs*, Soc. Pet. Eng. J. (Trans AIME), 3(228):245-255

[102] Weiler, M.H. (2001): *Mechanisms controlling macropore flow during infiltration - Dye tracer experiments and simulations*, Ph.D Thesis, Diss. ETHZ No. 14237, Swiss Federal Institute of Technology Zürich

[103] White, M.C. and Oostrom, M. (1996): *STOMP Subsurface Transport Over Multiple Phases: User's Guide*, PNNL-11218, UC-814, Pacific Northwest National Laboratory, Richland, Wasington

[104] Wu, Y.S., Bodvarsson, G. and Zellmer, K.E. (2004): *A triple-continuum approach for modeling flow and transport processes in fractured rock*, Journal of Contaminant Hydrology, Vol. 73, Issues 1-4

[105] Wienhöfer, J., Germer, K., Färber, A. and Zehe, E. (2008): *Subsurface flow observations at a steep forested hillslope using fiber-optic fluorometry*, Geophysical Research Abstracts, Vol. 10, EGU2008-A-07855

[106] Wienhöfer, J., Lindenmaier, F., Ihringer, J. and Zehe, E. (2008): *Characterization of Soil Hydraulic Properties on a Creeping Alpine Slope*, In: Marks, D. (ed.), Hydrology in Mountain Regions. Forthcoming IAHS Publication

[107] Wibbeler, H. (1995): *Entwicklung eines adaptiven Finite-Elemente-Modells zur Simulation seegangsinduzierter Strömungen in Wellenbrechern*, Dissertation, Institut für Bauinformatik, Technische Universität Darmstadt

[108] Yeh, J (2006): *Advanced Subsurface Hydrology - Chaper 8: Stochastic Conceptualization of Geology Heterogeneity*, Lecture Notes, University of Arizona, Tucson, USA

[109] Zehe, E. (1999): *Stofftransport in der ungesättigten Bodenzone auf verschiedenen Skalen*, Institut für Hydrologie und Wasserwirtschaft, 64. Mitteilungen des Instituts für Hydrologie und Wasserwirtschaft, Universität Karlsruhe (TH), Karlsruhe

[110] Zehe, E., Maurer, T., Ihringer, J. and Plate, E. (2001): *Modelling water flow and mass transport in a Loess catchment*, Physics and Chemistry of the Earth, Part B, 26: 487 - 507

[111] Zimmermann, R., Chen, T.H.G., and Bodvarsson, G. (1993): *A numerical dual-porosity model with semianalytical treatment of fracture/matrix flow*, Water Resources Research, 29:2127-2137

[112] Zyvoloski, G.A., Robinson, B.A., Dash, Z.V. and Trease, L.L. (1999): *Models and Methods Summary for the FEHM Application*, Report, Hydrology, Geochemistry & Geology Group (EES-6), Los Alamos National Laboratory